Egil Bergstøl Birkeland

High Voltage Subsea Connectors for Offshore Wind – Study of Interfaces

Master's thesis

NTNU
Norwegian University of Science and Technology
Faculty of Information Technology and Electrical Engineering
Department of Electric Power Engineering

NTNU
Norwegian University of
Science and Technology

Egil Bergstøl Birkeland

High Voltage Subsea Connectors for Offshore Wind – Study of Interfaces

NTNU
Norwegian University of
Science and Technology

Preface

This thesis is the master's thesis at the end of the 2-year master's program in Energy and the Environment at the Department of Electric Energy at the Norwegian University of Science and Technology(NTNU). The thesis is written over the entire spring semester of 2023 and accounts for 30 credits. The thesis is a continuation of a specialisation project conducted in the fall of 2022[1].

The development of technology related to renewable resources will be vital to reducing global warming. There is huge potential within offshore wind energy in regard to energy production. Large offshore wind farms are dependent on electrical equipment that can operate with high voltages to handle the considerable amount of generated energy. An important component of a well-functioning electrical grid for an offshore wind farm is the connector. This thesis is written in cooperation with SINTEF Energy, which is researching the design of a dry-mate 245 kV connector related to the CROWN project. The CROWN project is run by Baker Hughes with support from SINTEF and NTNU with the aim of developing the first subsea connector with a voltage rating of 245 kV in the world. The thesis examines how the interface between the electrode and insulation will impact the insulation performance. PD measurements and breakdown tests were conducted to research the impact of the various electrode surfaces.

Trondheim, 08/06/2023

Egil Bergstøl Birkeland

i

Abstract

The European Commission has set a goal to have 450 GW of offshore wind farms by 2050, and by that become the first carbon-neutral continent. It is vital to develop technology to reduce the price of floating wind farms located far from shore. An important component that needs development is dry-mate 245 kV connectors. A critical part of the design of such connectors is the interface between the electrode and the insulation material.

The interface can be examined by casting insulation cups around aluminium discs with known surface roughness parameters. The aluminium discs will function as electrodes that have undergone different kinds of surface preparation methods. The applied surface preparation methods in the thesis are sandblasting with two different particle types and polishing combined with hot AC anodising. All the test objects were cast with the casting procedure that was deemed best in the specialisation project.

The finalised insulation cups were taken into a test setup, designed for PD measurements and breakdown tests. PDIV and PDEV were found by increasing the voltage by 1 kV every two minutes until there were visible discharges and then decreasing by 1 kV in the same time interval until the discharges disappeared. Furthermore, the discharge magnitudes were used to examine electrical tree initiation and growth. Lastly, breakdown tests were conducted for the test objects without defects.

The profilometry results from the discs showed that the aluminium discs had relatively equal surface roughness within the surface preparation methods, which provided a foundation for an accurate comparison of the impact of surface roughness. The electrode surfaces sandblasted with aluminium oxide(0.5-1.0 mm) and glass orbs(0.25-0.42 mm) gave average S_a-values of 11.5 μm and 4.3 μm respectively. The electrode surfaces that were polished and hot AC anodised had an average S_a-value of 54 nm.

The impact of the surface roughness on electric field distribution was analysed with 2D simulations in COMSOL. The simulations showed that increasing the surface roughness increased the field enhancement, especially at the surface peaks. The results from the simulations were corroborated with the results from the laboratory testing. There was not a considerable difference in PDIV values, however, the average electrical field for electrical tree initiation was 14 kV/mm, 17 kV/mm and 21 kV/mm ranging from roughest to smoothest surface. Furthermore, the test objects with polished and hot AC anodised electrode surfaces gave the highest average breakdown strength at 38 kV/mm, while the roughest electrode surface sandblasted with aluminium oxide had an average breakdown strength of 26 kV/mm.

All the findings in the thesis are corroborating that the surface roughness will affect the insulation performance. Increasing the surface roughness will increase the field enhancement in the insulation layer, which will contribute to reducing the electric field at electrical tree initiation and when discharge magnitudes reach 1 nC, as well as decreasing the breakdown strength. Therefore, it can be concluded that an increase in surface roughness will cause a decrease in the insulation performance.

Sammendrag

Europakommisjonen har satt som mål å nå 450 GW med offshore vindparker innen 2050, og med det bli det første karbonnøytrale kontinentet. Det er nødvendig å utvikle teknologi for å redusere kostnaden av flytende vindparker langt fra land. En viktig komponent hvor det trengs utvikling er høyspent koblere med spenningsnivå på 245 kV. En kritisk del av designet vil være grensesnittet mellom elektroden og isolasjonsmaterialet.

Grensesnittet kan bli undersøkt ved å støpe isolasjonskopper rundt aluminiumsdisker. Aluminiumsdiskene vil fungere som elektroder som har gjennomgått ulike overflatebehandlinger. Overflatebehandlingene som har blitt brukt i denne oppgaven er sandblåsing med to ulike partikkeltyper og polering kombinert med varm AC anodisering. Alle testobjektene ble støpt med støpeprosedyren som ble funnet i spesialiseringsprosjektet.

De ferdiglagde isolasjonskoppene ble tatt videre til et testoppsett, som er designet for å måle partielle utladninger og gjennomslagstester. Tennspenningen og slukkespenningen for de partielle utladningene ble funnet ved å justere spenningen opp 1 kV annet hvert minutt helt til utladninger var synlige og så redusere med 1 kV i samme tidsintervall til utladningene forsvant. Videre ble størrelsen på utladningene undersøkt for å undersøke veksten av elektriske trær. Til slutt ble det gjennomført gjennomslagstester på koppene med tilfredsstillende kvalitet.

Resultatene fra profilometeret viste at diskene med samme overflatebehandling hadde relativt like overflateparametre, som legger til rette for nøyaktige sammenligninger mellom overflatebehandlingene. Elektrodeoverflatene som ble sandblåst med aluminiumsoksid(0.5-1.0 mm) og glasskuler(0.25-0.42 mm) ga gjennomsnittlige S_a-verdier på henholdsvis 11.5 μm og 4.3 μm. Elektrodeoverflatene som ble polerte og varm AC anodisert hadde en gjennomsnittlig S_a-verdi på 54 nm.

Påvirkningen av overflateruheten på fordelingen av elektrisk felt ble analysert ved hjelp av 2D simuleringer i COMSOL. Simuleringene viste at en økning i overflateruheten førte til en økning i feltforsterkning, spesielt i toppene på overflaten. Resultatene fra simuleringene ble bekreftet av resultatene fra laboratorietestingen. Tennspenningen hadde ikke noen betraktelig forskjell, men det gjennomsnittlige elektriske feltet for initiering av elektriske trær ble 14 kV/mm, 17 kV/mm og 21 kV/mm fra grovest til glattest overflate. Videre ga testobjektene med polerte og varm AC anodiserte elektrodeoverflater den høyeste holdfastheten med 38 kV/mm, mens den groveste elektrodeoverflaten hadde en holdfasthet på 26 kV/mm.

Alle funnene i avhandlingen bekreftet at overflateruheten vil påvirke isolasjonsytelsen. En økning av overflateruheten vil føre til høyere feltforsterkning som vil bidra til å redusere det elektriske feltet hvor elektriske trær er initiert og hvor utladninger kommer over 1 nC, samt redusere holdfastheten. Derfor kan det konkluderes med at en økning i overflateruhet vil redusere isolasjonsytelsen.

Contents

List of symbols

Symbol	Definition	Unit
a	Capacitance over test object excluding b and c	$[F]$
b	Capacitance between void wall and electrode	$[F]$
c	Capacitance over the void	$[F]$
E	Cavity free electric stress	$[kV/mm]$
E_h	Maximum electric stress	$[kV/mm]$
E_{min}	Minimum electric field	$[kV/mm]$
E_{max}	Maximum electric field	$[kV/mm]$
q_i	Charge injection	$[C]$
q_a	Apparent charge	$[C]$
R_a	Arithmetic mean deviation of a segment of a surface topography	$[\mu m]$
R_p	Highest peak value	$[\mu m]$
S_a	Arithmetic mean roughness of a surface	$[\mu m]$
S_p	Maximum peak height	$[\mu m]$
S_q	Root mean square average roughness of a surface	$[\mu m]$
S_v	Maximum valley depth	$[\mu m]$
S_z	Maximum height difference	$[\mu m]$
u, U	Voltage	$[V]$
u_a	Voltage across capacitance a	$[V]$
U_{r0}	Remanent voltage	$[V]$
U_{s0}	Ignition voltage	$[V]$
Z	Impedance	$[\Omega]$

Abbreviations

Term	Definition
AC	Alternating Current
BD	Breakdown
CT	Computerized Tomography
DC	Direct Current
PD	Partial Discharge
PDEV	Partial Discharge Extinction Voltage
PDIV	Partial Discharge Inception Voltage
PRPD	Phase Resolved Partial Discharge

List of Figures

List of Tables

1 Introduction

Reducing global warming will be vital for ensuring the future on Earth. The United Nations presented the Paris Agreement in 2015, which is an international treaty to limit climate change. The treaty set a global goal of keeping the temperature rise under $2°C$ in this century. The development of technology related to renewable resources will be crucial to keep within the limit. Wind energy has huge potential in energy production, especially with offshore wind farms. The European Commission has set a goal that Europe will have 450 GW of offshore wind power by 2050 to become the first carbon-neutral continent.[1–3]

Obtaining 450 GW offshore wind power requires large-scale floating wind farms, which comes with challenges regarding the price of the electric transmission grid. Especially in cases where the floating wind farms need to be located far from shore, and in deep waters. The price of the wind farms can be significantly reduced by placing substations on the seabed, combined with simplified component design and specifications tailored for floating wind farms. The substations will need to handle high voltages. An important component in the design will be dry-mate 245 kV connectors, which are yet to be developed at those voltage levels. The thesis is written in cooperation with the CROWN project, which has the goal of developing the first subsea connector with a voltage rating of 245 kV.[1, 4]

To develop these kinds of connectors, there are some critical parts of the design that needs to be examined. One of them is the interface between the electrode and insulation materials, including the influence on the insulation performance. Surface roughness of the electrode, adhesion, temperature, electric field, humidity, contaminants and defects will all be factors that impact the insulation performance of an insulation system.

A reliable manufacturing process will be vital to accurately examine how desired factors impact the insulation performance. The specialisation project[1] was used to determine which hardening method gave the best test objects without defects. The conclusion was that hardening in a pressure tank filled with 15 bar nitrogen at 150°C gave the highest possibility of test objects without defects.

1.1 Scope of thesis

This thesis will address the interface between the electrode and insulation materials for the development of technology to design dry-mate 245 kV connectors. It will be accomplished by utilising three preparation methods for aluminium discs to achieve various surface roughness parameters. Two of them were sandblasting with different particles and the last set of discs were polished and hot AC anodised. The aluminium discs will function as electrodes for insulation cups that will be cast around them with an epoxy resin mixture.

There are multiple factors that might affect the insulation performance of a connector, which is why the thesis is focusing on some specific factors. Factors that will be considered are surface roughness, electric field and adhesion. If other factors, such as defects or contaminants are detected, the cup is discarded. They are removed to ensure an even ground for the comparison of the surface preparation methods. Too many unknowns will make it challenging to determine which factors that affect the results and to what degree. The impact of the surfaces subjected to each preparation method will be examined through measurements with voltage stressing over the test objects. The objective of the thesis is therefore to examine the impact of electrode surface roughness on insulation performance.

There are not a lot of previous studies that have examined the impact of surface roughness at the interface between the electrode and insulation material on insulation performance. Some of the studies that do exist were used to determine where surface roughness parameters usually range. Additionally, results from similar problems were used to get an idea of how surface roughness can impact electrical properties. With those in mind, the hypothesis for the thesis is that an increase in surface roughness will decrease the insulation performance. The thesis is written with the assumption that the reader has knowledge in the field of electrical engineering.

1.1.1 Structure of the report

This section will provide a brief overview of all the sections included in the thesis:

Section 2 - Theory: The theory section will present the necessary theory to understand and provide a theoretical background for the discussion of the results. Additionally, some results and conclusions from earlier relevant studies are presented. A large part of the theory section is taken from the specialisation project[1] with some additions and improvements.

Section 3 - Methodology: The methodology section includes a description of the surface preparation methods that were used, how the surfaces were analysed with a profilometer and the casting process to manufacture the insulation cups. Additionally, it describes how the voltage tests were set up and conducted, as well as methods of post-test analysis. Lastly, a 2D COMSOL model used in the thesis is presented. The methodology section is based on the specialisation project [1], with improvements and new implementations.

Section 4 - Results and Discussion: Firstly the profilometry results from the profilometer will be presented. Furthermore, the results and discussion will include results from all the voltage tests that were conducted for the thesis, in addition to results from the COMSOL simulations. The presented results will be discussed continuously.

Section 5 - Conclusion: This section will include the most important results and conclude based on the findings.

Section 6 - Further work: This section will present suggestions for a continuation of the master thesis.

2 Theory

The theory section in the thesis is an improved version of the theory in the specialisation project report[1]. The improvements include additional figures, rewriting of some sentences for clarity and some additional topics.

A high voltage insulation system needs to withstand a variety of stresses which impacts the electric breakdown properties. The stresses reduce the breakdown strength, which eventually can lead to a breakdown. No matter the condition of the equipment, it will have internal stress due to the electrical fields. The magnitude of the internal stress is determined by the electrode and insulation design.[5]

The electrical properties, such as electric conductivity and permittivity, are essential when selecting insulation materials. Ideally, the conductivity is zero, while the permittivity is considered independent of frequency and temperature. In addition, the material should be homogeneous. If these requirements are met, the insulation material will be loss free and the field distribution is independent of voltage shape. However, these conditions will not be met in real scenarios. Insulation material is also known as dielectric.[5]

2.1 Surface roughness

A surface will never reach an ideal level of smoothness. In order to describe the finely spaced micro-irregularities that exist, surface roughness is a helpful parameter. Surface roughness can be divided into three components, which are called roughness, waviness, and form [6]. Some common parameters to characterise a surface is R_a and R_p. R_a is defined as the arithmetic mean deviation of a segment of a surface topography, while R_p is the highest peak value. In addition, the root mean square surface slope, R_{dq}, can be used to indicate the sharpness of surface peaks. These parameters are a good method of characterising a surface topography based on the roughness profile. Often in reports where the impact of surface roughness is included, the R_a-value is presented.[7]

Even though the R_a-value is often used, it cannot be solely trusted to characterise a surface accurately, due to peak handling. Every surface in Figure 2.1 has similar R_a-values, although they have different peak configurations. An important thing to consider is that the R-values are based on a two-dimensional roughness profile. It is therefore important to have more than one surface parameter for an accurate representation of a surface.
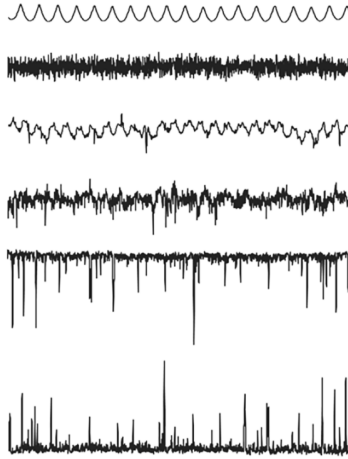
Figure 2.1: *Different surface profiles with similar R_a-values.[8]*

Surfaces can also be examined in three dimensions by utilising for example profilometry. The surface can then be characterised by S-parameters, which are equivalent to the R-parameters for three-dimensional analysis. Relevant S-parameters are S_a and S_q. S_a will be the equivalent to R_a, thus giving the areal average roughness. S_q gives the standard deviation of height distribution for the surface, which also can be expressed as the root mean square average. Usually, S_a and S_q are used for different kinds of surfaces, where S_a regularly is utilised for machined surfaces and S_q for optical surfaces. The S-parameters are used in reports where the surface has been examined in 3D, by for example a profilometer. In addition to S_a and S_q, the maximum peak height, S_p, the maximum valley depth, S_v, and the maximum height difference, S_z can be useful to characterise a surface. These additional parameters can be used to describe the magnitude of valleys and peaks for a surface. All the surface roughness parameters that have been used in the report are presented in Table 2.1.[9, 10]

Table 2.1: *Surface parameter definitions.*

Parameter	Definition
R_a	Arithmetic mean deviation of a segment of a surface topography
R_p	Highest peak value
S_a	Arithmetic mean roughness of a surface
S_p	Maximum peak height
S_q	Root mean square average roughness of a surface
S_v	Maximum valley depth
S_z	Maximum height difference

An additional way to characterise a surface is by using ISO-grade roughness numbers. ISO made a standard that divides roughness into twelve different categories that indicate how rough a surface is. A large number indicates a rough surface. For electrical equipment such as an electrode, the grade number will usually be in the lower range. A study conducted by *Tan [11]* presents their electrode roughness as quite high with an S_a-value of 0.166 μm. Additionally, a combination of studies [12] shows the surface roughness for several types of electrical equipment. The presented values are exclusively in the nanoscale and correspond to the first four ISO roughness grade numbers. After some time in operation, the surface might deteriorate which causes the surface roughness to increase.[11–13]

If the surface roughness parameters are known, they can be utilised to examine how the surface roughness will impact the electrical properties. *Feet et al.[7]* conducted a study on how surface roughness influences breakdown in air gaps. The experiments were conducted at atmospheric pressure under lightning impulse. R_a-values in the study ranged from $0.428 - 26.19 \mu m$. The study concluded that the surface roughness had a very limited effect on the breakdown voltage in air gaps at atmospheric pressure.[7]

A study conducted by *Kim et al.[14]* researched how surface roughness influenced the dielectric characteristics of various solid insulation materials. They did their simulations with a rod-to-plane electrode system with 60 Hz AC voltages applied to the rod, while the plane was grounded. The electrodes were divided by installing a solid insulation barrier. The electrode system was made of stainless steel.[14]

The surface roughness in the study ranged from $0.1 \mu m$ to nearly 20 μm. The influence surface roughness has on penetrating electrical breakdown, creep discharge, and sparkover voltage was examined. Experiments showed that all three were decreased as the surface roughness increased. Even though the surface roughness influenced the dielectric characteristics, the effects of changing insulation materials were larger for R_a-values under $20 \mu m$.[14]

Another study containing surface roughness influence on electrical properties is *Wei et al. [15]*. Their study examined how dielectric film affected insulation performance in air, SF_6 and SF_6/N_2 mixture with negative DC voltage applied. A spherical electrode was used with surface roughnesses ranging from $0.05 - 12.5 \mu m$. Every surface roughness was tested with different values of film thickness coated on both the spherical and plate electrode.[15]

Table 2.2: *ISO roughness grade numbers with corresponding R_a-values.*

ISO roughness grade number	$R_a[\mu m]$
N1	0.025
N2	0.05
N3	0.1
N4	0.2
N5	0.4
N6	0.8
N7	1.6
N8	3.2
N9	6.3
N10	12.5
N11	25
N12	50

The results from the experiments showed that increasing the surface roughness yielded a decrease in breakdown voltage for the three types of gas with all the applied methods of polyimide film coating. In addition, it showed that increasing the film coating thickness increased the breakdown strength. For all the experiments a coating of $100\mu m$ and surface roughness of $12.5\mu m$ gave higher gap breakdown voltage than no film coating and surface roughness of $0.05\mu m$.[15]

The effect on breakdown of electrode roughness in air-insulated apparatus has been studied in *Mahdy et al.* [16]. Local irregularities of the local electric field may form as a consequence of surface roughness, which can be created in tough operating conditions. The study simulated various surface roughnesses of an electrode by utilising a random events generator for the surface topography. The simulations showed that increasing the height of the surface roughness in a range of $0\text{-}140\mu m$ decreased the breakdown voltage to a corresponding range of 600-160 kV. The findings showed that the surface roughness could reduce the breakdown voltage by 50% compared to a smooth surface in a typical air gap.[16]

Another study, conducted by *Kantar et al.* [17], researched the longitudinal AC breakdown voltage of XLPE-XLPE interfaces based on surface roughness and pressure. The surfaces were examined with a profilometer, which gave S_a-values ranging from $0.27\mu m$ to 8.86 μm. The test objects were stressed with an AC voltage under different contact pressures. The experimental results showed that the interfacial breakdown strength was increased if the surface roughness was decreased for all the tested contact pressures. One reason given in the report was the substantial deviation in cavity size in the yz-plane between the roughest and smoothest surface, as a consequence of a significant difference in S_a-values. The cavities for the smoothest surface will be thinner in the vertical direction, thus having the lowest stress factor and highest breakdown strength.[17]

Objects with the same S-parameters were also used to research the tangential AC breakdown strength of solid-solid interfaces in a study by *Kantar et al.* [18]. The results were that a rougher surface decreased the breakdown strength.[18]

Impact of surface roughness on electrical field distribution.

The surface roughness of an electrode will affect the electrical properties, however, the importance of the effect will vary. One important property that is partly dependent on surface roughness is electrical field distribution. There will be microscopic regions on a surface which has a higher local electrical field compared to the average field of the entire surface. The higher local field leads to increased space charge in the insulation. Studies conducted by *Patrikar et al. [19]* and *Inagawa et al. [20]* corroborate that a rougher surface yields higher maximum electrical fields. A study conducted by *Taleb et al. [21]* examined how the electric field enhancement was affected by surface roughness at an electrode. Simulations in COMSOL showed that the field enhancement for an electrode with approximately S_a-value of $2\mu m$ was increased with a factor of around six compared to a flat electrode.[19–21]

Another study conducted by *Zhang et al. [22]* researched the relationship between the surface of a metal electrode and charge injection characteristics. Sandpaper with various grain sizes was used to create four surfaces with different surface roughnesses. Maximum depth and height were used to describe the surfaces. The maximum depth and maximum height were intervals of 0.38-6.33 μm and 0.21-4.59 μm, respectively. A surface profile from a section of each surface is presented in Figure 2.2. The simulations showed an increase in charge density for the rough surface, which might stem from an intensified electric field strength. The smoothest surface had a significantly smaller charge density, due to fewer sharp edges at the surface. Due to the findings, the study concluded that electrode surfaces should be treated to achieve smoother surfaces, thus improving the insulation's long-term performance.[22]
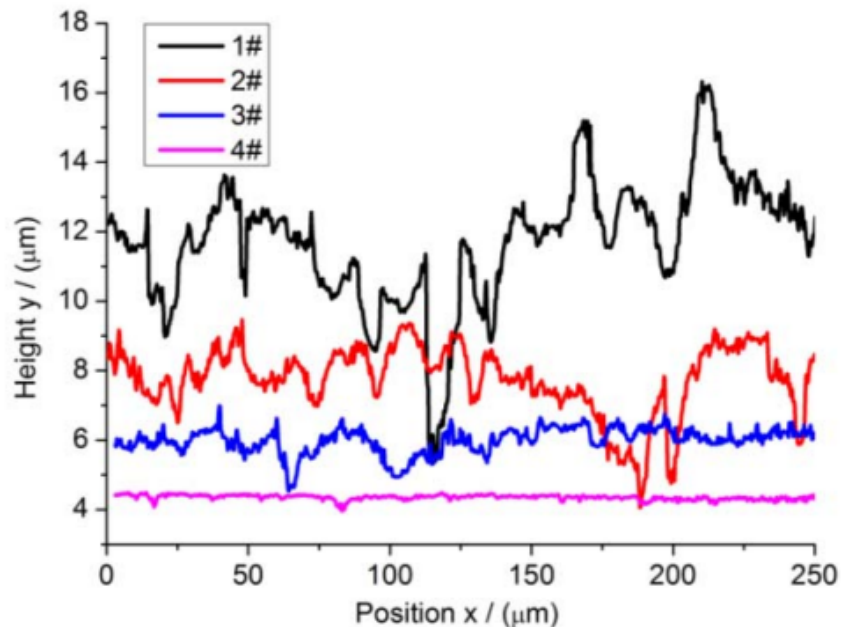
Figure 2.2: *Surface profile for the examined surfaces in the study conducted by Zhang et al.[22]*

2.2 Adhesion

In some electrical components, such as connectors, there will be interfaces between insulation materials and the electrode. A force or energy in the normal direction of the contact surface will be necessary if separation of the bodies is desired. The necessity of a force or energy is called the adhesion phenomenon. A high adhesion strength is desirable so the components stick together. Usually, the adhesion is given in adhesion force, which is the maximum necessary force for separation.[23]

The adhesion force will be influenced mainly by chemical bonds, intermolecular bonds, electrostatic force and meniscus force. The two main contributors to adhesion are the intermolecular and electrostatic forces. Intermolecular forces will exist everywhere, independent of the appearance of chemical interactions. Electrostatic forces occur when the net charges of two contacting surfaces are either the same or opposite. There are some discussions regarding the predominant force, but there are no doubts about the significant impact of electrostatic forces.[23]

Usually, the electric field in the electric double layer will generate electrostatic forces for the adhesion of solids. The electric double layer is occurring at an interface during two-body attachment because of charge exchange and redistribution. The electrical properties of the surfaces will determine how the electrical double layers form. Additionally, the form of matter and type of contact will impact how the electrons behave. A metal/polymer contact will be impacted by different effects than a metal/metal contact.[23]

The adhesion of epoxy-aluminium interfaces will be most relevant for this report. *Zhang et al.[24]* conducted a study to examine how the surface morphology influences the adhesion strength of epoxy-aluminium interfaces. The reason for the study was to determine which surface roughnesses will be best in designing based on the interfacial debonding of adhesively bonded aluminium joints. They found out that a rougher surface ended up with some isolated epoxy patches, while everything was removed for a smoother surface. The experimental results showed that the interfacial fracture resistance is increased with increasing surface roughness, which shows rougher surfaces have better adhesion strength. [24]

2.3 Progressive breakdown mechanisms

The main factors impacting the ageing phenomena of an energised solid insulation system are contaminants and imperfections in dry service conditions. Due to their impact on ageing, they will also be the main factor for determining the time to a breakdown. There are various defects that can impact the ageing time negatively and limit the breakdown strength of an insulation system. The defects can be in the form of cavities, particles that have intruded the insulation, interfaces and sharp points at the electrodes.[5]

Avoiding dust particles to intrude into the insulation is very challenging when producing it in an industrial process. In addition, cavities can quickly form if there are some air bubbles in the material used to produce the insulation. Furthermore, cavities can occur from mechanical or chemical stress after being manufactured. An electric stress greater than the breakdown strength of a gas enclosed in a cavity will cause the cavity to discharge.[5]

Partial discharge

A significant phenomenon that impacts the insulation performance and lifetime of electrical equipment with solid and gaseous or liquid insulation is partial discharges(PD). The gas will have a lower permittivity than the solid dielectric and the liquid will also usually have a lower permittivity. As a consequence, the dielectric strength is lower in the liquid or gaseous parts. PD can occur in different types depending on the location of the discharges. The discharges can either occur inside the material, at the material surface/interface or in gas. The discharges in a gas are also known as the phenomena Corona.[5, 25]

General erosion of the surface or cavity walls might initiate breakdown due to discharges. Eventually, cavities will develop into a pit of indefinite shape, which will develop further into electrical trees. Examples of where partial discharges can occur are visualised in Figure 2.3.
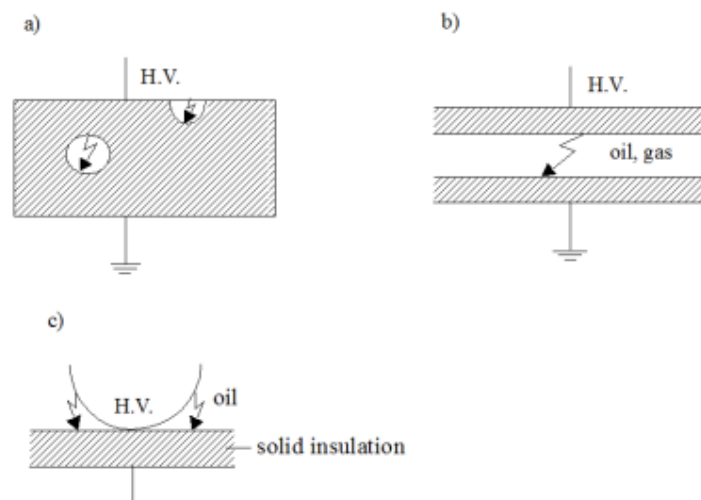
Figure 2.3: *Partial discharges in different kinds of devices.[5]*

It is desirable to manufacture solid insulation without gas inclusion, but that can be very challenging. Manufacturing processes such as casting, extrusion or impregnation all come with a risk of developing gas-filled cavities. In addition, poor adhesion between insulation and electrode can cause cavities. Therefore the impacts of partial discharges on high voltage equipment should be investigated to obtain reliable insulation.[5, 25]

The electric stress in a cavity is dependent on the shape of the gas-filled cavity. If it is spherical, the maximum electric stress, E_h is given by Equation 2.1. ϵ_r represents the relative permittivity of the solid insulating material and E represents the cavity-free stress in the solid dielectric. If the cavity is flat and perpendicular to the electric field, the maximum electric field is given by Equation 2.2.[5]

$$E_h = \frac{3 \cdot \epsilon_r}{1 + 2 \cdot \epsilon_r} \cdot E \tag{2.1}$$

$$E_h = \epsilon_r \cdot E \tag{2.2}$$

The equations show that the electric stress in the cavity will be higher than the solid dielectric. In many cases, the gas in the cavities will be air, which has a dielectric strength dependent on the air pressure, p, and electrode spacing, d. The electrode spacing will be the dimensions of the cavity in this case. If the two parameters are known, the dielectric strength can be found utilising a Paschen curve, as long as $p \cdot d$ is over the value corresponding to the lowest Paschen curve value. If the air is at room temperature and atmospheric pressure, the value can be set to 3 kV/mm. However, the electric stress of high-voltage equipment under normal operating conditions is usually higher.[5]

Some relevant parameters for measuring PD are the partial discharge inception voltage and extinction voltage. The partial discharge inception voltage is defined as the lowest voltage where partial discharges occur in a test arrangement when the stressed voltage is increased gradually from a voltage with no observations of such discharges. The partial discharge extinction voltage is defined as the voltage where repetitive partial discharges cease to occur when the stressed voltage is decreased gradually from a higher voltage value than the inception voltage. Even though there are defined values to the inception and extinction of PD, several tests with identical conditions may yield slightly different results. The reason is that PD is a stochastic variable, so the number of discharges can vary with the same stressed voltage.[5, 26, 27]

With stressed AC voltage, there are three methods of deterioration until the occurrence of a puncture. Before the puncture occurs, the partial discharges will repeat themselves at least once every half-cycle. The three methods of deterioration are:

1. Bombardment by ions and electrons around the discharge region of the insulation.
2. Chemical reactions in surrounding materials caused by temperature rise due to the discharges.
3. Radiation emitted from discharges. Bonds in organic substances can be broken by ultraviolet radiation.

Discharges through a cavity will occur in the field direction in a narrow channel. Eventually, the discharges will reach the dielectric surface, which will cause discharges along it. As a consequence, a significant percentage of the cavity surface is affected and a formation of a surface charge layer occurs. Immediately after discharge, the stress will be either zero or a little fraction of the value before discharge due to the surface charge layer. A discharge is developing fast, which means that the air will become insulating again in the fractions of μs.[5]

Partial discharges can also occur in oil-filled cavities in situations with oil present in the insulation. A common situation that leads to oil-filled cavities is when insulation distance is divided into alternate layers of solid insulation and oil. The design is made so there will be no sparkover at normal operating stress, however, discharges might occur in for example a 1-minute AC test. The partial discharges in oil will have high energy because the discharge path has a high voltage across it. Therefore, a failure may occur rapidly if discharges apply prolonged stress on the insulation.[5]

Measuring PD for different scenarios requires obtaining measurable quantities of an insulation system. Internal discharges due to a void in a test object can be represented by an equivalent diagram, as visualised in Figure 2.4a. The c in the circuit represents the capacitance of the void and b consists of a capacitance between the void wall and electrode on both sides of the cavity, as visualised in Figure 2.4b. The rest of the capacitance in the test object is represented by a. The stressed voltage is represented as a Thévenin equivalent with a voltage source, $u(t)$, and an impedance, Z_i.[5]
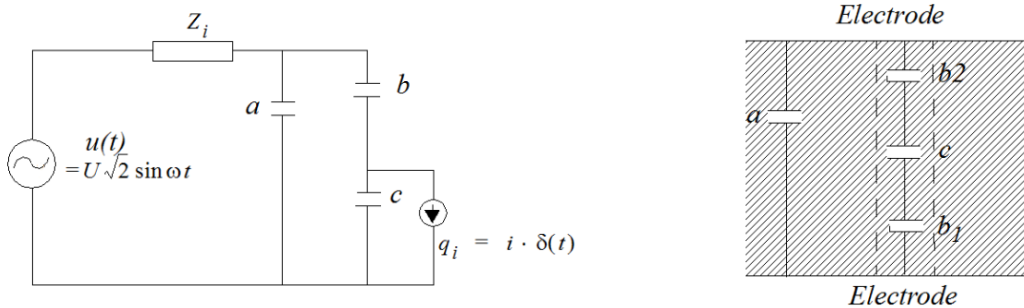
(a) The entire equivalent circuit.   (b) The configuration of the b-capacitances.

Figure 2.4: Equivalent circuit for discharges in a cavity. Figure 2.4a has been modified.[5]

The voltage across a void will nearly immediately fall to a remanent voltage, U_{r_0} after a discharge occurred when the ignition voltage, U_{s0} was reached. The voltage drop will correspond to an injection of a charge, q_i, across c, which can be expressed by Equation 2.3. For the discharge time of 10 nanoseconds, the current in the external circuit can be considered zero, as long as the impedance is assumed mainly inductive without any parallel capacitance. In the time interval of the discharge, the equivalent circuit can thus be represented as the abc-equivalent visualised in Figure 2.5.[5]

$$\Delta U = U_{s0} - U_{r_0} \tag{2.3}$$
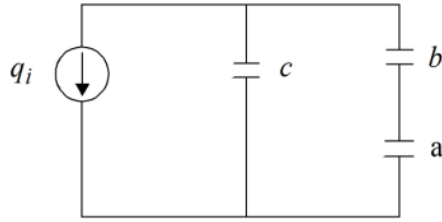
Figure 2.5: *Equivalent circuit during discharge time, often called abc-equivalent.[5]*

By utilising the abc-equivalent, an expression for the charge across c can be found. However, the charge cannot be directly measured in the external circuit. Contrarily, a voltage drop across a can be observed, expressed as presented in Equation 2.4.[5]

$$\Delta u_a = \frac{b}{a+b} \cdot \Delta U \approx \frac{b}{a} \cdot \Delta U \tag{2.4}$$

The test object will have the voltage across it restored immediately after the discharge by a transient current in the external circuit. By utilising the expression for voltage drop over a, a charge represented by the current can be expressed as shown in Equation 2.5. This charge is called the apparent charge and can be used to determine the magnitude of the discharge. The apparent charge is the necessary charge after a partial discharge to restore the voltage across the test object by transferring the charge from the external circuit to the test object.[5]

$$q_a = b(U_{s0} - U_{r0}) \tag{2.5}$$

If an AC voltage is stressed to the equivalent circuit, the voltage will be expressed as Equation 2.6, as long as there are no discharges. If the stressed voltage is lower than the ignition voltage, $u_1(t)$ will be equal to Equation 2.6. If the stressed voltage is higher than the ignition voltage, discharges will occur as visualised in Figure 2.6. The figure shows the immediate voltage drop after the discharge and the attempt to restore it. However, a new discharge will occur when the ignition voltage is reached again. The discharges will continue in both polarities until the voltage is reduced to the extinction voltage. The minimum limit for the extinction voltage is half the inception voltage.[5]

$$u_{c0}(t) = \frac{b}{b+c} \cdot \sqrt{2}U sin(\omega t) \tag{2.6}$$
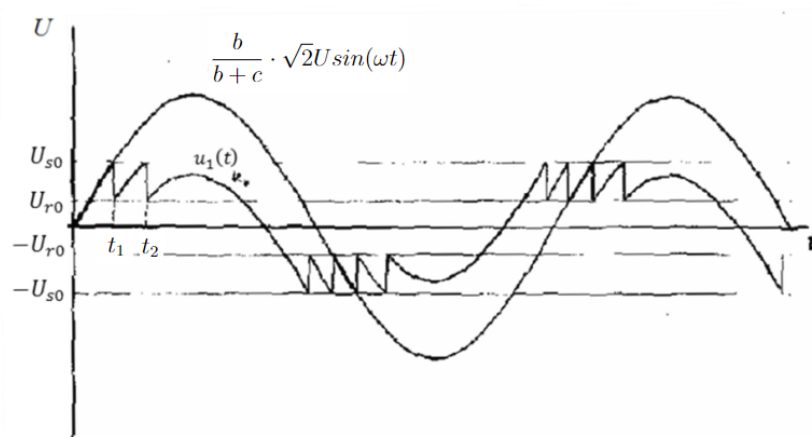
Figure 2.6: *The impact of a cavity on the voltage over time. The stressed voltage is also included. The figure has been modified.[5]*

14

Studying a Phase Resolved Partial Discharge(PRPD) plot can give an indication of the discharge locations in for example an electrical component where the electrode is isolated with epoxy resin. If discharges measured are symmetrical in the positive and negative half-periods, there is a void in the insulation. Contrary, if the discharges are asymmetrical, it indicates a void against the electrode.

Additionally, there are some common PD patterns that might occur when presenting a PRPD plot. The PD patterns are often called rabbit ear, turtle-like and wing-like named after the form created by the discharges. How the patterns generally look in a PRPD plot are visualised in Figure 2.7. Usually, the transition of the rabbit-like pattern to turtle-like will indicate growth of electrical treeing. The wing-like pattern will resemble an electrical tree and is visible after an electrical tree has grown. The maximum magnitude of the partial discharges will increase as the electrical tree is growing. The highest PD values will increase the branch length. The lower magnitude PDs can widen the channels, but they can not increase the length because the discharges do not reach the tree tips.[28–30]
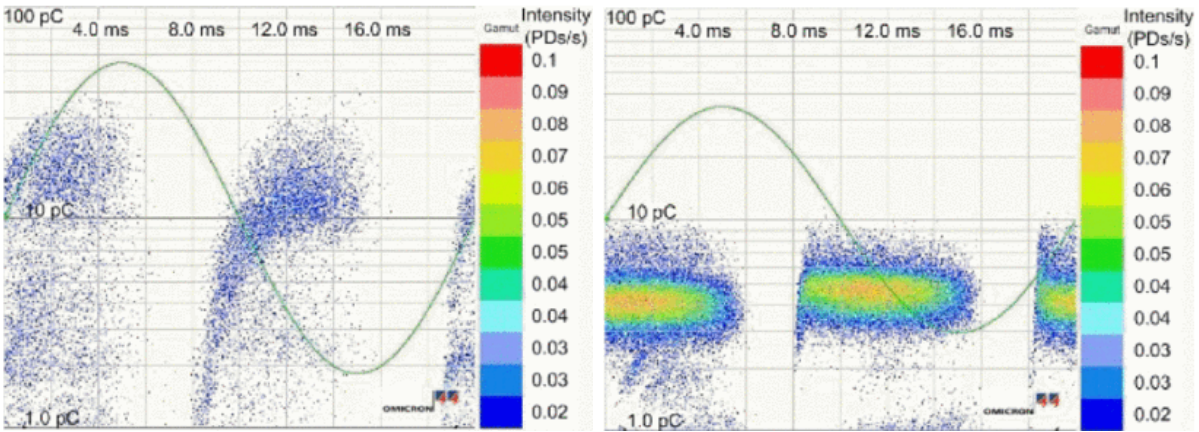
(a) *Wing-like.[30]*

(b) *Turtle-like.[30]*
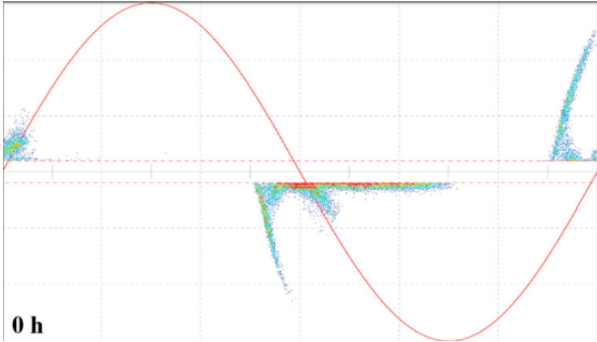
(c) *Rabbit ear.[29]*

Figure 2.7: *Common PD patterns under AC stress.*

Electrical treeing

During operation, the insulation quality of electrical equipment will deteriorate. The deterioration will impact the breakdown strength negatively in the form of for example cavities, sharp points at electrodes, particle contamination or interfaces. If dust particles enter an insulation system, voids can be created at the interface between the dielectric and the inclusion. In addition, voids might occur due to mechanical stress or chemical reactions.

The deterioration of the insulation might lead to electrical treeing, which is the initiation of tubular channels in the insulation. The tubular channels will grow with the same structure as a tree and typically has a diameter of $1 - 10 \, \mu m$. The phenomenon of electrical treeing is occurring in solid dielectrics. Examples of how electrical trees might look at different voltage levels are presented in Figure 2.8. Gaseous discharges from the electrode will cause growth of the electrical tree when it goes through the tubules. In addition to gaseous discharges, the growth of tree channels might stem from divergent fields caused by field enhancement points.[31]
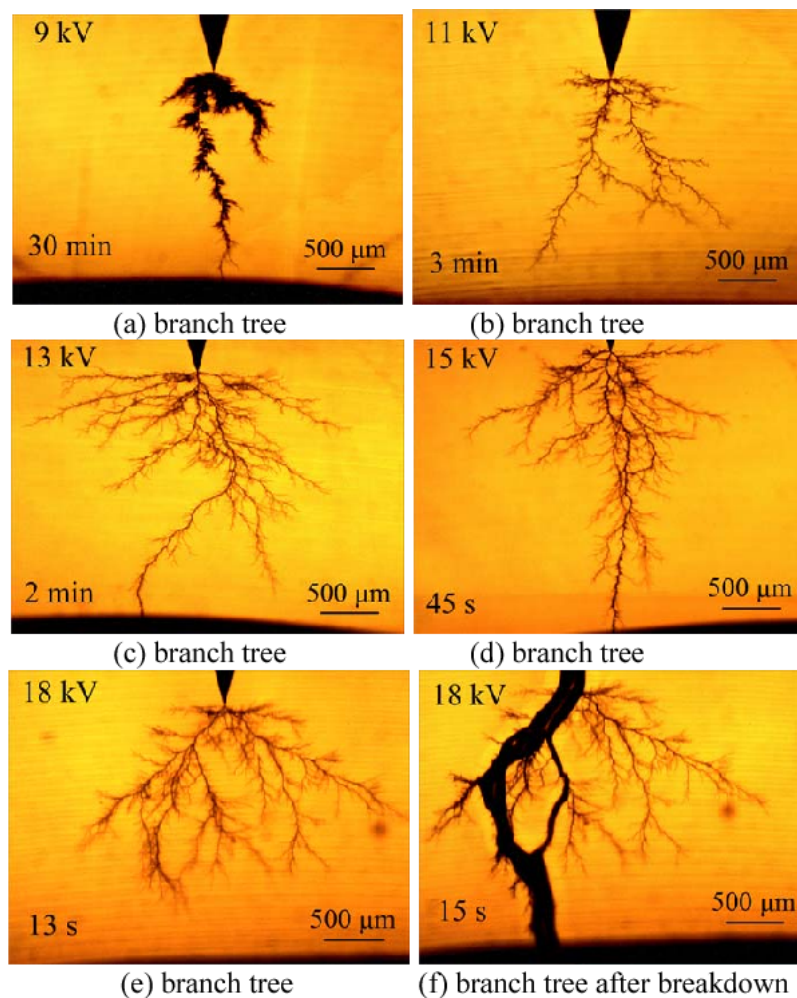
Figure 2.8: *Electrical tree initiation at different voltage levels.[32]*

The electrical trees will grow and develop new branches due to acoustic emission, partial discharge activity, light pulses and imperfections. The discharge magnitude will quickly enhance as a consequence of the expansion of electrical trees. The electrical trees will eventually bridge the insulation, however, the time frame may vary from minutes to hours. An electrical breakdown will probably occur immediately after the insulation has been bridged. An example of bridged insulation is visualised in Figure 2.8(f). A breakdown is usually developed in the positive half period of a stressed AC voltage. As for PD, the breakdown voltage or breakdown time are stochastic variables that may be slightly different for identical test conditions.[5, 31]

Gas discharges in a void will yield a different tree initiation than a cavity-free condition. The first phenomenon regarding tree initiation from cavities is the gaseous discharges, which can occur at relatively low voltage. The treeing growing process is heavily dependent on the shape and size of the cavity. A cylindrical, ellipsoidal or spherical cavity with an approximate size of μm will have tree initiation from partial discharges leading to erosion of cavity walls. A needle-shaped cavity will cause rapid tree growth. The erosion of cavity walls will have a much slower growth of electrical trees in comparison to needle-shaped cavities.[31]

As mentioned previously, tree initiation can occur without gaseous discharges. An increasing quality of insulation production decreases the magnitude of imperfections in the insulation. As a consequence of fewer voids in the insulation layer, tree initiation in a discharge-free condition becomes more interesting to research. In those cases, there will be void formation due to a divergent field.[31]

One way of detecting electrical tree propagation is by measuring partial discharges. A study conducted by *Vogelsang et al. [33]* researched how the partial discharge measurements could be used to interpret the electrical tree propagation in epoxy resin for winding insulation. The experiments recorded electrical tree inception by continuous PD measurements while simultaneously conducting optical analysis of the tree growth. The study divides the electrical tree growth into three stages to better characterise the process. The first stage is the initiation of tree growth, which will only be detectable by sensitive measuring methods. The next stage covers a range from the first small branches that appear until the tree reaches the opposite electrode. The last stage is when the small branches widen up and reach a pipe-shaped structure and eventually cause breakdown.[33]

The study found that the various stages had different values of PD. In stage 1, the PD was some pC, which can only be picked up by sensitive equipment. For stage 2, the branches will only have some μm diameters, which makes it possible for them to penetrate the insulation without causing breakdown. Due to the narrowness, the discharges are only some tenths of a pC. When the branches widen in stage 3, the discharges increase to some nC. Therefore, the rise in PD may indicate that a breakdown is imminent. However, it is important to note that PD can occur due to different mechanisms. Thus, making it a method that requires some caution when utilised.[33]

2.4 Hot AC anodising

Anodising is a way to treat a metal by making it the anode in an electrolytic cell. The treatment is done to create a protective coating to enhance the performance of a surface. For an aluminium surface, the anodising will develop a layer of aluminium oxide on the surface. The layer will protect against corrosion and provide additional adhesion for lacquer. There are several methods of anodising, including hot AC anodising, an efficient treatment process for aluminium.[34, 35]

The utilisation of DC anodising requires degreasing of the aluminium surface to remove contaminants. Hot AC anodising enables the degreasing step to be eliminated due to the combination of hot, acidic electrolytes and the production of vigorous gas evolution that comes as a result of electrolytic action. The surface will be degassed and cleared of contaminants without adding an extra step. As a consequence, the hot AC anodising is faster and more cost efficient.[36]

A study conducted by *Knudsen et al.[36]* investigated various methods of anodising as pre-treatment for aluminium alloys. The performance impact of chromating, DC and hot AC anodising were compared. The cathodic current density was significantly decreased for both hot AC anodising and chromating. The study concluded that hot AC anodising gave better performance compared to DC anodising. Additionally, hot AC anodising was found to be an alternative for chromating both in regard to speed and environmental impact. The corrosion protection for hot AC anodising is comparable to chromating and it does not contain any heavy metals while still maintaining a robust process due to current-voltage control. These properties are all contributing to making it a good alternative. A disadvantage is that old chromating equipment is incompatible with hot AC installations, which requires new installations of power supply.[36]

Johnsen et al. [37] conducted a study to examine how the durability of bonded aluminium joints was affected by AC and DC anodising pretreatments. Both the AC and DC pre-treatments were conducted with phosphoric acid and sulfuric acid as electrolytes. The DC anodising was 20 minutes for both electrolytes, while the AC anodising was 12 and 30 seconds for sulfuric and phosphoric respectively. Additionally, the DC methods had the substrates etched prior to the anodising. It was discovered that hot AC anodising had a performance almost as good as the traditional DC anodising method with phosphoric acid solution and significantly better than DC with sulfuric acid.[37]

3 Methodology

This section will contain the methods used in manufacturing insulation cups around aluminium discs, as well as the test setup used for PD measurements and breakdown tests. Firstly, the preparation of the electrodes will be provided. Furthermore, the casting process used to create the insulation cups and the test setup is presented. Additionally, ways of post-test analysis and a 2D COMSOL model for electric field simulations are introduced. Some of the parts in the methodology are taken from the specialisation project[1] and improved.

3.1 Test object pretreatment

The master thesis will consist of test objects with aluminium discs that have undergone various surface treatments. The preparation method that is used will determine the surface roughness parameters for the electrode surfaces. All the test object will be insulation cups that is cast around aluminium discs that have a height of $1\,cm$ and $6.5\,cm$ diameter.

Polishing

One way of pre-treatment is to utilise a polishing machine. The principle of the machine is a rotating disc where sandpaper can be attached magnetically. The roughness of the sandpaper is adjusted to the desired grade of polishing. For the smallest grain sizes, a diamond suspension and a lubricating liquid are added to the sandpaper to ensure successful polishing.

The first batch of discs was polished with sandpaper with decreasing grain size from 30-3 μm. Six different types of sandpaper were used within the grain size interval. The times at the rougher grain sizes were determined by using the first disc as a reference point. One disc was ground down until the deepest scratches were gone. The other discs were ground until they looked identical, which varied some in regard to time due to different initial conditions. The finest grain sizes were used for an equal amount of time, which yielded the same reflection level. The end result yielded surfaces that could be used as a mirror with S_a-parameters in the nanoscale.

Hot AC anodising

Another way of pretreatment used in the master thesis is hot AC anodising, which is described in section 2.4. Hot AC anodising was conducted on the polished discs by Sintef Industry. The specifics from the anodising process are presented in Table 3.1. The discs were submerged into the electrolyte and stressed with 50 Hz AC voltage as visualised in Figure 3.1. The orbs around the anodising cup are there to reduce evaporation. There were in total 12 polished discs that were hot AC anodised, to have some extra discs in case of unsuccessful test objects.

Table 3.1: *Anodising specifics.*

Parameter	Value
Current source	50 Hz AC
Electrolyte	150 g/l H_2SO_4
Current density	20 A/dm^2
Time	10 seconds
Temperature	80±1°C

Figure 3.1: *The anodising setup.*

Sandblasting

Sandblasting was used to obtain different surface roughnesses on the test objects. Varying the particle size and types yield a wide range of surface roughnesses. There is a strong correlation between particle size and average surface roughness for surfaces that have undergone sandblasting. Increasing the particle size will increase the S_a-value of a surface. Two different particles, aluminium oxide(0.5-1.0mm) and glass orbs(0.25-0.42 mm) were used to obtain the various surface roughnesses in the thesis.[38]

3.2 Profilometry analysis

The next step after surface pretreatment was to measure the surface roughness with a profilometer. The profilometer measures surface roughness by sending infrared light through an objective lens from a semiconductor laser. The infrared light will focus on a spot, which will reflect the light. A sensor in the profilometer will use the light reflection to give a profile of the surface roughness. The profilometer will only examine a small area of the surface, thus making it important with even sandblasting across the entire disc. An examination of the entire surface is possible, but it will be extremely time-consuming. Time can be saved by examining multiple randomly chosen spots of the surface and finding the average values of the surface roughness parameters.[39]

The profilometer is connected to a computer with Vision 64 software for result analyses. Correct input into the software is vital for accurate results. Adjustments of the light intensity must be conducted to examine all parts of the desired surface. Too high light intensity will lead to missing topography due to bright reflections and too low intensity will not detect the entire surface. There will still be some missing points from the surface even if the light intensity is well adjusted. As long as the profilometer picks up at least 75% of the data points, the results can be used. An example of how it may look with 80% data points is presented in Figure 3.2. There is a built-in function to approximate the missing points in the topography. The R_a-parameter will in most cases keep approximately the same with and without the function.
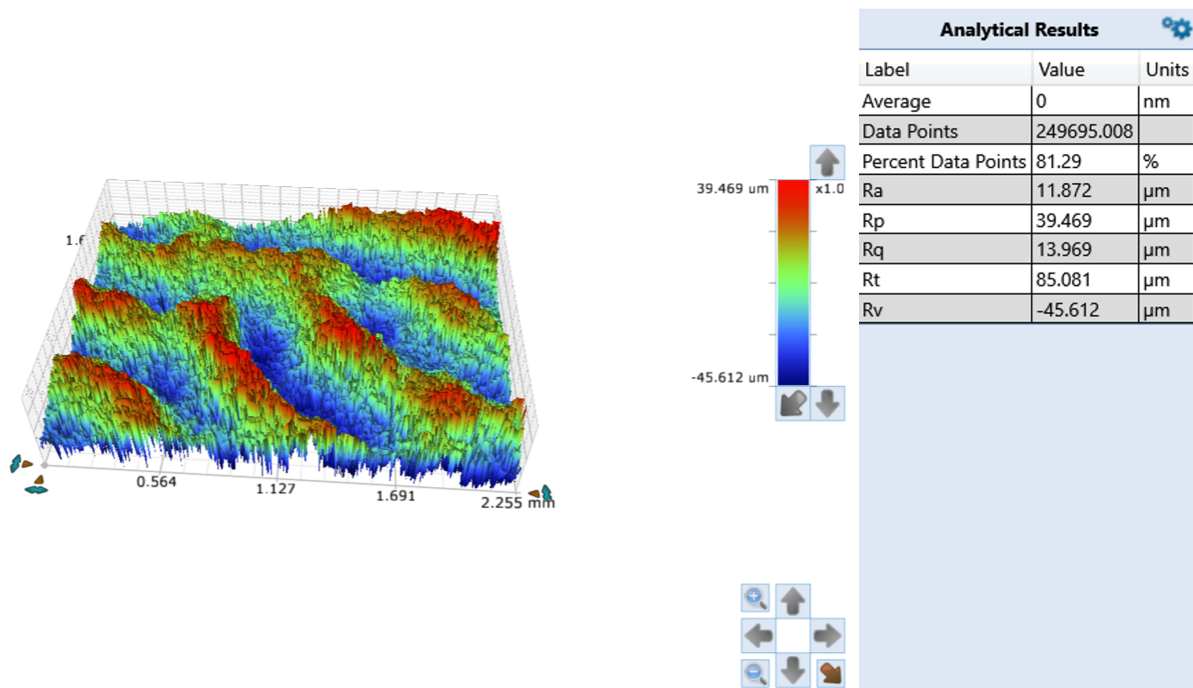
Figure 3.2: *Example of profilometry results.*

It is necessary that the profilometer focuses properly to get any results for the software. The focus is adjusted by examining for fringes in the live feed. The fringes will appear first at the top and move down when the distance between the test sample and the sensor is decreased. Eventually, they will disappear at the bottom. The measurement interval is found by subtracting the height when the fringes disappear with the height they appear. The profilometer is set to the upper value and will automatically move down when the measurements are initiated.

The profilometer stand will not be completely levelled, due to a slight linear tilt in the profilometer. For measurements in the microscale, the slight tilt will be picked up in the results. Useful built-in functions that remove the tilt and curvature are "Terms removal(F-operator)" and "Remove tilt". By applying these functions only the surface topography will be accounted for in the data analysis without the impact of a tilted measuring plate surface. The functions are already applied in Figure 3.2.

Surface roughness parameters are automatically calculated by the software after the profilometer is done scanning the surface. The desired values can be accessed by choosing either the basic stats or S-parameters. Both types of surface roughness parameters can be chosen on top of other built-in functions. However, the S-parameters will remove the tilt automatically without activating the functions. The S-parameters can still be chosen under the tilt removal functions, but the results will be unchanged. The values will be presented in the top right corner, as in Figure 3.2. The most important parameters from the basic stats are the per cent data points and R_a. From the S-parameters, useful information is S_a, S_p, S_q, S_v, and S_z.

3.3 Casting process

The casting of the insulation cups is a vital part of the test object manufacturing process. The specialisation project [1] was used to find a casting process that gave consistent PD and breakdown measurements for approximately identical insulation cups. This section will be used to describe that process.

The casting process was performed in a casting lab, which contain a casting chamber, a pressure tank, a heating cabinet and premanufactured moulds along with several other useful tools. The moulds are produced for the dimensions of the aluminium discs and will create an insulation layer of 1 mm over the electrode. A thorough cleaning of the equipment is the first step in the casting process. Every piece that will be in contact with either the epoxy or the aluminium discs must go through a cleaning process to ensure that the risk of contaminants and unwanted void formation stays low. In addition to the cleaning, the moulds are applied with a lubricant to make the extraction process easier when the insulation cups are finished. The assembled moulds are put into a heating cabinet for preheating to 130 °C.

The procedure after the cleaning will be determined by the type of epoxy. Different types of epoxies will require specific mixture ratios and temperatures to ensure the insulation gets the desired properties. The epoxy used for the master thesis is a two-part epoxy from Georg Jordan, which consist of epoxy resin and hardener. The epoxy resin and hardener are kept in separate containers in the first steps of the material preparation. The first step in material preparation is to heat the material to 60-65 °C and stir them for approximately five minutes. The stirring will contribute to reducing air bubbles in the materials and mix in a top layer that appears when the materials are left untouched for a while.

The next step is to measure the necessary amount of resin and hardener into separate cups. The ratio between the two materials should be 1:1 in regard to the weight. Further, the cups are put into a vacuum cabinet at 80-85 °C for degassing. After about an hour, the cups are moved into the casting chamber as visualised in Figure 3.3. The materials can be mixed within the chamber by tilting the cups from the outside panel. The orange equipment attached to the mixing cup is a heating element set to 70 °C. The mixing cup has a mixer that rotates to mix the materials with a vacuum in the chamber. The viscosity is at the highest point before the hardener and resin are mixed together. The initial speed is therefore set to 25 rpm to ensure enough power to rotate the whisker. Shortly after, the speed is reduced to 10 rpm. After about 90 minutes of stirring at 10 rpm in a vacuum, the mixture is ready for casting. Stirring in a vacuum will remove air bubbles in the epoxy resin mixture.
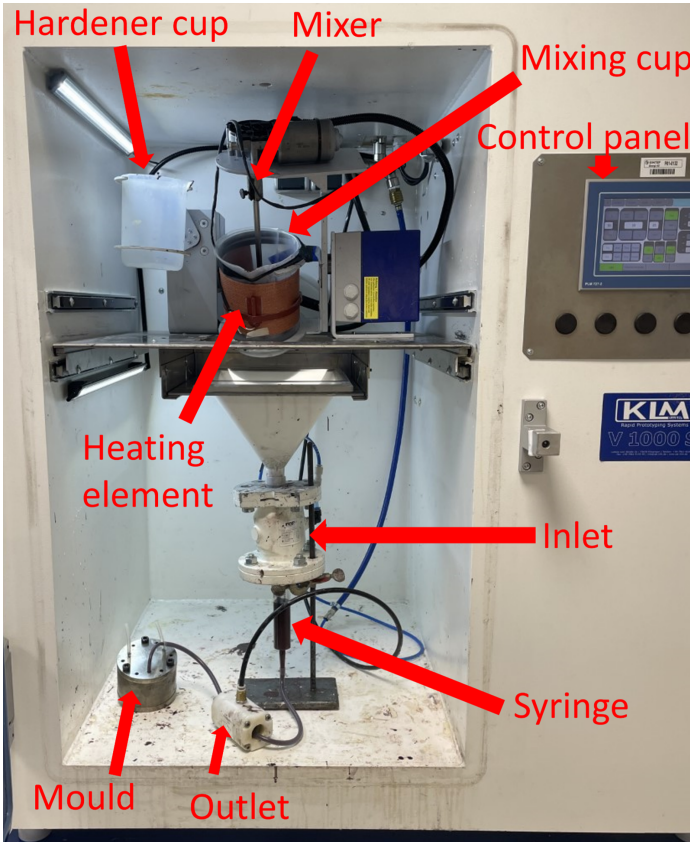
Figure 3.3: *The setup in the casting chamber.*

In addition to the material preparation, the flow line of the material in the casting chamber needs to be prepared. The material needs to be transferred from the main cup and into the mould. The epoxy will be led by silicone hoses that go through a syringe, an outlet and an inlet. The main cup can be tilted to pour the epoxy mixture into a funnel which leads through a silicon hose with a diameter of 8 mm and into the syringe, which is used to measure up the correct amount of epoxy to fill a mould. The 8 mm hose is going through an inlet valve, which can be used to stop or start the flow into the syringe.

From the syringe, the flow line is continued with a silicon hose with a 6 mm diameter. This hose is going through the outlet valve and towards the mould. At the end, the hose is extended with a 3 mm silicon hose that leads into the mould. Additionally, two 3 mm silicon hoses are put into the mould to determine when the mould is full and reduce spilling. The complete setup for the material flow is presented in Figure 3.3. Additionally, each component has been named to better visualise the flow line.

With both the material and flow line prepared, the last stage is to fill the mould with epoxy. Firstly, the outlet valve must be closed. Then, the mixer is stopped and the epoxy is poured into the syringe until it reaches approximately 45 ml. When the syringe is filled, the vacuum chamber is vented so the preheated moulds can be inserted. The 3 mm silicon hose is lead into the mould and both the valves remain closed when the vacuum is turned back on. The outlet valve is opened when the chamber reaches 400 mBar, which initiates the filling of the mould. The outlet valve is kept open until epoxy comes out from the overflow holes.

Subsequently, the moulds filled with liquid epoxy are set to harden. The results from the specialisation project report showed that the best hardening method was at 150 °C in a pressure tank containing 15 bar nitrogen. The moulds are kept in the pressure tank for 20 hours before the temperature is turned off. They are left an additional day to cool down before extracting the insulation cups.

The final step after extruding the insulation cups from the moulds is to apply conductive paint on the bottom and approximately 3 mm along the inner walls. The conductive paint is applied to function as a protective layer to reduce corona discharges on the insulation surface. Two layers of the conductive paint CoronaShield P8003 diluted with "rectified spirit" were applied. The mixture consisted of a mixing ratio of 5:1 with 5 parts of CoronaShield to 1 part spirit. They were mixed by an ultrasound mixer. An even paint job was ensured by applying electrical tape, as visualised in Figure 3.4a. The first layer was set to dry for at least 30 minutes before applying the second layer. The end results will be something like the insulation cup visualised in Figure 3.4b.[40]

(a) *Example of the conductive paint process.*

(b) *Finalised manufactured insulation cup.*

Figure 3.4: *The last steps in the manufacturing process of the insulation cups.*

3.4 Measurement circuit

The insulation cups need to be stressed with a voltage to examine PD occurrence and breakdown strength. The circuit used to conduct the measurements will include the PD measuring equipment MPD800, a transformer, a coupling capacitance, and a voltage source. A diagram of the measuring circuit is presented in Figure 3.5. DUT stands for the device under testing, which in this case is the insulation cups. CPL 1 in the diagram is a measuring shunt. As visualised, it is connected to a unit, MPD800, that is powered by a battery, RBP1. The unit sends the signal out from the high-voltage area by fibre optical cables. Outside the high-voltage cage, the fibre optic cables connect to a computer through a control unit. The results can be recorded and analysed with the OMICRON MPD Suite software. The software will present the discharges from the measurements in a PRPD plot.
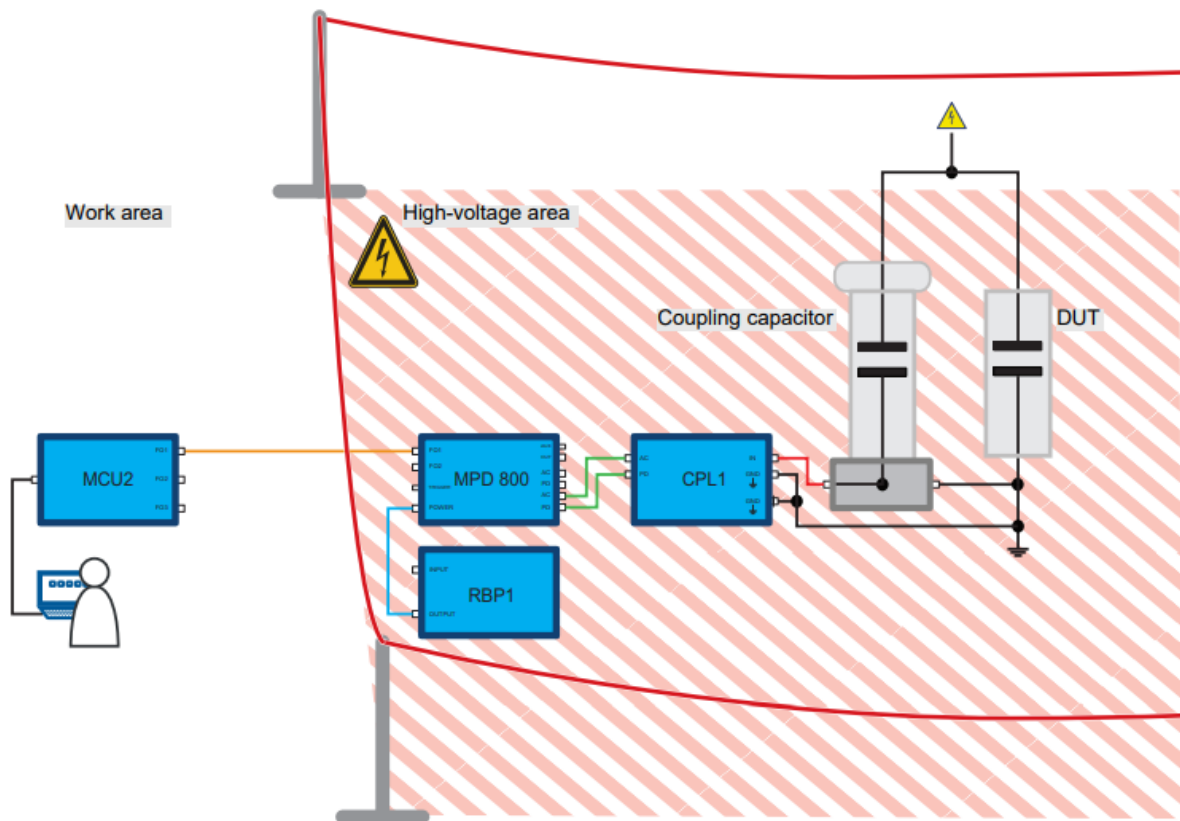
Figure 3.5: *Test circuit used for PD measurements and breakdown testing.[41]*

The measurements in the high-voltage cell were conducted with two slightly different setups. The PD measurements used the measurement circuit from 3.5. The PD measuring equipment was removed for the breakdown tests and the coupling capacitor was replaced with an insulator. Additionally, a water resistance was added between the transformer and the insulator. The test objects were placed identically for the two tests in a container filled with silicon oil, as visualised in Figure 3.6.
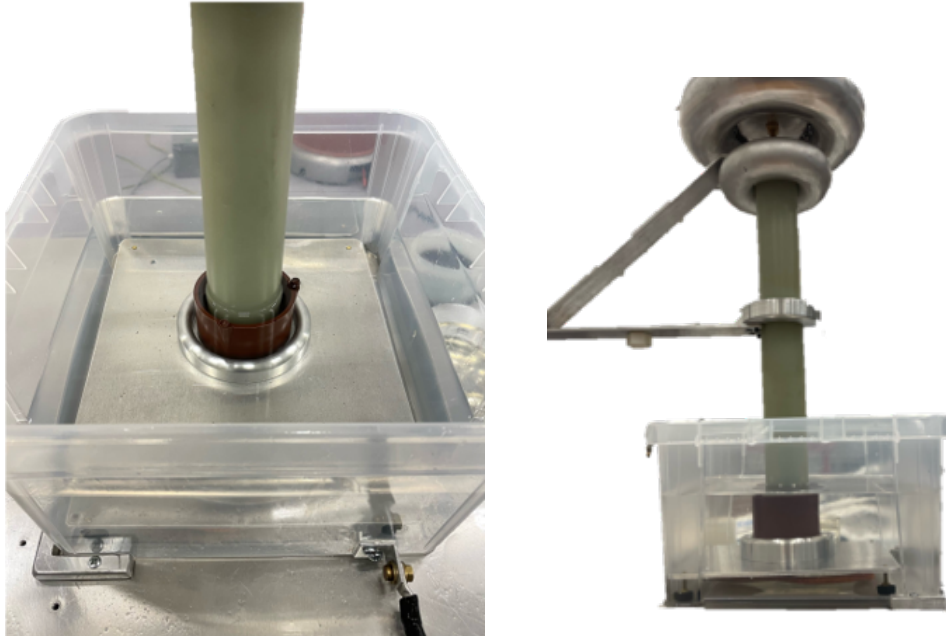
(a) *The insulation cup looking from above.* (b) *The insulation cup looking from the side.*

Figure 3.6: *The measurement setup for the insulation cups used to conduct both PD and BD measurements.*

Before any measurements could be done, the software must be calibrated to the test setup. A calibrator was used to calibrate the charge by applying 10 pC over the test object and adjusting the software to correspond to the same value. The transformer ratio of 220V/100 kV and the stressed voltage from the low-voltage side were used to calibrate the voltage. The measurements were divided into three steps. The first step is a screening process to determine which of the insulation cups has sufficient quality to continue testing by finding PDIV values and the corresponding discharge magnitudes. It will function as a quality check to ensure there are no voids that will give misleading results for the objective of the tests. The PDIV measurements were conducted by increasing the voltage by 1 kV every two minutes until PD was visible. Subsequently, the voltage was reduced by 1 kV in the same time interval until the extinction voltage was found. The same tests were done three times for each test object to ensure that the data were correct and not skewed by disturbances.

The second step of the testing, Phase 2, is to increase the voltage until PD measurements indicate electrical tree growth. In the specialisation project tests[1], it was found that the discharge magnitude began gradually increasing around the same electric field for all the successful insulation cups with the same surface roughness. Figure 3.7 visualises the gradual increase over time for a typical insulation cup tested in the specialisation project. The increase in magnitude indicates that electrical trees are growing. The second step is conducted by increasing the voltage in the same time interval until the discharge magnitude reaches 1 nC. In addition to the electric field necessary for reaching 1 nC, the electric field where the gradual increase in charge magnitude began is determined.
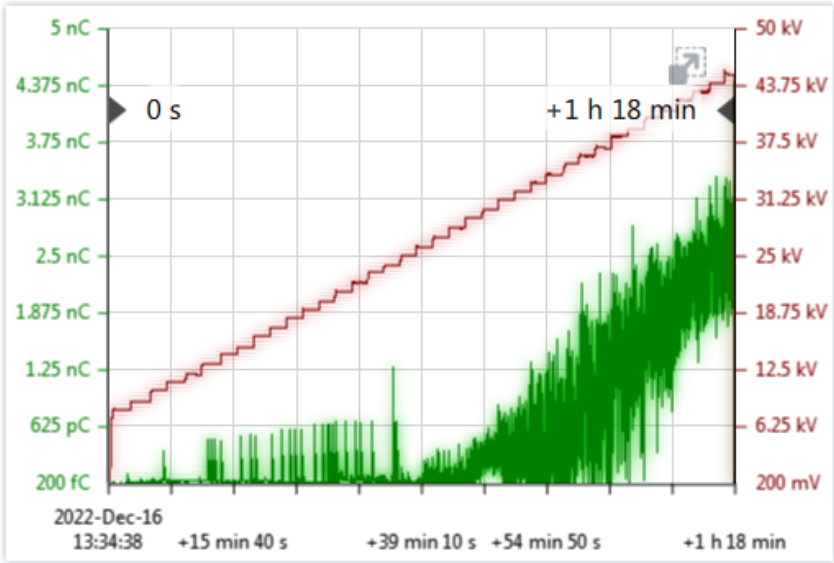
Figure 3.7: *Typical development of PD during the specialisation project tests.[1]*

The last step is breakdown testing. The PD measurement equipment is removed from the setup to preserve it before a potentially damaging breakdown occurs. Additionally, a water resistance is added to reduce the breakdown channel size. Smaller breakdown channel size enables microscopical examination of electrical trees. The setup in the specialisation project did not include a water resistance, which made the breakdown channel hide all traces of electrical tree formation. The start voltage for the breakdown tests is set to the individual values found for each insulation cup where the charge magnitude began to gradually increase. Further, the voltage was increased by 1 kV with a two minute interval as for all the other tests.

The first two measurement steps were conducted as non-destructive tests. A non-destructive test is a way to determine the physical conditions of a test object without harming its abilities within its desired function. Contrarily, destructive testing will harm the ability of the test object, so it no longer can fulfil its desired function. Determining the breakdown strength of the test object will be a destructive test, thus only possible to conduct once at each test object.[42, 43]

3.5 Post test analysis

To get a greater understanding of why a breakdown occurred in the insulation cups, some of the cups were analysed further. Two different methods were used to examine the breakdown channel, the surrounding epoxy layer and the electrode surface in the proximity of the breakdown.

The first method was to cut the insulation cup in two and grind it with sandpaper until the breakdown channel was reached. Furthermore, the breakdown point was examined under a microscope. The breakdown channel size, traces of electrical treeing and the electrode surface around the breakdown can be used to examine the cause of the breakdown.

The second method is to utilise industrial tomography. To increase the possibility of a successful scan, the insulation was separated from the aluminium disc. The results from a CT scan might be skewed if there is aluminium present, especially if it is close to the interesting area. The aluminium will be creating noise, which might make it impossible to see the breakdown channel and electrical tree initiation. The insulation was separated by utilising a blow torch under the aluminium disc. The increased temperature of the aluminium disc separated the insulation without harming it, as visualised in Figure 3.8. [44]
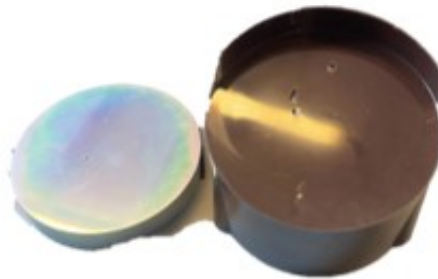
Figure 3.8: *Example of separated insulation from the aluminium disc.*

The separated insulation part of the insulation cup was scanned. The scan was analysed by utilising the software myVGL, which allows the user to select sections of the scan for analysis. The scan will provide a model of the entire disc as visualised in Figure 3.9. There are planes in the x,y and z-axis that can be adjusted to analyse desired parts of the test objects in a 2D plane.

Figure 3.9: *Example of a CT-scanned insulation cup.*

3.6 COMSOL model

The preparation methods used in the master thesis resulted in different surface topographies, which yield varying electrical field distributions. To better understand how the electrical field will behave on surfaces with various surface roughnesses, a 2D COMSOL model was created. The model consists of a 1 mm thick epoxy layer with an aluminium terminal at each side. One terminal is for the stressed voltage and the other is ground. The surface between the ground and the epoxy is imported as a polygon from profilometry results. Additionally, the filet function is applied to the peaks of the surface. The filet will round off the peaks, which gives more accurate electric field simulations. If the peaks are too pointy, the electrical field can get unrealistically high.

The geometry for all the COMSOL simulations will be created as presented in Figure 3.10. The only difference between the models from various preparation methods will be the surface roughness between the insulation and the ground terminal. The material properties for the epoxy presented in Table 3.2 are input in a blank material to model typical epoxy resin properties. For the simulations, a voltage of 10 kV is stressed, which gives an electric field of 10kV/mm in the epoxy without factoring in field enhancement. [45–48]

Table 3.2: *Material properties for the epoxy.*

Property	Value
Relative permittivity	3.6
Density	1300 $[kg/m^3]$
Electrical conductivity	$10^{-9}[S/m]$
Thermal conductivity	0.2 $[W/(m \cdot K]$
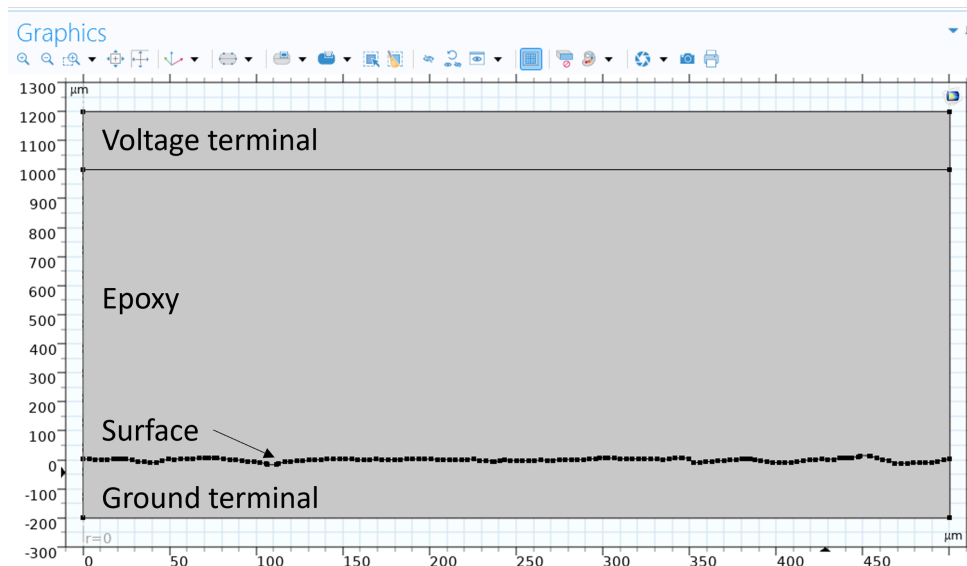
Figure 3.10: *The geometry of the COMSOL model.*

30

4 Results and Discussion

The laboratory work for the project yielded results for surface roughness parameters for the aluminium discs used as electrodes, PD measurements in the insulation cups and breakdown voltages. All voltage values found in the text and tables are given as RMS values. Due to the width of the insulation layer being 1 mm, the ratio of voltage and electric field will be 1 kV:1 kV/mm for all the measurements in the thesis. The presented results will be discussed continuously.

4.1 Surface parameters

Every disc used as an electrode for the insulation cups had the surface roughness parameters measured with a profilometer. This section will present the results of the measurements.

4.1.1 Polished and hot AC anodised electrode surface

The profilometry results from the polished and hot AC anodised discs are presented in Table 4.1. The polished discs had a surface with an ISO roughness grade number of around N2. The ISO roughness grade number shows that the polishing yielded smooth surfaces. S_a-values for the polished discs were measured to around 54 nanometers. Every average S_a-value was within a reasonable range of each other, with the biggest deviation being only 9.25 nanometers between the smallest and largest S_a-value.

In regard to the remaining surface roughness parameters, the measurements are relatively close. Some dissimilarities are to be expected due to the low magnitude of the measurements. The largest deviations are found in the S_z-values. Since S_z only takes the highest peak into account, a range from 1.07-4.43 μm is negligible. Therefore, the surface parameters are deemed close enough to initiate insulation cup casting and partial discharge measurements.

Table 4.1: *Surface parameters for the polished and hot AC anodised aluminium discs.*

Object	$S_a[nm]$	$S_q[nm]$	$S_p[\mu m]$	$S_v[\mu m]$	$S_z[\mu m]$
1	57.32	78.54	2.53	-1.89	4.43
2	50.57	65.80	0.73	-0.58	1.31
3	56.10	74.83	0.74	-0.86	1.60
4	50.73	65.93	0.66	-0.58	1.24
5	54.57	71.25	0.62	-0.45	1.07
6	55.92	72.15	0.75	-0.41	1.16
7	55.25	72.86	0.92	-1.17	2.09
8	53.29	69.88	0.62	-0.93	1.56
9	58.79	76.40	0.67	-0.52	1.18
10	53.72	71.49	1.98	-1.63	3.62
11	49.54	65.70	0.86	-1.31	2.17
12	50.43	67.31	1.48	-1.62	3.09

The deviations between measured spots on each polished disc were also found, yielding the results presented in Table 4.2. Although most of the S_a-value deviations are below 10 nanometers, some of them are conspicuous. The largest deviation is found for test object 8 with 21.31 nanometers between the highest and lowest value. Therefore, the individual measurements were studied more thoroughly. The measurements conducted for the surface of disc 8 had both the highest and the lowest S_a-value for all the measurements at the polished discs. However, the remaining 3 measurements were all within 2 nanometers of each other. Additionally, the measurements are in nanometers, which makes the relative deviation small. Still, if it is necessary to use an insulation cup as a dummy test object for additional testing of the setup, disc 8 will be first in line.

Table 4.2: *The largest deviation in S-parameters between the measured spots on each polished and hot AC anodised disc.*

Object	$\Delta S_a[nm]$	$\Delta S_q[nm]$	$\Delta S_p[\mu m]$	$\Delta S_v[\mu m]$	$\Delta S_z[\mu m]$
1	15.94	20.68	5.72	2.74	8.22
2	8.94	11.62	0.13	0.50	0.59
3	10.81	13.96	0.16	1.43	1.56
4	9.88	12.79	0.1	0.58	0.64
5	6.49	8.36	0.13	0.24	0.23
6	9.81	12.40	0.29	0.10	0.24
7	9.20	11.63	0.58	1.22	1.51
8	21.31	26.33	0.29	1.07	1.01
9	11.46	14.53	0.28	0.58	0.66
10	3.90	10.09	5.73	3.45	9.12
11	3.85	6.85	0.48	1.92	2.40
12	5.95	9.22	3.67	2.62	6.17

A typical 3D plot from the profilometry results for the polished surfaces is presented in Figure 4.1. The S_a-value for the measured spot in the figure is 57.36 nm. The plot clearly shows a smooth surface with 0.684 μm as the highest peak surface. The upper left corner shows a small collection of peaks. Those peaks were present for all the measurements for every disc. Therefore, it might be a slight unevenness with the profilometer stand that affects measurements in the nanoscale. The software is automatically removing tilt when calculating the S-parameters, so the small collection of peaks can be neglected.
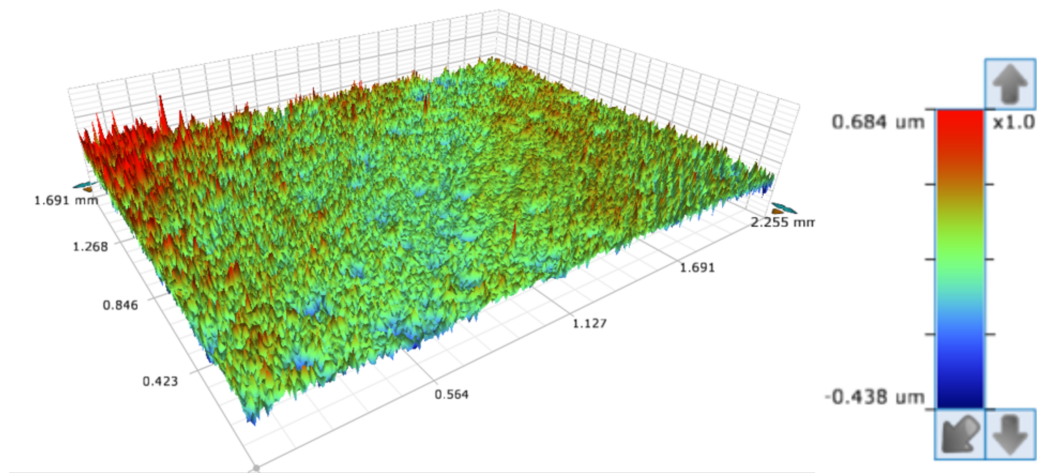
Figure 4.1: *Profilometry result for a spot at disc 5 of the polished surfaces. The spot has a S_a-value of 57.36 nm.*

An additional measurement was conducted for disc 5 of the polished discs to examine if the conducted measuring method gives reliable results. Every measurement only gets a small spot of approximately 1.5X2mm, which leaves a large amount of the disc unmeasured. By applying a stitching function, a much larger area could be measured. The results are presented in Figure 4.2. This kind of measurement took approximately 20 hours, so it would be too time-consuming to implement it at every disc. The figure shows the surface is slightly curved, with the highest point in the centre. The reason is probably that the force applied while polishing was higher around the edges. The highest point is at 19.284 μm and the lowest point is at -11.381μm. The difference looks more dramatic in the figure, but 30 μm is unproblematic. The most important thing is that there are no parts where the surface is sticking out. Even though it is curved, the surface roughness at random spots seems similar. The similarities were confirmed in the normal measurements at five random spots. Therefore, the measuring method is deemed satisfactory.
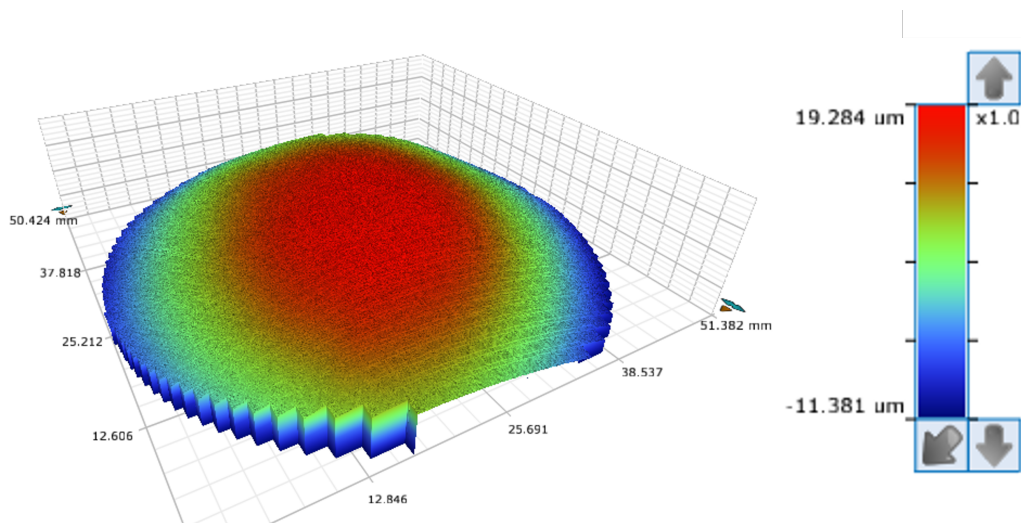
Figure 4.2: *Profilometry result for a large portion of test object 5 pretreated with polishing and hot AC anodising.*

4.1.2 Electrode surface sandblasted with aluminium oxide(0.5-1.0 mm)

Profilometry results from the aluminium discs sandblasted with aluminium oxide with a particle size of 0.5-1.0 mm are presented in Table 4.3. The surfaces have S_a-values corresponding to ISO grade number N10, which is a huge difference compared to the polished and hot AC anodised discs. The S_a-values for all the rough sandblasted discs are within a reasonable range of each other. The largest deviation is found at disc 10 with a S_a-value of 10.70 μm, however, the deviation is not problematic for the continuation of voltage testing. Furthermore, all the other surface parameters are within a satisfactory range to proceed with casting around the discs.

Table 4.3: *Surface parameters for the discs sandblasted with aluminium oxide(0.5-1.0 mm).*

| Object	$S_a[\mu m]$	$S_q[\mu m]$	$S_p[\mu m]$	$S_v[\mu m]$	$S_z[\mu m]$
1	11.29	14.42	58.86	-78.90	137.76
2	11.70	15.05	63.45	-72.20	135.65
3	11.04	14.01	52.64	-75.45	128.10
4	11.64	14.90	60.33	-83.12	141.45
5	11.41	14.58	60.36	-76.45	136.81
6	11.72	14.77	57.24	-80.57	137.81
7	11.73	14.87	58.67	-82.09	140.77
8	11.57	14.70	56.85	-91.77	148.62
9	11.86	15.01	58.61	-84.56	143.17
10	10.70	13.60	53.37	-77.53	130.90

The deviations between results at various randomly chosen spots at each disc sandblasted with aluminium oxide are presented in Table 4.4. There are some rather large deviations for the S_z-values, however, considering this value is a composite of two peak values, some deviations are expected. For the other parameters, there are no alarming deviations, which deemed all the discs sufficient for casting.

Table 4.4: *The largest deviation in S-parameters between the measured spots on each rough sandblasted disc.*

Object	$\Delta S_a[\mu m]$	$\Delta S_q[\mu m]$	$\Delta S_p[\mu m]$	$\Delta S_v[\mu m]$	$\Delta S_z[\mu m]$
1	1.04	1.17	18.67	29.19	27.73
2	0.66	1.19	31.72	2.96	32.18
3	1.64	2.30	16.30	27.15	43.45
4	1.30	2.09	27.52	31.83	39.85
5	0.22	0.28	20.93	24.38	40.04
6	1.74	2.12	28.21	32.34	27.19
7	1.35	1.69	14.59	34.83	47.61
8	0.58	1.01	14.38	25.05	28.44
9	1.34	1.74	20.47	36.17	46.18
10	0.81	1.12	13.96	41.76	48.96

A typical 3D plot for a surface sandblasted with aluminium oxide is presented in Figure 4.3. There are a lot more visible peaks with higher magnitudes compared to the polished discs. The seemingly random peak pattern is in the same form as for the surfaces sandblasted with smaller aluminium oxide particles in the specialisation project. The only notable distinction is that the peaks have larger magnitudes and therefore higher S-parameters. The profilometry results validate the theory that the S_a-values of a sandblasted surface are heavily dependent on particle size.
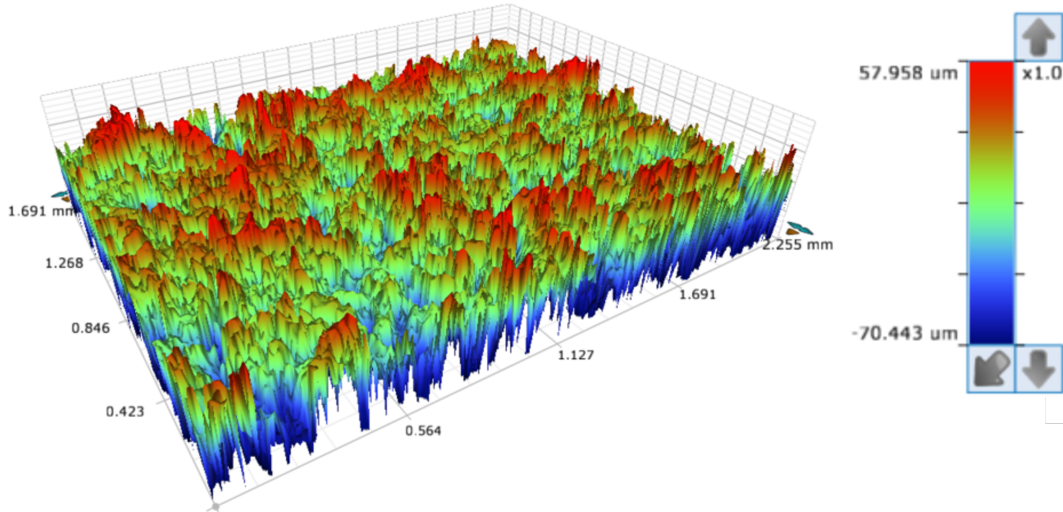
Figure 4.3: *Profilometry results for disc 1 sandblasted with aluminium oxide. The S_a-value of the spot is 11.69 μm.*

4.1.3 Surface sandblasted with glass orbs(0.25-0.42 mm)

The profilometry results from the discs sandblasted with glass orbs with a particle size of 0.25-0.42 mm are presented in Table 4.5. The measured S_a-values, with an average of approximately 4.3 μm, correspond to an ISO roughness grade number N8. As for the other preparation methods, the surface parameters are within a reasonable range of each other to advance into insulation cup casting. The values of the remaining surface parameters are all in close proximity, which shows that the discs are sufficiently treated to initiate PD measurements.

Table 4.5: *Surface parameters for the discs sandblasted with glass orbs(0.25-0.42 mm).*

Object	$S_a[\mu m]$	$S_q[\mu m]$	$S_p[\mu m]$	$S_v[\mu m]$	$S_z[\mu m]$
1	3.99	5.04	22.19	-30.53	52.72
2	4.33	5.46	26.03	-39.21	65.24
3	4.98	6.25	31.85	-38.55	70.41
4	4.21	5.29	22.91	-29.34	52.25
5	4.18	5.23	27.39	-27.83	55.23
6	4.58	5.76	26.73	-34.20	60.93
7	4.09	5.13	21.72	-27.07	48.79
8	3.98	5.00	22.85	-27.77	50.61
9	3.93	4.96	22.77	-34.96	57.72
10	4.30	5.39	27.16	-31.13	58.29

Table 4.6 presents the deviations between measured spots on each polished disc. As expected there are some small deviations at each spot. They are practically impossible to prevent, especially when the sandblasting is done by hand. Even though there are some deviations, none of them are large enough to impact the results significantly. The discs are therefore deemed sufficient to function as a baseline for a surface sandblasted with glass orbs.

Table 4.6: *The largest deviation in S-parameters between the measured spots on each disc sandblasted with glass orbs(0.25-0.42 mm).*

Object	$\Delta S_a[\mu m]$	$\Delta S_q[\mu m]$	$\Delta S_p[\mu m]$	$\Delta S_v[\mu m]$	$\Delta S_z[\mu m]$
1	0.35	0.44	8.63	11.41	16.52
2	0.55	0.58	4.66	28.09	32.76
3	0.73	0.96	15.16	14.57	22.28
4	0.19	0.24	5.14	11.06	10.61
5	0.27	0.33	9.89	8.97	14.77
6	0.24	0.30	12.68	7.94	19.45
7	0.62	0.72	7.94	8.02	7.27
8	0.59	0.66	10.67	11.09	20.73
9	0.47	0.58	6.42	14.76	11.67
10	0.19	0.26	10.58	8.32	8.21

In addition to the difference in S_a-values, the surface topography is distinctive for the glass orbs compared to the other surface pre-treatments. Sandblasting with glass orbs yielded a surface with peaks in valley formations, as visualised in Figure 4.4. The discs sandblasted with aluminium oxide had sharper edges at the surface peaks with no clear pattern. Due to valley formations, the surface peaks are not as sharp for the discs sandblasted with glass orbs. Consequently, the maximum electric field will be lower even if the S_a-values were similar. The clear variance in surface topography shows the importance of analysing surfaces more thoroughly than only the S-parameters.
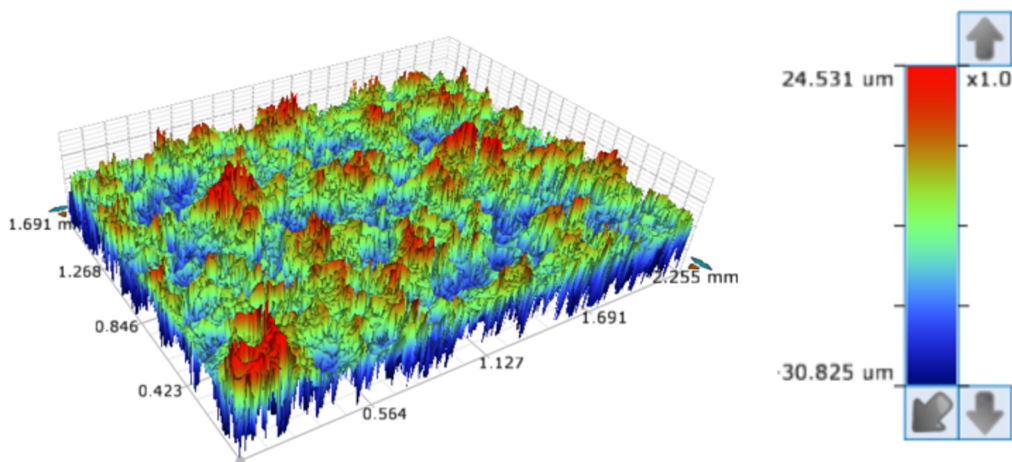

Figure 4.4: *Profilometry results for disc 6 sandblasted with glass orbs. The S_a-value of the spot is 4.623 μm.*

4.2 Electric field simulations

Electric field simulations were conducted for every surface pre-treatment utilised in the thesis. The simulations are used to determine how the electric field distribution will be affected by the surface roughness. All the simulations are conducted for 2D models based on surface profiles extracted from profilometry results. The reliability of the electric properties of all the models was confirmed by checking the voltage distribution over the epoxy layer. If the voltage distribution matched the results in Figure 4.5, the electrical properties were deemed to function as expected. A simulation was conducted for each method of surface preparation. Additionally, simulations with varying distances between surface peaks were done to examine how the peak distribution affects the local electrical field distribution. The profilometry results for a randomly selected test object within each surface preparation category were used for the models. A profile of 0.5 mm was chosen for every model, with the exception of the polished and anodised test object which was decreased to 0.1 mm. The reason for the decrease is to get approximately the same amount of peaks in each model. Too many peaks yield around the same results, but make them harder to analyse. The electric field without any enhancements from surface peaks will be 10 kV/mm corresponding to a voltage of 10 kV over a 1 mm thick insulation layer.
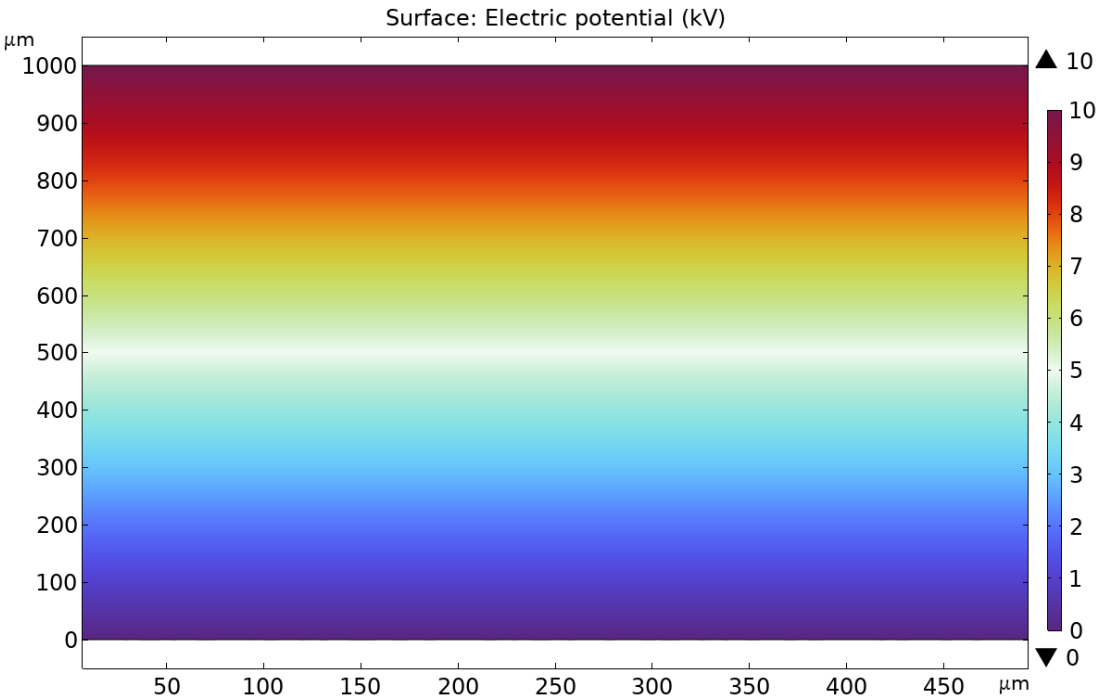
Figure 4.5: *Typical voltage distribution in the epoxy layer for all the COMSOL simulations.*

Impact of surface peak positions

Simulations in this section were conducted in 2D to examine how the distance between peaks impacts the electric field distribution along a surface. The simulations were done by constructing four peaks with a circular arc with a diameter of 5 μm. The value was chosen to emulate the peaks of previously analysed surfaces. The initial condition was to separate each peak by 100 μm, as visualised in Figure 4.6a. The distance between them was reduced by 5 μm until only 15 μm separated the peaks, as visualised in Figure 4.6b.
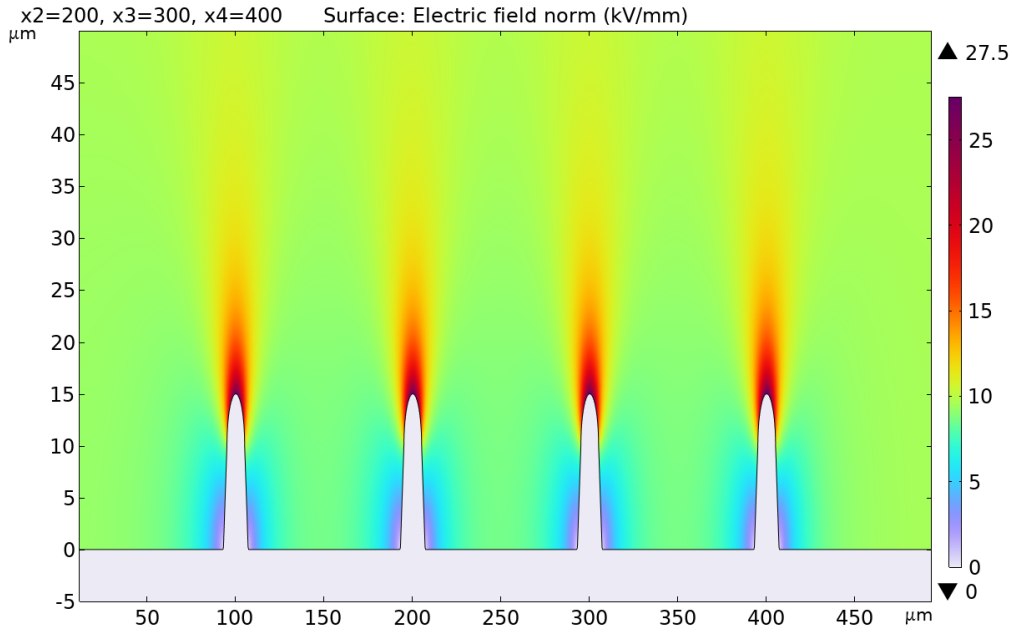
(a) *Peaks separated with 100 μm.*
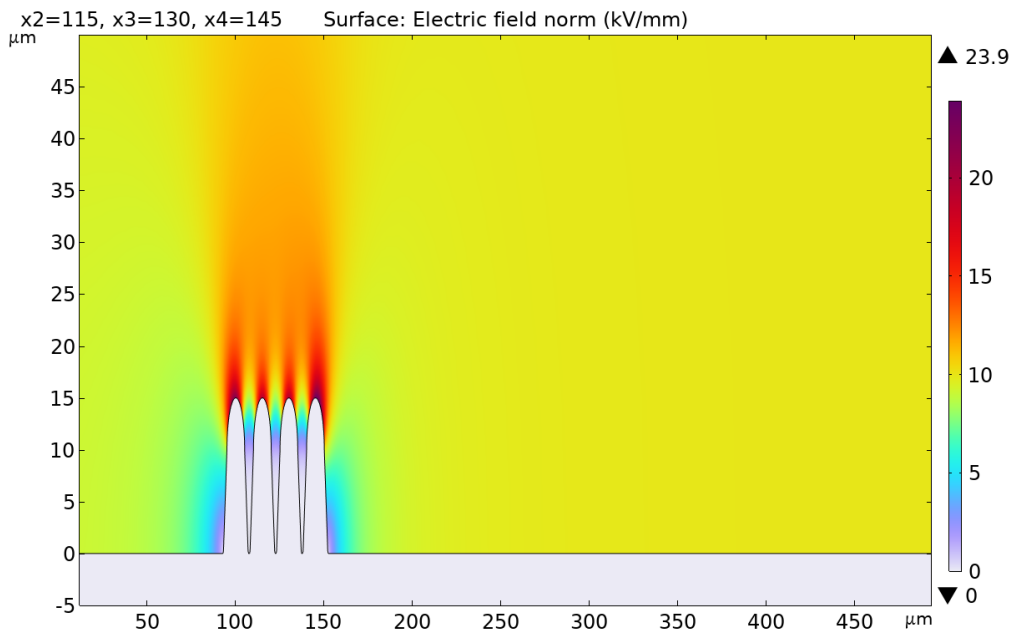
(b) *Peaks separated with 15 μm.*

Figure 4.6: *The four peaks at the maximum and minimum distance between them.*

The results from the electric field simulations are gathered as a graph in Figure 4.7. The graph shows the maximum and minimum electric field values in the epoxy layer with varying distances between peaks. The simulations show that for the maximum distance, the electrical field at a peak will not be affected by the other peaks. When the distance reached around 65 μm both the maximum and minimum electric field began decreasing. The maximum field is close to a linear decrease when the distance between peaks is decreased, while the minimum field has a more exponential decrease. When the peaks are at their closest, COMSOL calculates the minimum electric field to 0 kV/mm. There are very sharp edges between the peaks, which can cause COMSOL problems in the calculations in such small areas. Therefore, the minimum electric field might not be exactly zero in an actual situation, although it will be close.
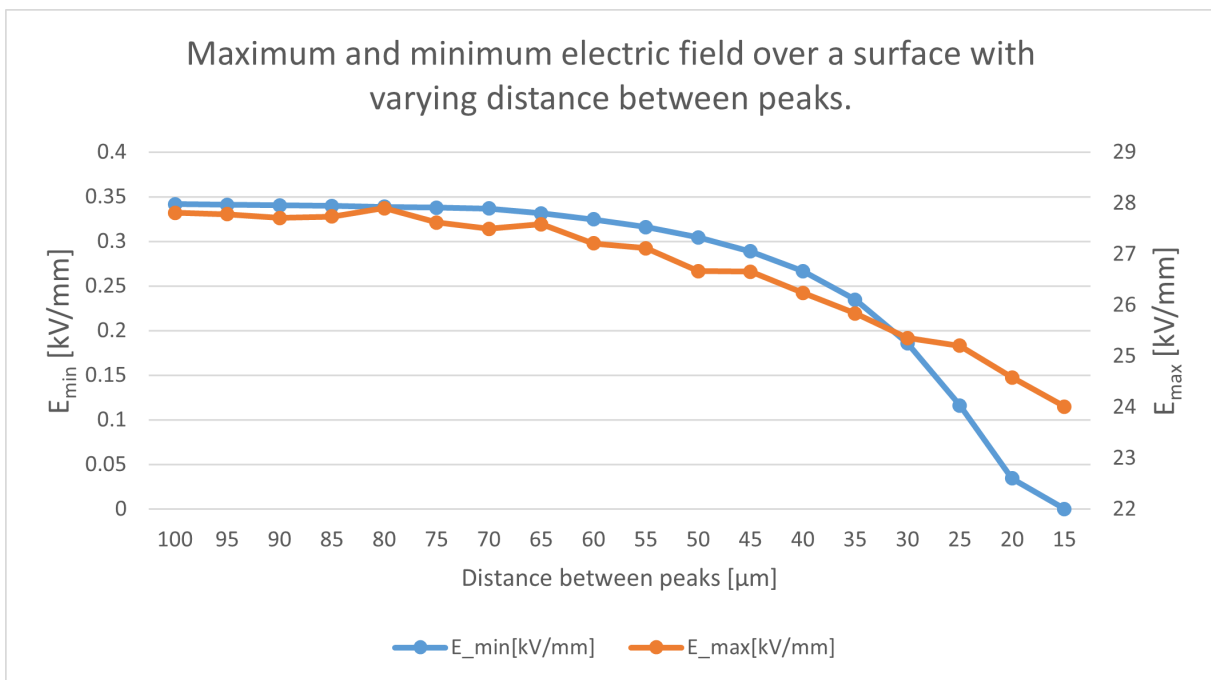
Figure 4.7: *Graph showing the maximum and minimum electric field over a surface with varying distance between peaks.*

The simulations show that if surface peaks are located in close proximity, the maximum electrical field will be decreased. The local fields for each peak will then be affected by the others, which causes the maximum electric field to decrease. This is both interesting and vital information to determine possible breakdown locations. By using the results it is clear that the highest peak is not necessarily the point with the highest field strength. If there are several peaks close by, the electric field can be decreased. Therefore, a smaller peak may have a higher local electric field if there are no other peaks nearby.

Polished and hot AC anodised electrode surface

The electric field simulation for a randomly selected surface profile of a polished and hot AC anodised disc is presented in Figure 4.8. The analysed surface profile is belonging to disc 10, which had a S_a-value of 53.72 nm. The maximum electric field in the epoxy layer is 10.5 kV/mm, which is only a 5% increase from the average background field without roughness. With the highest peaks at around 0.1 μm, a low impact is reasonable. The field distribution looks extreme in the figure, but in reality, there is a close to negligible difference in the epoxy layer.
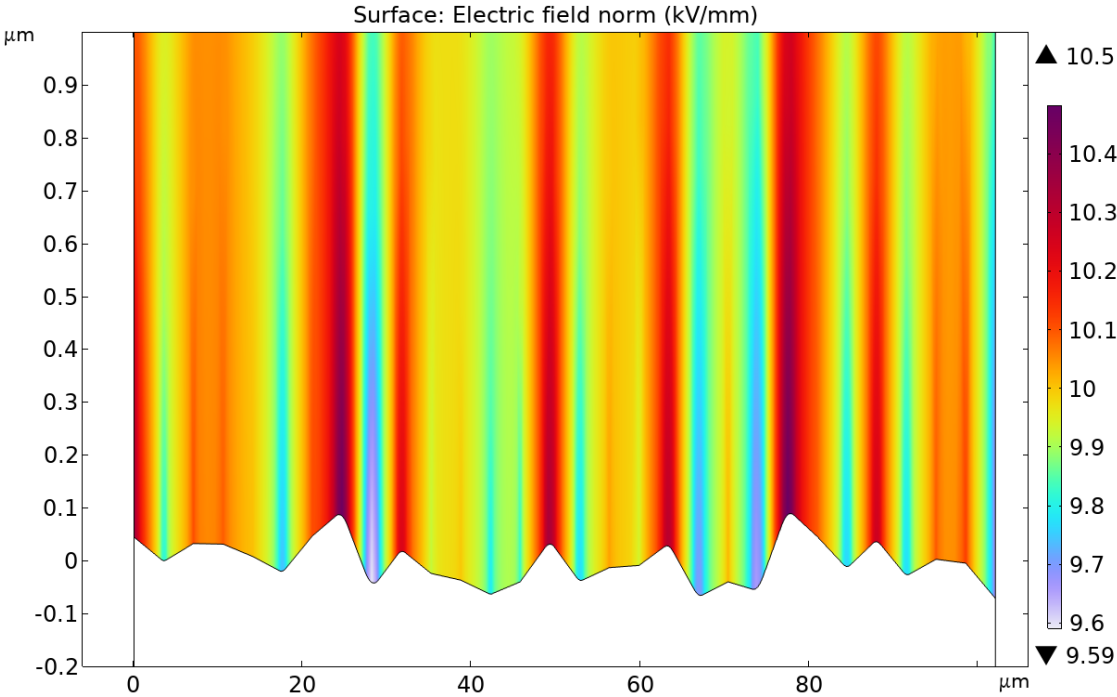

Figure 4.8: *Electric field distribution along the surface of test object 10 for the polished and hot AC anodised discs.*

Electrode surface sandblasted with aluminium oxide(0.5-1.0 mm)

The simulation results for a rough surface sandblasted with aluminium oxide(0.5-1.0 mm) are presented in Figure 4.9. It is clear that the surface topography is impacting the electrical field distribution in the epoxy layer. The surface profile is exported from disc 1, which had a S_a-value of 11.29 μm. As a consequence of higher roughness, there are higher surface peaks. A maximum electric field of 36.4 kV/mm is reached at the first peak from the left with the highest point around 26 μm. An electric field of 36.4 kV/mm corresponds to a field enhancement of 264%, which is a significant increase compared to the polished surface.

Figure 4.9: *Electric field distribution along the surface of test object 1 for an aluminium disc sandblasted with aluminium oxide(0.5-1.0mm).*

The peaks on the right side do not reach the same electric field, even though their highest point is approximately 31 μm. The results is corresponding to the parametric sweep conducted to learn how the positions of surface peaks is impacting the electric field. There are three peaks located within an interval of around 50 μm on the right side, which are close enough to affect each other. The results show the importance of accounting for peak positions and not only the highest peaks.

Electrode surface sandblasted with glass orbs(0.25-0.42 mm)

The results from the COMSOL simulation conducted for a surface sandblasted with glass orbs(0.25-0.42 mm) are presented in Figure 4.10. The surface profile was extracted from test object 6, which had a S_a-value of 4.58 μm. In addition to a lower S_a value than the surface sandblasted with aluminium oxide, the peaks are shaped differently. The edges are not as sharp, which contributes to a lower electric field. The maximum electric field was calculated to be 21.6 kV/mm at the peak located at approximately x=300 μm. The highest peaks yielded the highest field in this case. There were no other peaks surrounding with a similar height, which heavily reduces the impact from other peaks at the surface. The maximum electric field gives a field enhancement of 116%. The field enhancement is significantly higher than the polished discs, however, still considerably lower than for the surface sandblasted with aluminium oxide.

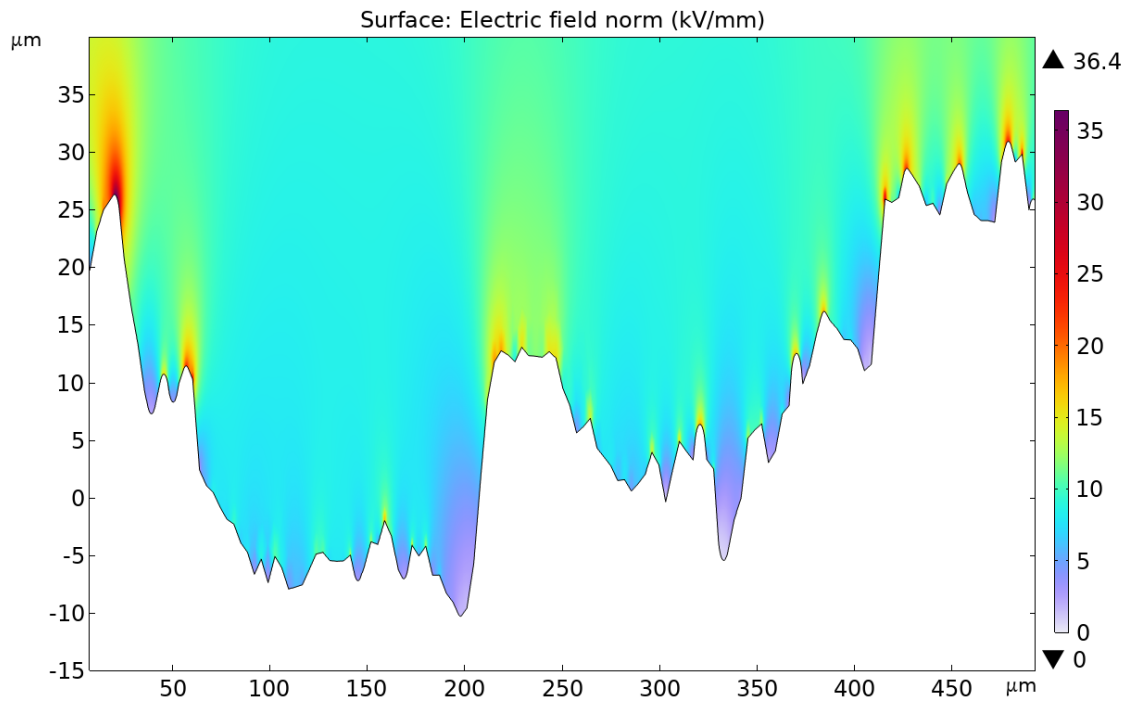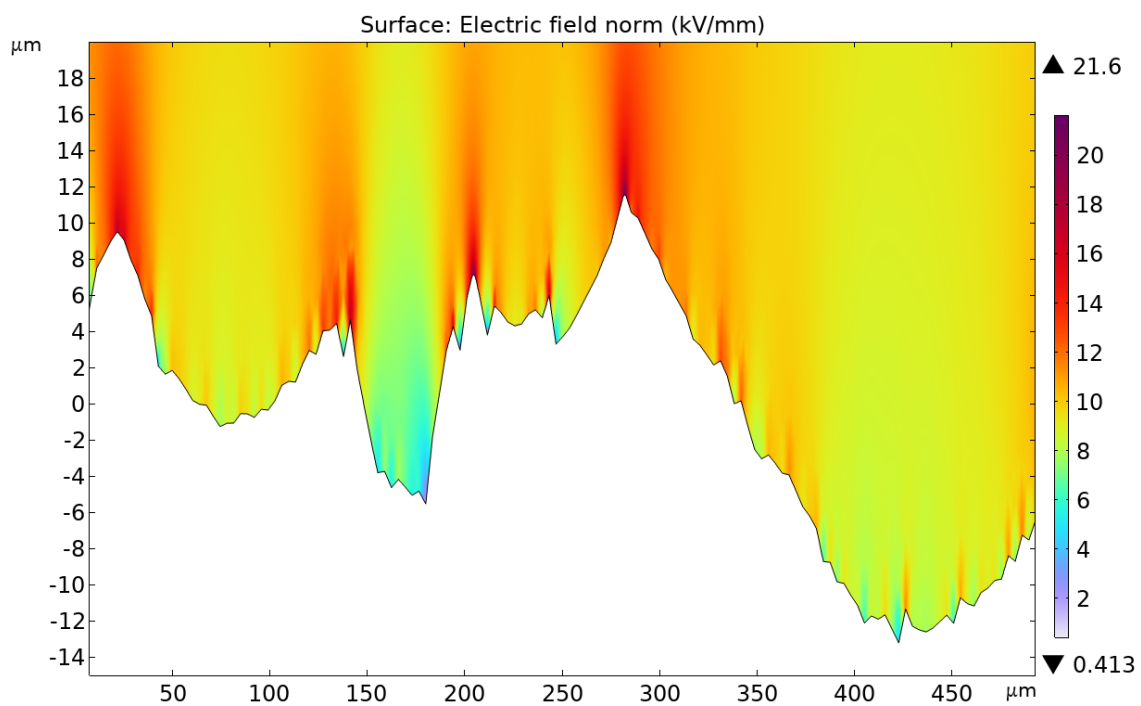**Figure 4.10:** *Electric field distribution along the surface of test object 6 for an aluminium disc sandblasted with glass orbs(0.25-0.42 mm).*

4.3 PD screening measurements

PD screening measurements were conducted for every insulation cup that was successfully cast. To ensure that the cups had high enough quality to examine the effect of surface roughness, the PDIV and charge magnitudes were measured. If PD occurred before reaching 5 kV or if the charge magnitudes exceeded 10 pC, the insulation cup was deemed to be inadequate for its purpose due to probable defects. The value was set by comparing with the measurements for the successful cups conducted in the specialisation project. Additionally, the PDIV value was decreased due to an adjustment in the threshold of PD measurements. The charge threshold was first decreased to 1 pC, compared to 2 pC in the specialisation project. The adjustment made the PD detectable earlier, thus reducing the PDIV compared to the specialisation project values. For the two last pretreatments, the minimum threshold was further decreased to 200 fC so the equipment would register background noise.

The level of background noise is dependent on the activity surrounding the cell, but some background noise are constant. The constant background noise for the measurements was at about 500 fC, as visualised in Figure 4.11. Every measurement at every voltage level had these disturbances, so it is probably from the voltage source. This section will provide a selection of PRPD plots for some test objects from each pre-treatment, while plots for the remaining test objects can be found in Appendix A.
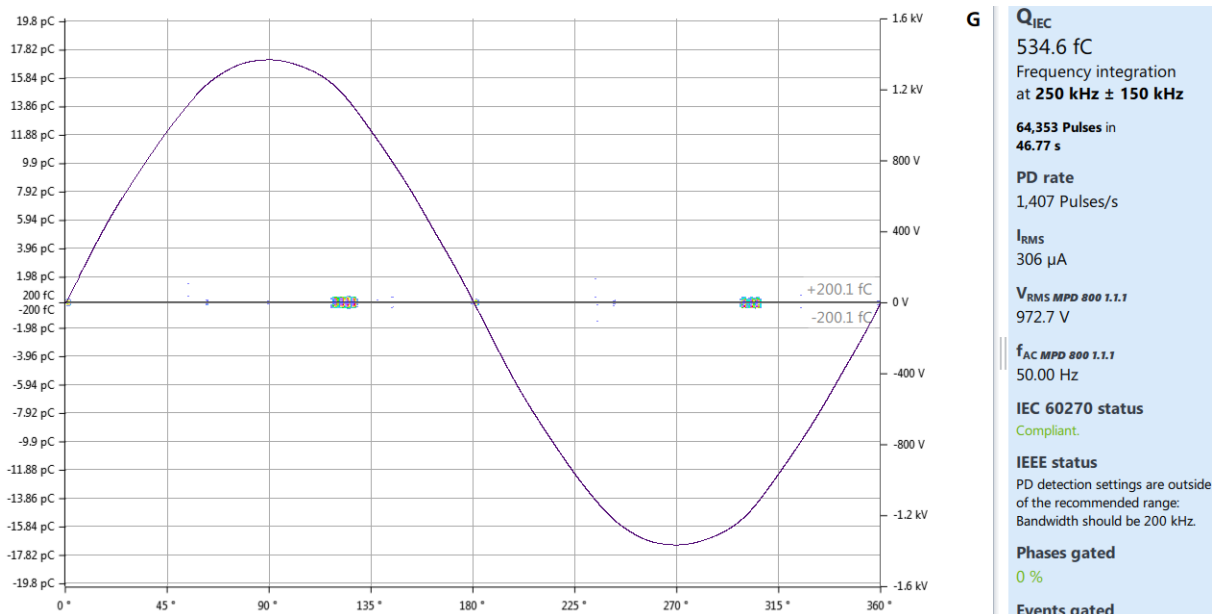

Figure 4.11: *Constant background noise in the PD measurements.*

4.3.1 Polished and hot AC anodised electrode surface

The PD screening measurements for the insulation cups with polished and hot AC anodised electrode surfaces are presented in Table 4.7. The test objects that are missing from the table were not tested due to unsuccessful casting with visible holes down to the electrode through the epoxy. The cups were cast in three batches in numerical order.

Table 4.7: *PD measurement data for the insulation cups with the polished and hot AC anodised electrode surface.*

Test object	PDIV [kV]	PDEV [kV]	Charge pos.[pC]	Charge neg.[pC]	Void location
1	9	1	80	80	Insulation
3	7	5	0.5	1.5	Electrode surface
4	10	7	2.5	2.5	Insulation
6	6	4	2.5	2.5	Insulation
8	3	2	150	100	Electrode surface
9	10	8	3.5	3.5	Insulation
10	3	2	800	800	Insulation
11	8	6	4	4	Insulation
12	8	6	1	1	Insulation

The first batch yielded two unsuccessful cups. The reason for the two inadequate cups from the first batch is hard to determine. The casting of insulation cups does not have a success rate of 100% even if the process is followed. Test object 1 had a clearly visible hole through the epoxy, thus making it unfit for voltage stressing. As visualised in Figure 4.12, a cavity is present in the insulation layer over the electrode. Every other cup with such visible imperfections did not get tested, however, this one was tested to have a foundation of how a void would impact the measurements.
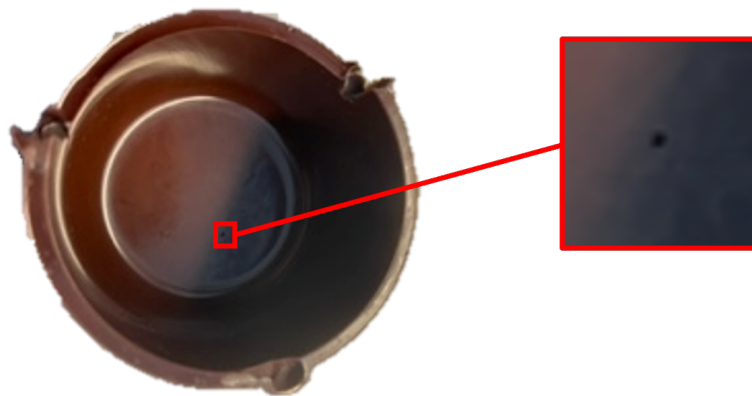

Figure 4.12: *Insulation cup around polished disc number 1. A cavity at the epoxy surface can be seen.*

The presence of a cavity in test object 1 is distinctly visible from the charge magnitudes in the PD measurements. Even though there was a visible void in the insulation layer, the first PD measurements did not yield an inception voltage until 12 kV, then with discharge magnitudes of around 80 pC. For the third screening of the test objects, the PDIV was decreased to 6 kV. Figure 4.13, presents the PD distribution at 6 kV for test object 1. The discharge pattern has higher magnitudes in the negative half-period than the positive, thus making an asymmetrical pattern. The PD patterns indicate a void at the electrode surface, in addition to the visible void at the surface.
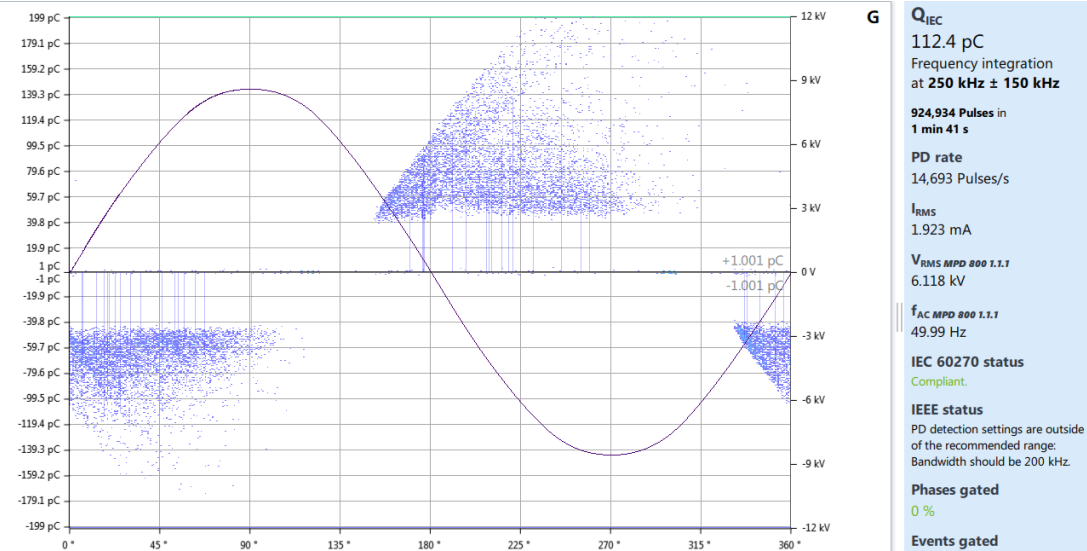

Figure 4.13: *PD measurement for test object 1 with a polished and hot AC anodised electrode surface.*

The second batch was unsuccessful with only one adequate insulation cup for further testing. The PDIV for this cup was at only 6 kV, so there might still be some imperfections that can cause a breakdown in phase 2. The reason is probably a power surge that occurred during the casting process. Usually, it takes about 15 minutes to fill a mould with epoxy. However, the filling time for the second batch varied from 30-60 minutes. Increased filling time indicates that the viscosity of the liquid epoxy was higher than for the other fillings. Viscosity is generally decreased when the temperature increases, making an error with the heating element the probable cause of unsuccessful casting. Even though, the heating was turned on in the control panel the power surge could have caused an error.

The third batch had three successful cups with similar results, which gives a total of six cups to advance to breakdown tests. Generally, the discharge patterns for the successful cups are similar to each other, especially the ones with the same charge magnitude. An example of the formation is shown in Figure 4.14. The figure is from test object 11 and shows the same PD patterns as test objects 4, 6 and 9.
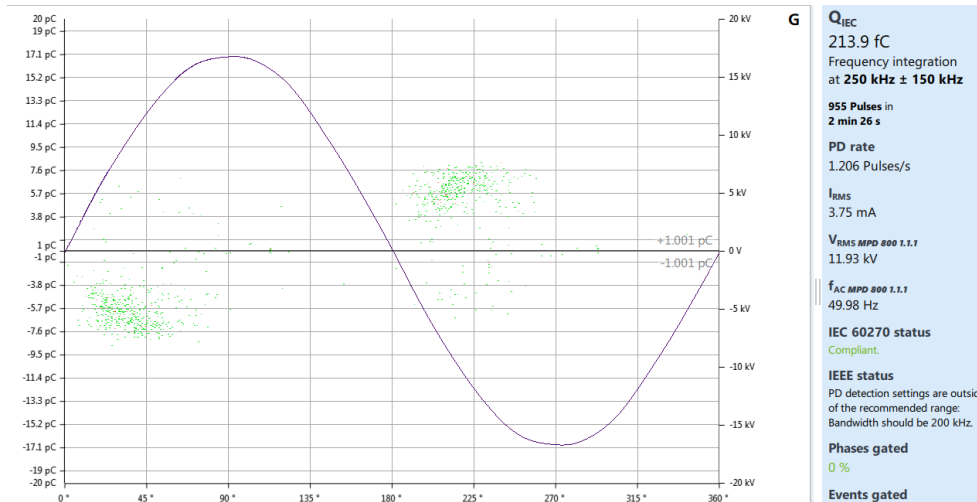

Figure 4.14: *Discharge pattern from the PD measurements at test object 11.*

The PD pattern for test object 12 was slightly different, as shown in Figure 4.15. The discharges are close around the x-axis around 1 pC, but still symmetrical. The frequency of discharges is shown with the colours in the plot. Green indicates a higher frequency of discharges, and the lighter blue is a smaller frequency. Even though there were fewer discharges with higher magnitudes, they were constant in the measurements, so it might be a small void in the insulation. The pattern from test object 3 also had the same level of PD around 1 pC, however, there were some additional discharges of higher magnitude in the negative half cycle. Thus, it seems like test object 3 has its void location at the electrode surface. All the other successful insulation cups were symmetrical, indicating the insulation as the void location.
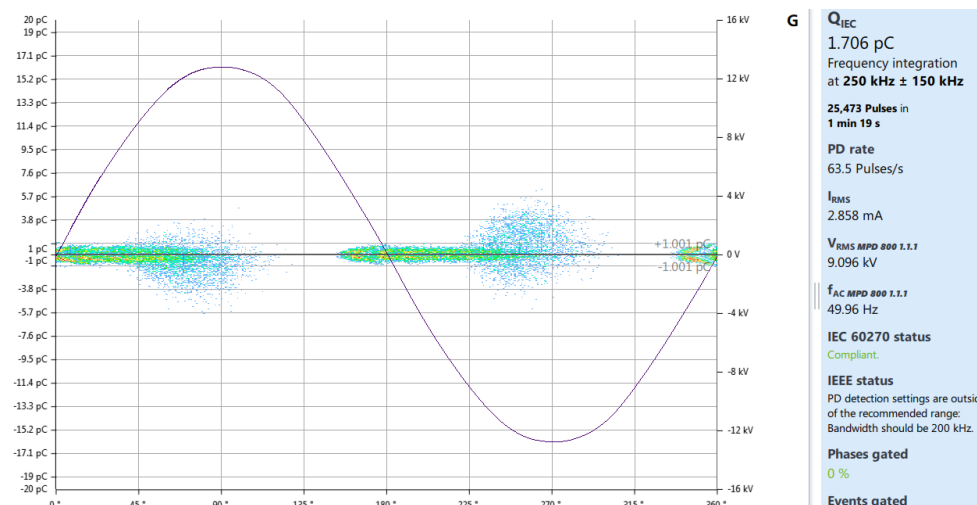

Figure 4.15: *Discharge pattern at PDIV measurements for test object 12.*

4.3.2 Electrode surface sandblasted with aluminium oxide(0.5-1.0 mm)

The PD measurements for the electrodes sandblasted with aluminium oxide with a particle size of 0.5-1.0 mm are presented in Table 4.8. Six insulation cups were successfully cast without visible imperfections in the insulation, while the remaining four were unsuccessful. Generally, for the test objects with rough electrode surfaces, the PDIV was lower than for the polished electrodes.

Table 4.8: *PD measurement data for the insulation cups with electrode surfaces sand-blasted with aluminium oxide(0.5-1.0 mm).*

Test object	PDIV [kV]	PDEV [kV]	Charge pos.[pC]	Charge neg.[pC]	Void location
1	5	3	2	2	Insulation
4	6	4	7	7	Insulation
6	3	2	25	25	Insulation
8	6	4	4	4	Insulation
9	9	7	1.5	1.5	Insulation
10	7	4	2	2	Insulation

None of the measurements yielded identical PDIV and charge magnitudes, although some of them are close. Test object 9 had the highest PDIV of 9 kV, while test object 6 was the lowest with 3 kV. Additionally, test object 6 had a high charge magnitude in both half-periods compared to the other measurements. As visualised in Figure 4.16 several discharges were measured up to around 40 pC with an average of around 25 pC. Charge values of this magnitude indicate that the cup is unfit for further testing due to its condition.
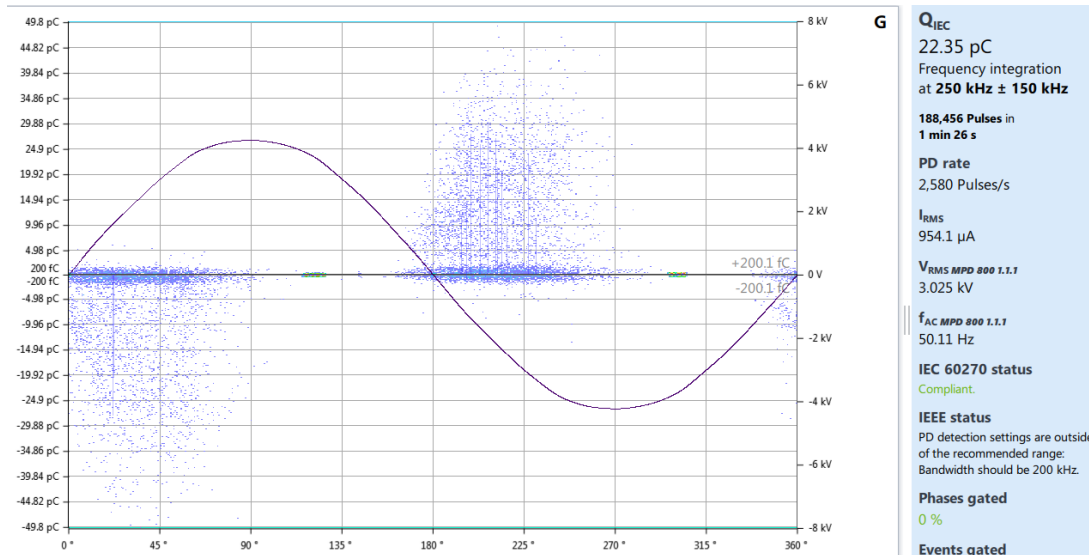

Figure 4.16: *PRPD plot for test object 6 of the electrodes sandblasted with aluminium oxide(0.5-1.0 mm).*

The discharge patterns for test objects 1, 9 and 10 were of similar magnitude and relatively similar. The discharges in both half-periods were kept under 2 pC, thus making them satisfactory for further testing. The PRPD plot for test object 1 in Figure 4.17 shows the symmetrical discharges at around 2 pC.
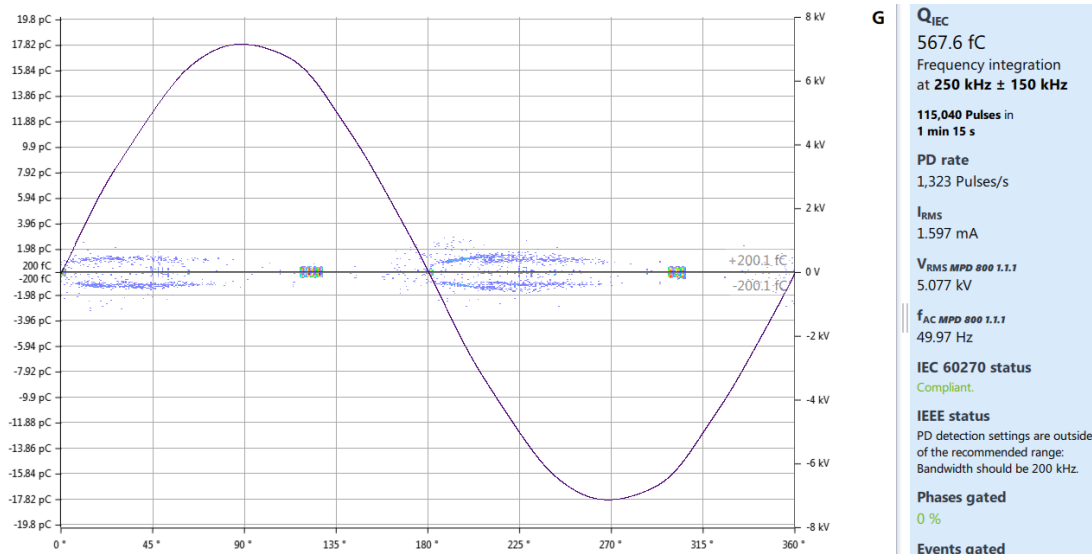

Figure 4.17: *PRPD plot for test object 1 of the electrodes sandblasted with aluminium oxide(0.5-1.0 mm).*

Test objects 4 and 8 had charge magnitudes slightly higher, but still within the threshold of 10 pC. The patterns between them are similar as in Figure 4.18, which displays the PRPD plot for test object 8. The pattern for test object 4 was similar, albeit shifted to a slightly higher magnitude. Compared to the typical PD patterns in the theory, it is challenging to pinpoint an exact match to any of them. The closest match for Figure 4.18 some discharges that remind of rabbit ear discharge pattern, indicating a cavity within the insulation.
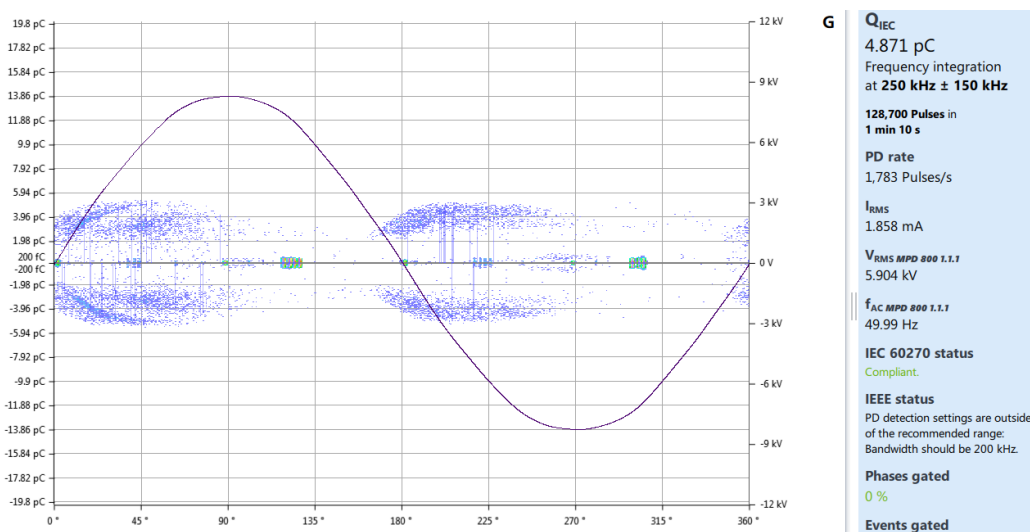

Figure 4.18: *PRPD plot for test object 8 of the electrodes sandblasted with aluminium oxide(0.5-1.0 mm).*

48

As mentioned previously, the PDIV values were lower in these measurements compared to the polished and hot AC anodised discs. The results make sense due to the increased maximum electric field and space charges that come as a consequence of the rough surface. Additionally, there might be some minuscule air gaps between the electrode surface and the insulation due to insufficient adhesion. Both of these factors might affect the electrical properties, thus making the lower PDIV values reasonable.

4.3.3 Electrode surface sandblasted with glass orbs(0.25-0.42 mm)

The casting of the insulation cups with an electrode surface sandblasted with glass orbs yielded eight successful test objects. The results for the PD screening measurements are presented in Table 4.9. The PDIV values for the measurements ranged from 6-10 kV and all of the cups were within the charge threshold of 10 pC, thus passing the quality test. Therefore, all the cups were deemed sufficient to advance to phase 2.

Table 4.9: *PD measurement data for the insulation cups with the electrode surface sandblasted with glass orbs(0.25-0.42 mm).*

Test object	PDIV [kV]	PDEV [kV]	Charge pos.[pC]	Charge neg.[pC]	Void location
1	6	4	10	10	Insulation
3	7	5	2	2	Insulation
4	9	7	0.7	0.7	Insulation
5	9	6	2	2	Insulation
6	7	5	2	2	Insulation
8	8	6	0.8	0.8	Insulation
9	6	4	2	2	Insulation
10	10	8	2	2	Insulation

With the exception of test object 1, the charge magnitude in both half-periods did not exceed 2 pC. All the measurements that yielded a charge magnitude of 2 pC look similar to the PRPD plot for test object 3 presented in Figure 4.19. Although the patterns are similar, the PDIV and PDEV values have slight variations. Due to PD being a stochastic variable, some variations are non-problematic for further testing. In regard to typical PD patterns, the closest visual match is the turtle-like pattern. However, the screening measurements show no sign of electrical tree growth, as the turtle-like patterns often indicate.
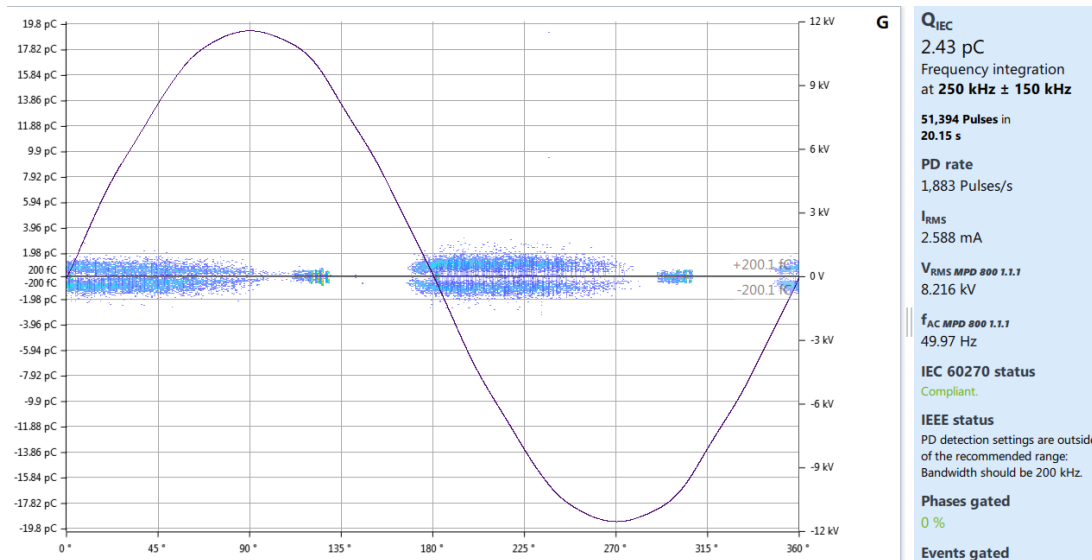
Figure 4.19: *PRPD plot for test object 3 of the electrodes sandblasted with glass orbs(0.25-0.42 mm).*

Test objects 4 and 8 had charge magnitudes of 0.7 and 0.8 pC, respectively. The PRPD plot for test object 4 is presented in Figure 4.20. The plot is well fit to represent both test objects 4 and 8 due to their similarities. The discharges are close to the x-axis due to the low charge magnitude. Such low charge values indicate that the cups are well suited for further testing.
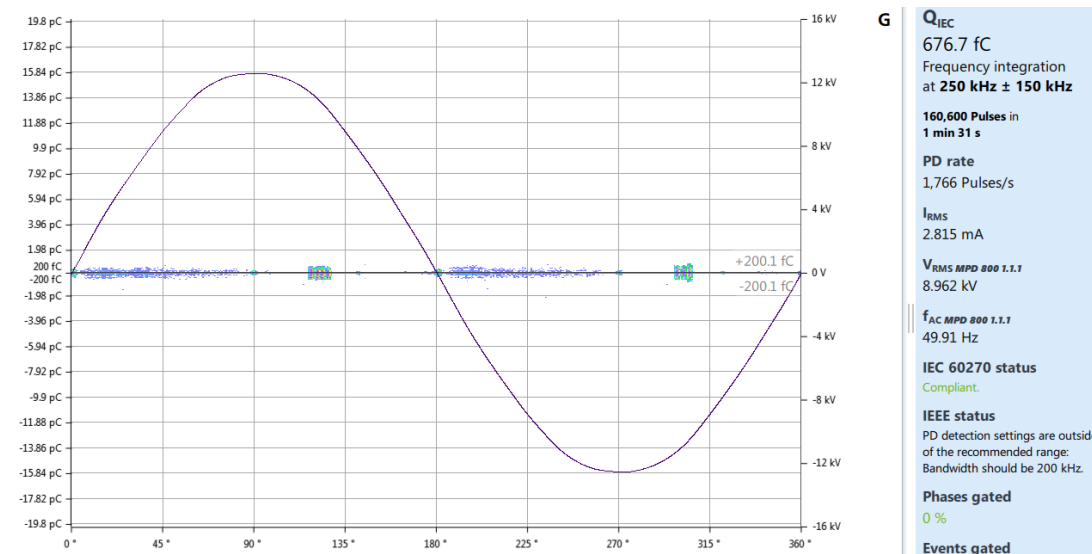

Figure 4.20: *PRPD plot for test object 4 of the electrodes sandblasted with glass orbs(0.25-0.42 mm).*

Based on the PD screening measurements, the insulation cups with the highest breakdown strength are test objects 4,8 and 10. Test object 10 is included due to the highest PDIV value of the test objects with an electrode surface sandblasted with glass orbs. The other two are chosen due to the lowest charge magnitude while still having high PDIV values, which indicate the smallest voids in the insulation.

50

The last test object pretreated with glass orbs was dissimilar from the other test objects. Test object 1 had the lowest PDIV and PDEV value combined with the highest charge magnitudes. As visualised in the PRPD plot in Figure 4.21, there are discharges up to around 15 pC, with the largest concentration below 10 pC. At the far left of the discharges in both half-periods, there are some discharge patterns that remind of the typical PD pattern, rabbit ear. Compared to the example of the rabbit ear PD pattern, there are a lot more discharges with magnitudes at the same charge level as the rabbit ear. Therefore, it is hard to determine if the PD pattern is definitely a rabbit ear formation. Due to the higher discharge magnitudes, test object 1 was removed before Phase 2 was initiated.
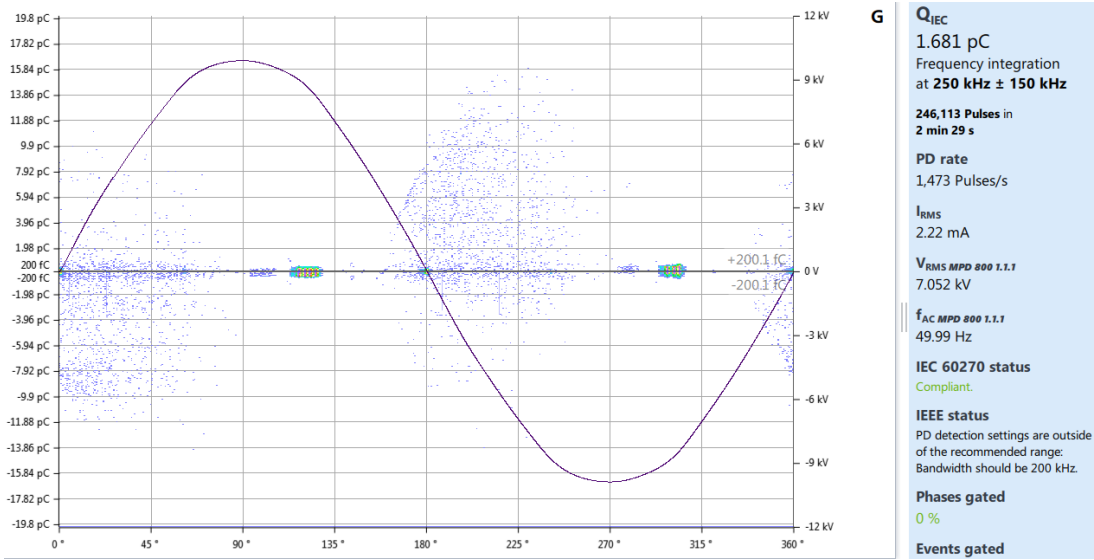

Figure 4.21: *PRPD plot for test object 1 of the electrodes sandblasted with glass orbs(0.25-0.42 mm).*

4.4   PD measurements to initiate electrical treeing

Six of the insulation cups for each preparation method that passed the screening process were taken to Phase 2 of the testing. The amount was chosen due to the number of successful insulation cups. The insulation cups were stressed with voltage until the discharge magnitudes reached 1 nC to ensure there was some electrical tree initiation. Additionally, the voltage where the electrical tree growth began was found. As for the PD screening process, the section is divided into a unique subsection for each electrode surface pretreatment. The selected PRPD plots shown are from the voltage level where discharges above 1 nC were found. The remaining PRPD plots from Phase 2 are presented in Appendix B.

4.4.1   Polished and hot AC anodised electrode surface

The results from the measurements conducted in Phase 2 for the test objects with a polished and hot AC anodised electrode surface are presented in Table 4.10. The table shows at what voltage level the electrical tree growth began and when the discharge magnitude reached 1 nC. Additionally, it is presented if a breakdown occurred accidentally during Phase 2. This is the case for both test objects 6 and 12 for the polished and hot AC anodised electrode surfaces. Test object 12 reached a breakdown before discharges at 1 nC occurred and test object 6 had a breakdown just as the first discharges with a magnitude of 1 nC developed.

Table 4.10: *Results from Phase 2 for the test objects with a polished and hot AC anodised electrode surface.*

Test Object	Electrical tree initiation [kV/mm]	Voltage at 1 nC [kV/mm]	Breakdown reached during Phase 2 [kV/mm]
3	23	30	-
4	24	34	-
6	15	19	19
9	20	21	-
11	18	25	-
12	13	-	16

The PRPD plot right before the breakdown in test object 12 is presented in Figure 4.22. The discharges are symmetrical over the half-periods and concentrated up to around 500 pC, which suggests that several voids or channels are present. If the discharges had come from electrical tree growth, the positive half-period would have higher discharges than the negative and the patterns would be shaped more wing-like. A void might have gone undetected in the screening process for test object 12. The measurements for test object 6 were also nearly symmetrical over the half-periods, but some larger discharges were present in the positive half-period. It seems like some electrical tree growth began in the insulation, but a preexisting imperfection caused a breakdown before the electrical tree breached the insulation layer.
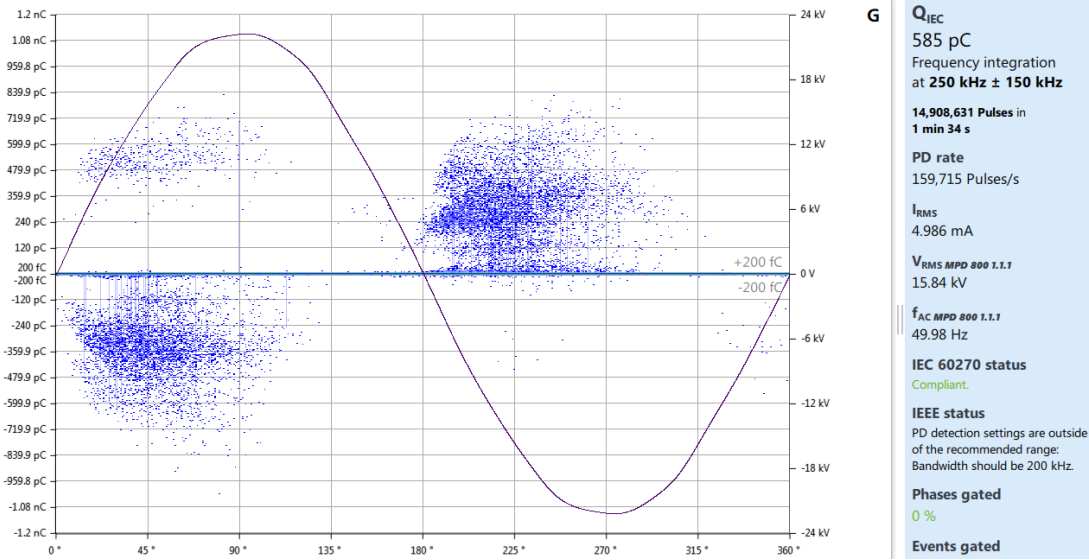

Figure 4.22: *PRPD plot right before breakdown for test object 12 with a polished and hot AC anodised electrode surface.*

The remaining four insulation cups shared similar patterns as visualised in Figure 4.23, although the voltage level varied. These PD patterns are more as expected for an insulation cup where electrical tree growth has initiated. There is a clear difference in the discharge magnitude between the positive and negative half-period and a wing-like pattern shows an electrical tree has grown.
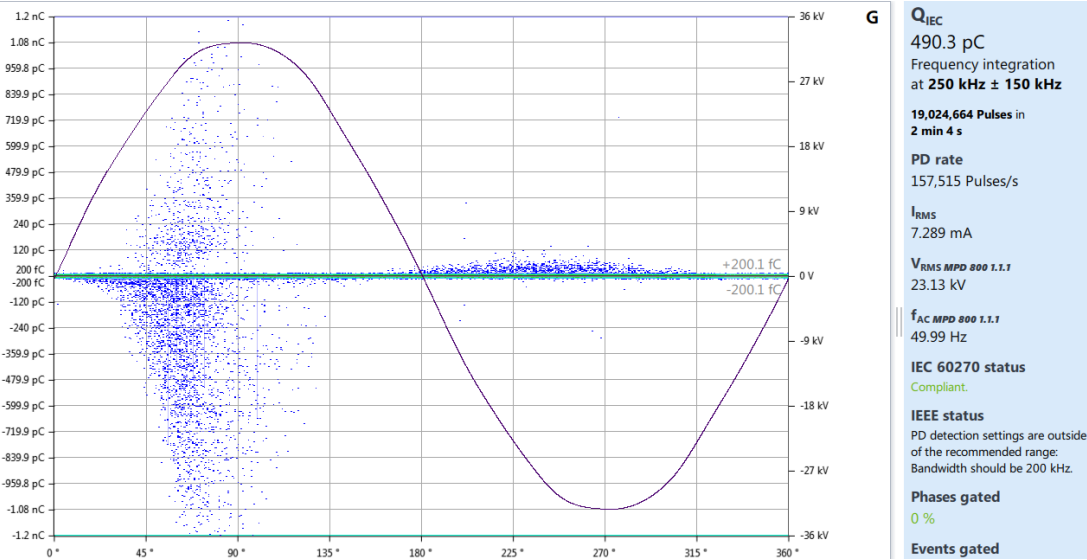

Figure 4.23: *PRPD plot when discharge magnitudes of 1 nC were reached for test object 11 with a polished and hot AC anodised electrode surface.*

Test objects 3 and 4 did not reach discharges at 1 nC before 30 and 34 kV/mm, while test objects 9 and 11 reached 1 nC at 21 and 23 kV/mm. The deviation between them is significant even though both of them yielded successful results. The casting process was identical, so it is hard to determine what causes the large deviation. It might be related to the adhesion between the epoxy resin and electrode surface due to the low surface roughness combined with hot AC anodising, or an unknown problem might have affected the casting procedure.

An interesting observation between the test objects that reached breakdown before 1 nC and the rest is how the PD patterns can be differentiated. In Figure 4.23 the number of discharges is highest close to the x-axis and gradually decreases outwards. Contrarily, the PD pattern in Figure 4.22 has a gap up to around 120 pC. The presence of such gaps can therefore be used to differentiate between electrical tree growth or voids in the insulation.

4.4.2 Electrode surface sandblasted with aluminium oxide(0.5-1.0 mm)

The results from the measurements conducted in Phase 2 for the test objects with an electrode surface sandblasted with aluminium oxide are presented in Table 4.11. None of the insulation cups reached breakdown during Phase 2 for these measurements. Test object 6 is included even though the thresholds in the screening process were exceeded. It was taken further into Phase 2 to reach six test objects and give an even foundation for comparison. The tests discovered that the first PD measurements for test object 6 were slightly inaccurate, with a PDIV of 5 kV instead of the earlier determined 3 kV. Since the insulation cup was tested three different times in the screening process, there must have been some disturbances that skewed the results for test object 6. As presented in Table 4.11, all the electric field values were within close proximity to each other.

Table 4.11: *Results from Phase 2 for the test objects with an electrode sandblasted with aluminium oxide(0.5-1.0 mm).*

Test Object	Electrical tree initiation [kV/mm]	Voltage at 1 nC [kV/mm]	Breakdown reached during Phase 2 [kV/mm]
1	13	19	-
4	14	19	-
6	14	21	-
8	14	19	-
9	17	19	-
10	14	17	-

The PRPD plot for test object 1 is shown in Figure 4.24. All the test objects yielded similarly distributed PD patterns with clear wing-like patterns, which show the growth of electrical trees. Due to the similarities in both voltage levels and PD patterns, the insulation cups with an electrode surface sandblasted with aluminium oxide are applicable for comparison with other pretreatments.
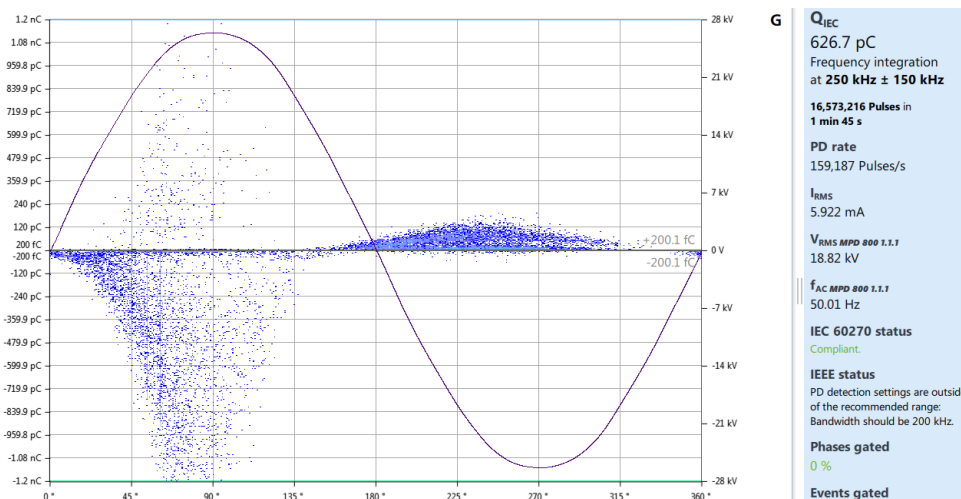

Figure 4.24: *PRPD plot when discharge magnitudes of 1 nC were reached for test object 1 with an electrode surface sandblasted with aluminium oxide(0.5-1.0 mm).*

4.4.3 Electrode surface sandblasted with glass orbs(0.25-0.42 mm)

The insulation cups with an electrode surface sandblasted with glass orbs yielded the results presented in Table 4.12. Six insulation cups were tested to keep the number of test objects even for all the surface pretreatments. Test object 1 had worse electrical properties than the rest, so it was removed. Additionally, test object 9 was removed because it had the lowest PDIV value among the surfaces pretreated with glass orbs. The table shows that electrical tree initiation all started between 15-18 kV/mm and reached 1 nC discharge magnitudes between 24-29 kV/mm. Test object 5 reached breakdown during the tests, however, the analysis of the PRPD plot showed it reached discharge magnitudes of above 1 nC before the breakdown.

Table 4.12: *Results from Phase 2 for the test objects with an electrode sandblasted with glass orbs(0.25-0.42 mm).*

Test Object	Electrical tree initiation [kV/mm]	Voltage at 1 nC [kV/mm]	Breakdown reached during Phase 2 [kV/mm]
3	16	24	-
4	15	27	-
5	17	25	27
6	16	-	19
8	18	29	-
10	18	24	-

The PRPD plots for all the measurements clearly showed the presence of electrical trees. Figure 4.25 is showing the PRPD plot when discharge magnitudes of 1 nC were reached. The typical wing-like pattern is representative of all the six test objects tested with electrode surfaces sandblasted with glass orbs. The measurements yielded similar voltage levels, thus setting a good foundation for comparison with other pretreatments.
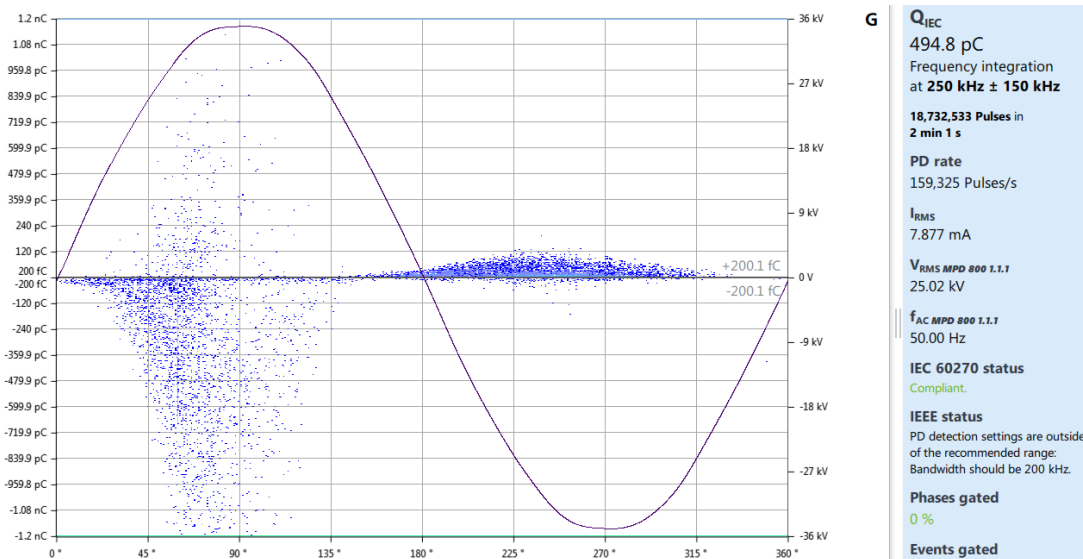

Figure 4.25: *PRPD plot when discharge magnitudes of 1 nC were reached for test object 5 with an electrode surface sandblasted with glass orbs(0.25-0.42 mm).*

4.4.4 Comparison of the surface preparation methods

As described earlier, both the test objects with sandblasted electrode surfaces yielded results applicable for comparison. Contrarily, the polished discs had large deviations between the test objects for the Phase 2 measurements, which makes it hard to conclude how the pretreatment affected the electrical properties. However, the average electric field for electrical tree initiation is still significantly better than the other preparation methods. Figure 4.26 shows the relationship between what voltage level electrical tree growth is initiated and the electrode surface preparation method. The plot displays that the roughest electrode surface needs the lowest voltage for electrical tree initiation. Additionally, the polished and hot AC anodised surfaces have the highest voltage levels. Although one of the polished values is lower than the highest value for the electrode surfaces sandblasted with glass orbs, the results indicate that an increase in surface roughness decreases the voltage for electrical tree initiation.
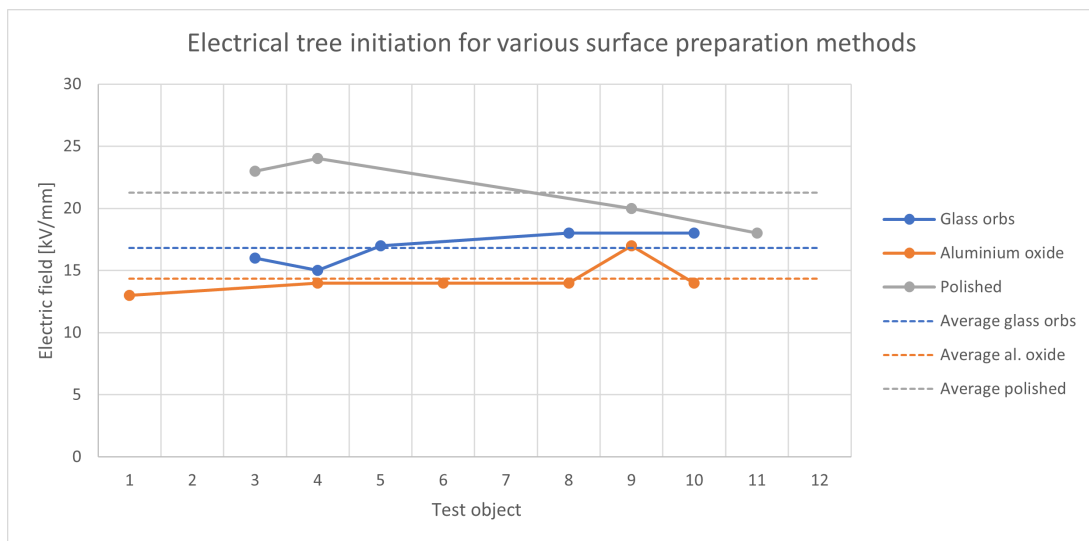

Figure 4.26: *Voltage level for electrical tree initiation for various surface preparation methods.*

Figure 4.27 shows a similar pattern for the voltage level when discharge magnitudes of 1 nC are reached. It is clear that surfaces sandblasted with glass orbs have higher voltage levels than the ones sandblasted with aluminium oxide. These findings correspond with the theory that an increase in surface roughness will decrease the quality of the electrical properties. The deviation for the polished discs has increased, which places half the measurements at the highest voltage levels, while the remaining measurements are worse than the surfaces sandblasted with glass orbs. Evidently, the quality of the insulation cups with polished electrode surfaces was inadequate for accurate comparison.
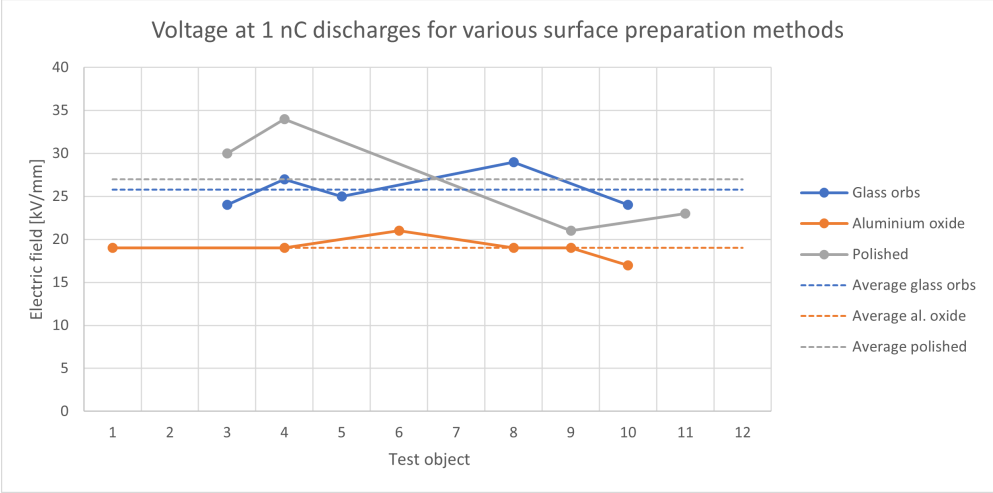
Figure 4.27: *Voltage level when discharge magnitudes reach 1 nC for various surface preparation methods.*

The polished and hot AC anodised electrode surfaces still give the highest average electric field, but it is close to the electrode surfaces sandblasted with glass orbs. The exact value of discharges with 1 nC was chosen when a discharge in the graph went over 1 nC, disregarding the peaks when the voltage was adjusted. For example, the graph presented in Figure 4.28 for test object 11 with a polished and hot AC anodised electrode surface reaches 1 nC at 25 kV/mm. These kinds of measurement may therefore differ by some kV/mm even if two identical test objects were tested.
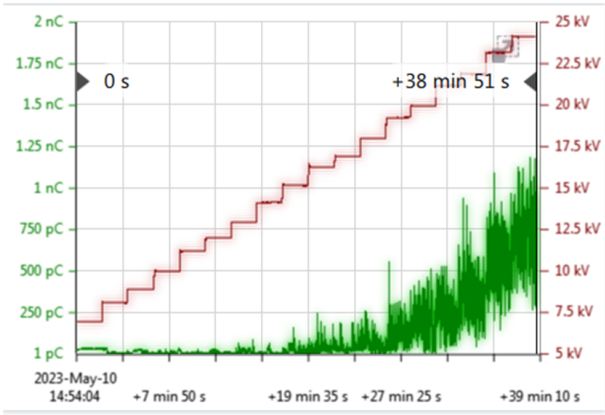

Figure 4.28: *The evolution of discharge magnitudes with increasing voltage for test object 11 with a polished and hot AC anodised electrode surface.*

4.5 Breakdown tests

The last step of the laboratory experiments was the breakdown tests. All the remaining insulation cups that did not reach breakdown during Phase 2 were tested in the new setup, as described in Section 3.4. The PD measurement equipment was disconnected to ensure it would not be broken, thus providing no PRPD plots from the breakdown measurements.

4.5.1 Polished and hot AC anodised electrode surface

The breakdown voltages for the selected test object with a polished and hot AC anodised electrode surface are presented in Table 4.13. The results are considerably deviating with values between 16 and 47 kV/mm.

Table 4.13: *Breakdown strength for the insulation cups with polished and hot AC anodised electrode surfaces. A "*" signifies that the breakdown occurred in Phase 2 testing.*

Test object	Breakdown strength [kV/mm]	BD at edge?
3	38	no
4	47	no
6	19*	no
9	33	yes
11	34	yes
12	16*	no

Breakdown at the edge is if the breakdown occurred in spots like for test object 11, as visualised in Figure 4.29. The breakdown at the edge might stem from a local field enhancement due to an uneven conductive paint layer or a void in the insulation. The insulation layer directly over the electrode could therefore possibly have withstood higher voltages, thus making test objects 9 and 11 closer to test objects 3 and 4 in breakdown strength. It is impossible to determine how much higher voltages it could withstand before a breakdown occurred directly over the electrode. Based on the measurement in Phase 2, the breakdown strength would still be lower than test objects 3 and 4 for the insulation cups with a breakdown away from the edge.
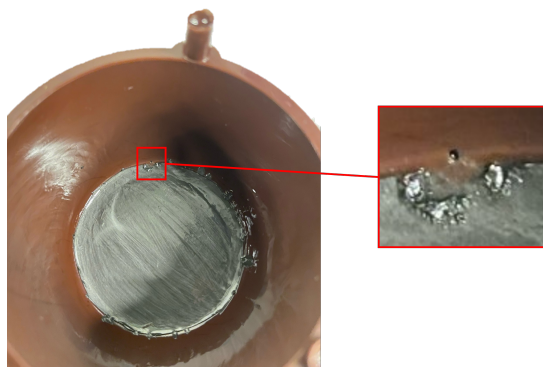

Figure 4.29: *Breakdown location for test object 11.*

Test object 3 was cut open to examine the breakdown channel with a microscope. The result is presented in Figure 4.30, which shows a breakdown channel of around 340 μm. Only the insulation layer is shown in the figure because the electrode detached when the cup was cut in two. There are no visible signs of electrical trees in the insulation around the breakdown channel and the electrode surface in the centre of the breakdown channel cannot be examined due to the separation. The breakdown point at the disc was examined with a profilometer, but the results were not useful to determine the cause of the breakdown at this point.
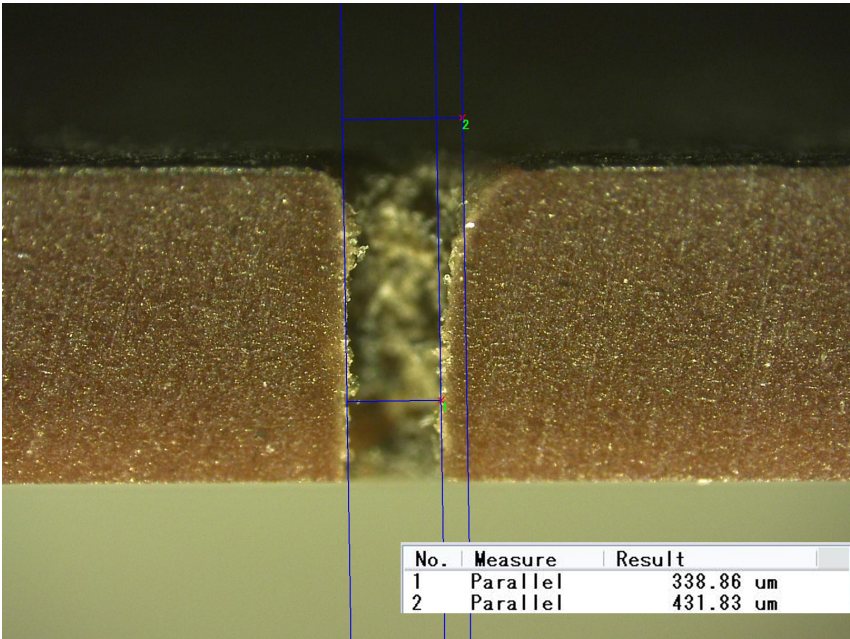
Figure 4.30: *The breakdown channel for test object 3 with a polished and hot AC anodised electrode surface.*

Additionally, test object 12 was cut open to search for defects in the production of the insulation cup. A defect was detected when the breakdown location was examined in a microscope. As visualised in Figure 4.31, a large part of the insulation was removed beside the breakdown channel. Figure 4.31a was taken before the insulation was polished right over the breakdown channel and shows an electrical tree from the surface which goes about 500 μm deep in the insulation layer. When the cup was polished further, a large part of the insulation was gone, with a width of nearly 2 mm. It is clear that the test object was defective with some kind of imperfection. The imperfection might be a void in the insulation, or some kind of contaminant either in the insulation or at the surface. Anyhow the cause, the cup is defective, thus it should be removed from the comparison graphs.
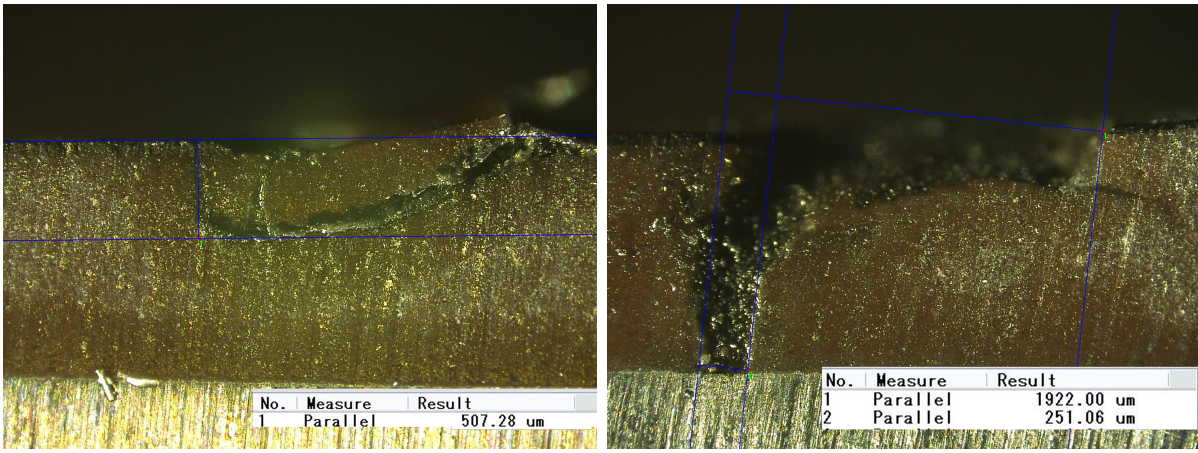
(a) *The insulation close to the breakdown channel.*

(b) *At the breakdown channel.*

Figure 4.31: *Images around the breakdown channel for test object 12 with a polished and hot AC anodised electrode surface.*

Test object 6 did also reach breakdown for a low voltage level. Even though it seemingly passed the quality test in the screening process, it reached a breakdown in Phase 2. There were some concerns with the test object due to the problem with the heating element, which caused higher viscosity in the epoxy mixture. Every other insulation cup in that batch had several holes in the insulation due to the issues, so it is safe to assume a defect in test object 6 as well. Therefore, it is not taken further to the comparison of the surface preparation methods.

The insulation and electrode were separated and CT scanned for test object 4. The entire insulation part was scanned, which created some challenges with the resolution. Figure 4.32 shows the breakdown channel, and also shows the challenges related to resolution. The resolution levels made it hard to determine the presence of electrical trees and where the electrical tree that led to the breakdown was initiated from. Electrical trees might be too small to be detected in the scan without cutting the cup into smaller pieces where it is a known electrical tree.
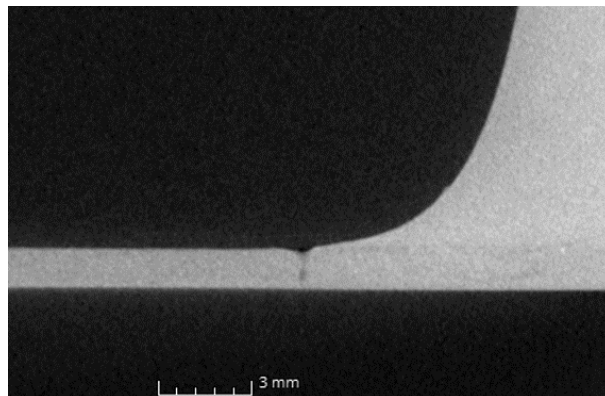

Figure 4.32: *Breakdown channel found in the CT scan for test object 4 with a polished and hot AC anodised electrode.*

4.5.2 Electrode surface sandblasted with aluminium oxide(0.5-1.0 mm)

The results from the breakdown measurements for the test objects with an electrode surface sandblasted with aluminium oxide are presented in Table 4.14. The breakdown for all the insulation cups was reached within an interval of 23-29 kV/mm. As for the previous testing, the results are in a reasonable range from each other. Six objects with around the same measurement results are a reliable source of how a rough surface has impacted the electrical properties of the component.

Table 4.14: *Breakdown strength for the insulation cups with electrode surfaces sandblasted with aluminium oxide(0.5-1.0 mm).*

Test object	Breakdown strength [kV/mm]	BD at edge?
1	23	no
4	25	no
6	29	yes
8	27	yes
9	26	no
10	28	yes

Test object 4 was cut and polished down until the breakdown channel was reached. The microscopic analysis revealed some traces of electrical treeing, as visualised in Figure 4.33. The electrical tree channel is located in the red oval at the left side of the breakdown channel and is seemingly going upwards. This indicates that the electrical tree initiation began from the electrode surface, which is the desired way for the experiments. If the tree had begun from the other side, it would indicate a defect such as voids or contaminants.
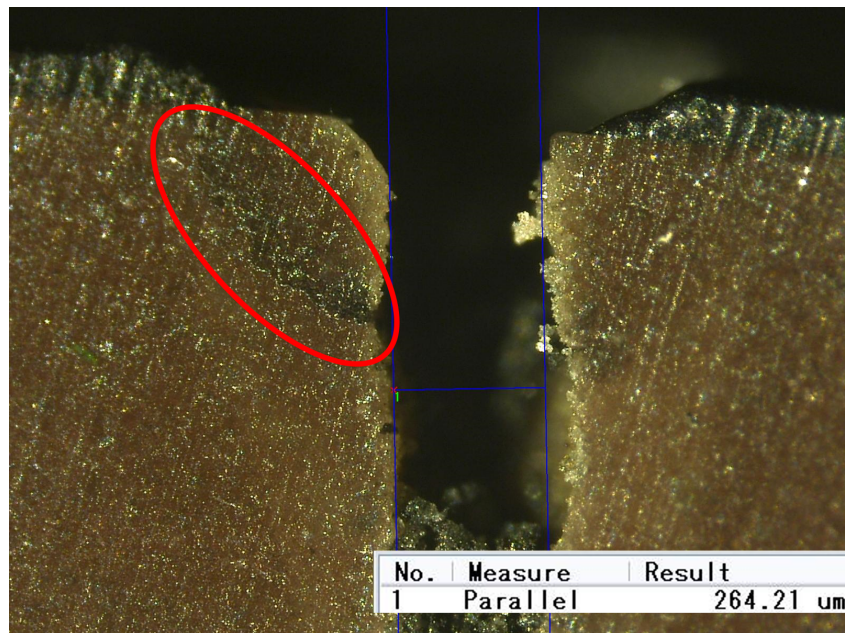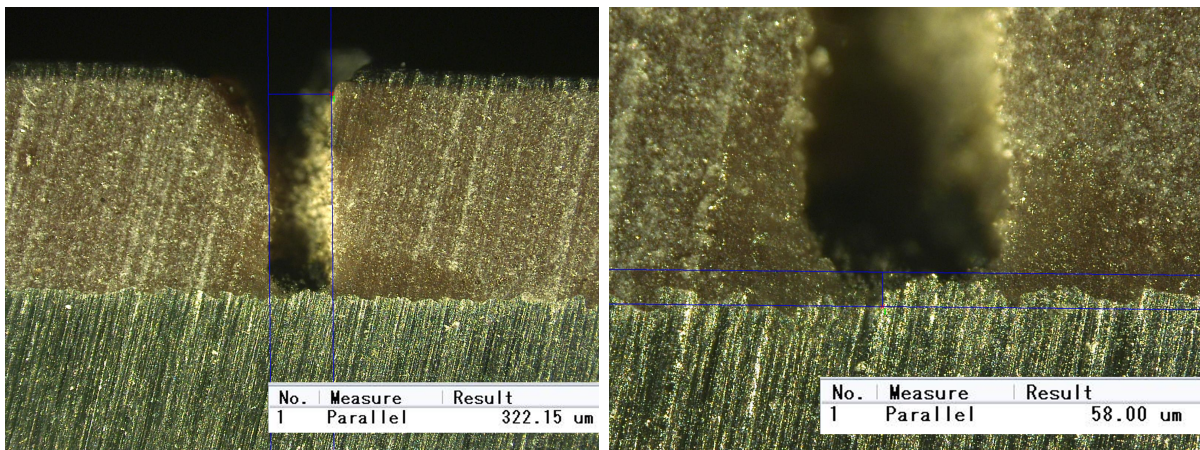

Figure 4.33: *The breakdown channel for test object 4 with an electrode sandblasted with aluminium oxide(0.5-1.0 mm).*

The insulation did not separate from the electrode for this test object when it was cut, which indicates strong adhesion. Figure 4.34 shows that the insulation is still directly in contact along the whole interface between the insulation and electrode. Additionally, the figure can be used to examine the electrode surface in the centre of the breakdown channel. The breakdown channel had a size of approximately 320 μm. The electric tree that was visible in Figure 4.33 disappeared when the cup was polished to the centre of the breakdown channel, and left a missing part of the insulation creating a slightly increased width at the top of the breakdown channel.

Figure 4.34b gives a closer inspection of the electrode surface in the breakdown channel. A peak of around 60 μm is directly in the centre of the breakdown channel. There are no peaks with the same height to decrease the field enhancement in the section analysed in the microscope. The distance between the peaks is around the same for the examined surface, thus giving the smaller peaks lower electric field enhancement. This indicates that the local field enhancement at the centre of the breakdown channel is higher than the rest of the surface. The electric field simulations correspond well with the highest peak having the highest electric field enhancement when there are no other peaks to impact the field distribution.

(a) *Entire breakdown channel.*

(b) *Electrode surface peaks around the break-down channel.*

Figure 4.34: *Images around the breakdown channel for test object 4 with an electrode surface sandblasted with aluminium oxide(0.5-1.0 mm).*

The insulation sent to a CT scan for the electrodes sandblasted with aluminium oxide was test object 9. The scan over the breakdown channel is presented in Figure 4.35. This scan yielded the clearest image of the breakdown channel compared to the other CT scans. Anyhow, the resolution is not good enough to examine the breakdown channel more closely.
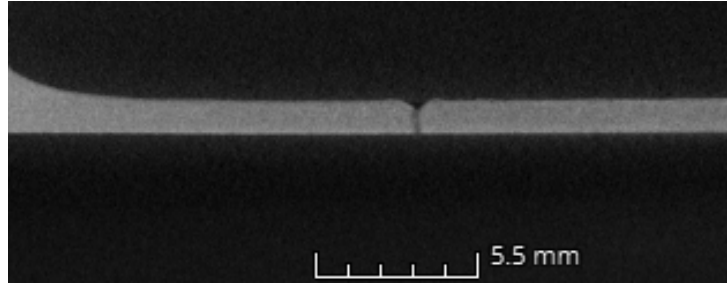

Figure 4.35: *Breakdown channel found in the CT scan for test object 9 with an electrode sandblasted with aluminium oxide.*

4.5.3   Electrode surface sandblasted with glass orbs(0.25-0.42 mm)

The results from the breakdown measurements for the test object with an electrode surface sandblasted with glass orbs are presented in Table 4.15. With the exception of the two cups that reached breakdown in Phase 2, the breakdown strength of the test objects is within a range of 33-37 kV/mm. In addition, the lowest in the range reached breakdown at the edge, thus making it a possibility for an even smaller deviation between the measurements.

Table 4.15: *Breakdown strength for the insulation cups with electrode surfaces sandblasted with glass orbs(0.25-0.42 mm). A "*" signifies that the breakdown occurred in Phase 2 testing.*

Test object	Breakdown strength [kV/mm]	BD at edge?
3	33	yes
4	37	no
5	27*	no
6	19*	no
8	35	no
10	34	no

One of the insulation cups with similar breakdown values was chosen for further analysis. Figure 4.36 visualises the breakdown channel and shows the electrode surface around the breakdown channel. The figure shows that the insulation loosened to a gap of around 70 μm from the aluminium disc in the cutting process. The disc and insulation did not completely separate, which indicates a stronger adhesive force than for the test object with a polished and hot AC anodised electrode surface. From Figure 4.36b it is visible that the breakdown occurred in the middle of a peak at the electrode surface. The surface around the breakdown is evenly distributed with no clear peaks, while a peak with a height

of about $30\mu m$ is in the centre of the breakdown channel. The surface profile under the breakdown is similarly shaped to the electric field simulations for the discs sandblasted with glass orbs. The peak in the breakdown channel is therefore probably the point with the highest electric field enhancement, which caused the breakdown in this specific location.
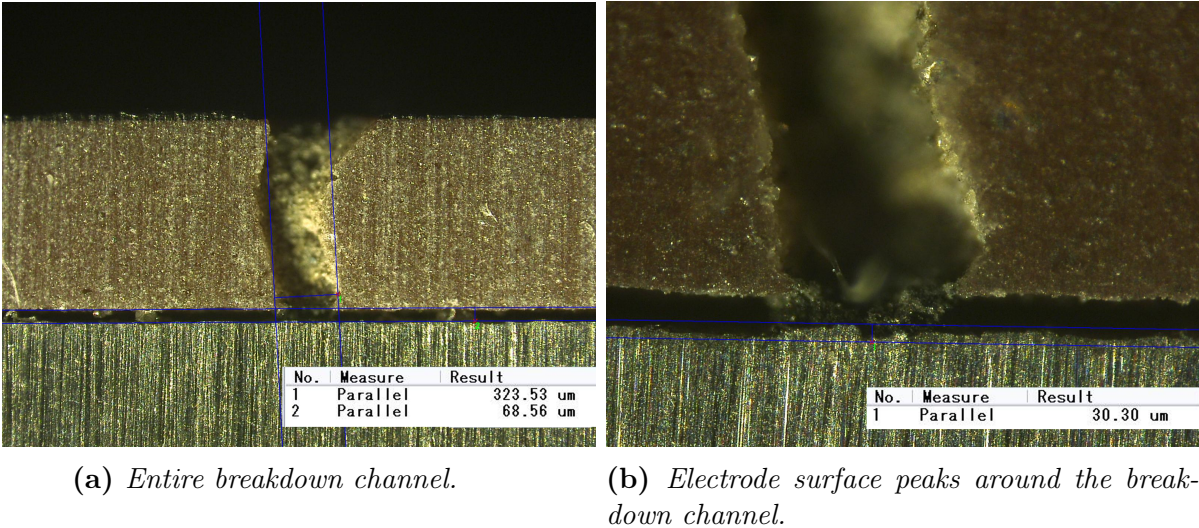

(a) *Entire breakdown channel.*

(b) *Electrode surface peaks around the breakdown channel.*

Figure 4.36: *Images around the breakdown channel for test object 10 with an electrode surface sandblasted with glass orbs(0.25-0.42 mm)*

To examine the cause of low breakdown strength for test object 6, it was cut open. If a defect is found, the value can be neglected in the final comparison of surface preparation methods. Figure 4.37 shows the breakdown channel for test object 6. There are no imminent defects visible in the figure, but a larger portion of the paint layer has burned off compared to in Figure 4.36a.
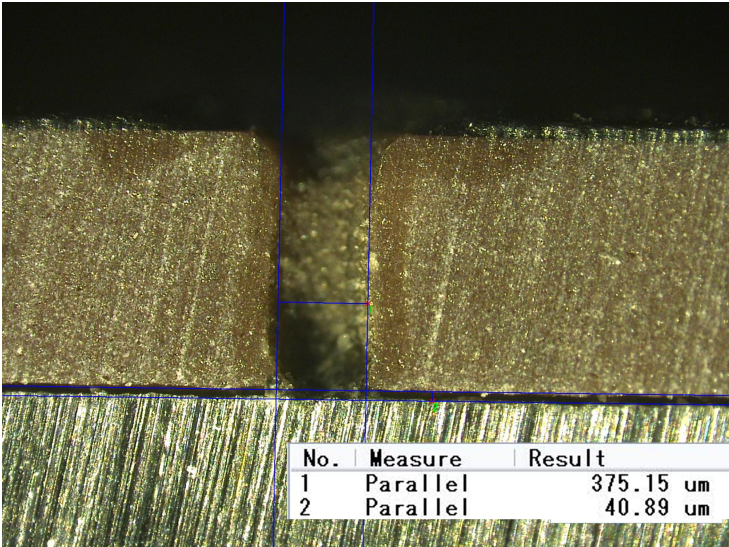
Figure 4.37: *Breakdown channel for test object 6 with an electrode surface sandblasted with glass orbs(0.25-0.42 mm)*

Due to no apparent defects around the breakdown channel, the PD measurements conducted in Phase 2 were examined further. Figure 4.38 displays the PRPD plot which shows discharges up to 30 pC at only 6 kV. The screening process showed PDIV at 7 kV, with only 2 pC discharge magnitudes as presented in Figure A.17. The cause might be a smaller void, with a similar form as in test object 1 for the polished and hot AC anodised discs, which had a clearly visible void. For test object 1, the void went undetected in the PD measurements until about 12 kV for the first test. The PDIV for the following screening tests decreased significantly. Given the difference in the size of the voids, it is plausible that it could go undetected up to 8 kV for test object 6. It is therefore assumed that such spots also were present at the breakdown location, thus enabling the measurement to be neglected in the comparison of surface preparation methods.
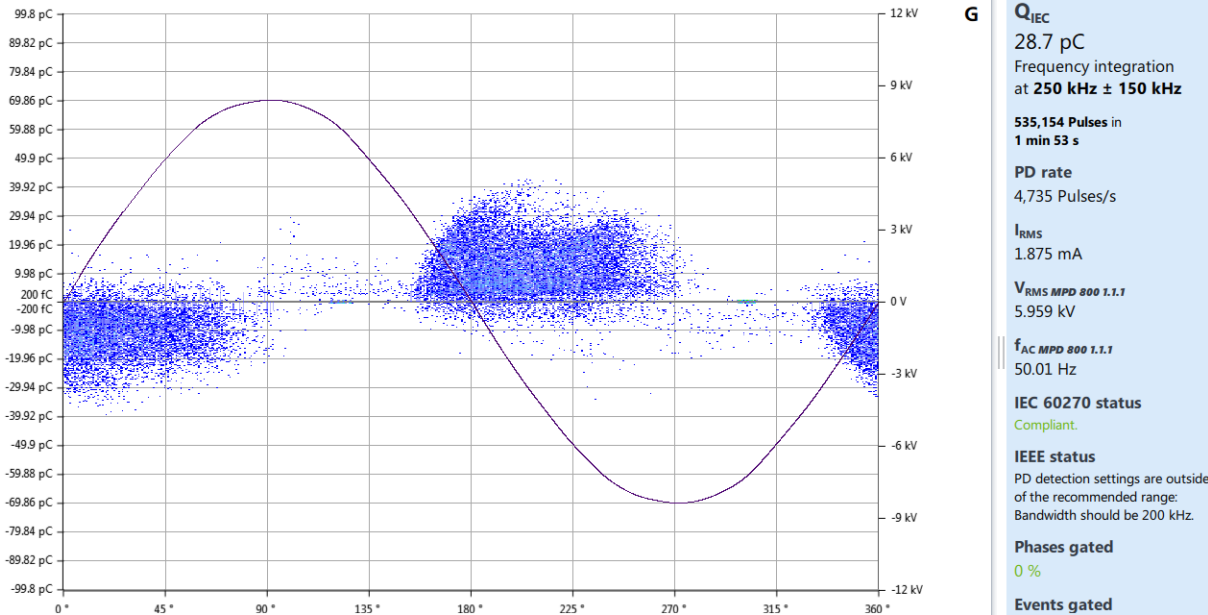
Figure 4.38: *PRPD plot for test object 6 sandblasted with glass orbs from the early stages in Phase 2 testing.*

Test object 5 did also reach breakdown during Phase 2, but it did not get cut open and examined in a microscope. The PRPD plots for Phase 2 were analysed, but no imperfections as the ones in test object 6 were found. Although there might still have been voids or other defects in the insulation layer, the value will be included in the comparison of breakdown strength. It is included due to the fact that no defect was found, and a defect should not be assumed without any other indications than a bad result.

A test object from the insulation cups with electrodes sandblasted with glass orbs was also sent to industrial tomography. The breakdown channel was found in the scan, as visualised in Figure 4.39. The scan has the same issues as the others in regard to resolution. The breakdown channel can be seen, however, it does not have a high enough resolution to determine anything conclusive.
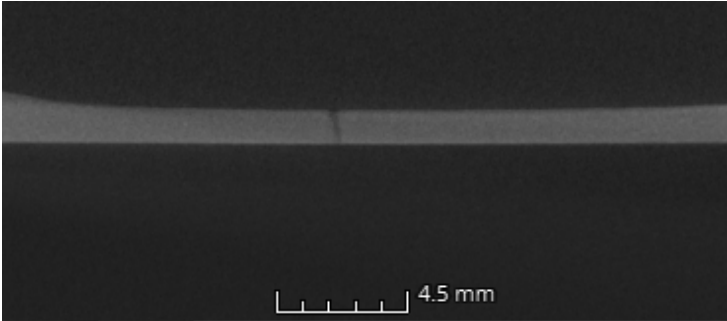

Figure 4.39: *Breakdown channel found in the CT scan for test object 8 with an electrode sandblasted with glass orbs.*

4.5.4 Comparison of the surface preparation methods

Each of the various surface preparation methods used for the aluminium discs used to obtain different surface roughnesses was tested separately. They were screened with PD measurements, and the initiation of electrical trees was found. The results from the breakdown tests for all the test objects that were deemed to not contain defects are presented in Figure 4.40. The objects where a defect was discovered either in the screening process or in further analysis are removed.
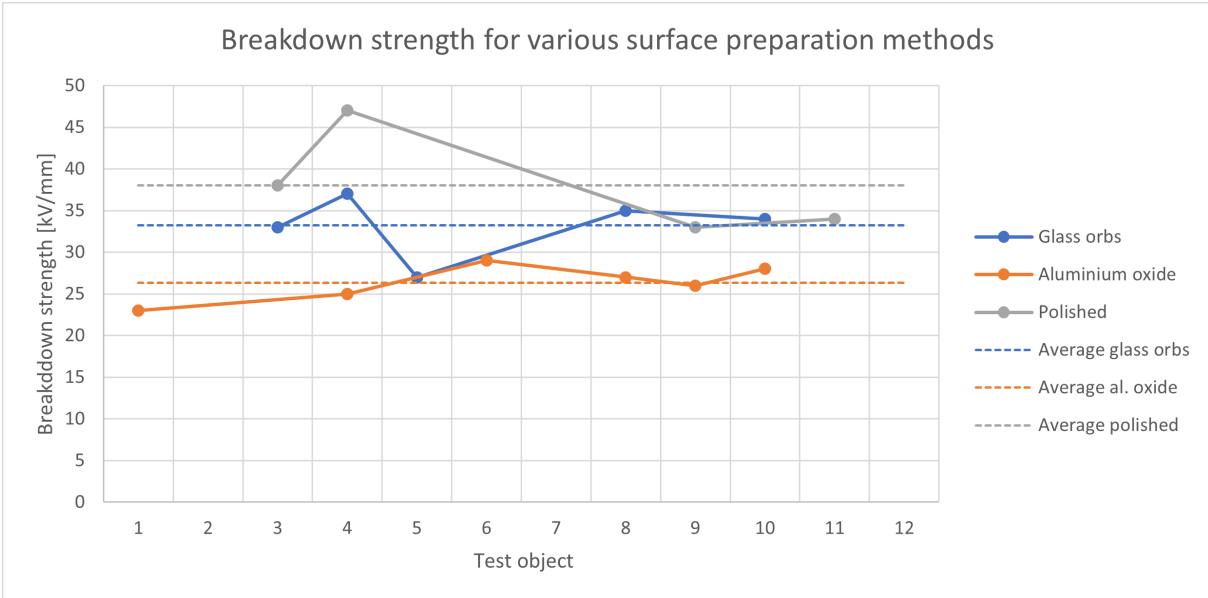
Figure 4.40: *A comparison of the breakdown voltage for the test objects that were deemed of sufficient quality without defects.*

Figure 4.40 clearly shows that the surface preparation method will impact the breakdown strength of the test objects. There is a significant difference in the results between the surface sandblasted with aluminium oxide and the polished and hot AC anodised surface with average breakdown strengths of 26 kV/mm and 38 kV/mm, respectively. The breakdown strength was decreased by around 30% when the surface roughness was increased from polished to rough sandblasted, which corresponds to S_a-values of around 54 nm and 11.5 μm. The average breakdown strength of the glass orbs was approximately in the middle, albeit a bit closer to 38 kV/mm, with a breakdown strength of 33 kV/mm. The average S_a-value was around 4.3 μm, which means there is a strong correlation between the surface roughness of the electrode and the breakdown strength in the test objects. The results show undoubtedly that the breakdown strength is decreased with an increase in the surface roughness.

The results from both the PD measurements and the breakdown strength is as expected based on the electric field simulations conducted in COMSOL. The simulations showed that an increase in surface roughness increased the field enhancement. The field enhancement will negatively impact the breakdown strength, which is clearly shown in Figure 4.40. Additionally, the simulations displayed that the highest surface peaks with no similar peaks close by gave the highest field enhancement. The examinations with a microscope showed the highest surface peaks in the centre of the breakdown channels, which corroborated the simulations.

The difference in surface roughness was the only adjusted factor for all the test objects in the thesis, however, other factors did also change as a consequence. Cutting the cups open and examining them with a microscope showed differences in the adhesion strength for the surface preparation methods. The insulation layer did not separate from the electrode surface for the test objects that were sandblasted with aluminium oxide. For the objects sandblasted with glass orbs, which had a lower surface roughness, the insulation separated slightly from the electrode while still maintaining the cup. The polished and hot AC anodised disc separated completely from the insulation when it was cut open. These results show that adhesion is affected by surface roughness. The adhesion strength seems to increase with the surface roughness, which means that the better values in breakdown strength come with a cost of worse adhesion.

5 Conclusion

The objective of the thesis was to examine the impact of electrode surface roughness on insulation performance. It was accomplished by applying three different surface preparation methods to aluminium discs, which yielded three sets of different surface roughnesses.

- The three different sets of test objects consisted of electrodes sandblasted with either aluminium oxide(0.5-1.0 mm) or glass orbs(0.25-0.42 mm), while the last set of discs was polished and hot AC anodised. The results from the surface preparation methods were average S_a-values of 11.5 μm, 4.3 μm and 54 nm, respectively. Although there were some small deviations within each set of preparation methods, they were deemed negligible in the comparison of the different methods.

- Simulations for a surface from every preparation method were conducted in COMSOL to examine the impact of surface roughness on the electric field distribution. The results showed that an increase in surface roughness will increase the local field enhancement in the insulation layer. Additionally, it was concluded that if there are several surface peaks in close proximity to each other, the maximum field at each peak will be reduced by the surrounding peaks. The highest peak is therefore not necessarily the point with the highest local electric field.

- PD measurements were conducted as a screening process to eliminate insulation cups that were defective. For the successful insulation cups, the PDIV values and the charge magnitudes of the various surface preparation methods were not considerably different. They were not identical, with the polished and hot AC anodised electrode surfaces as well as the surfaces sandblasted with glass orbs having generally slightly higher PDIV values and slightly lower charge magnitudes than the surfaces sandblasted with aluminium oxide.

- The differences in the surface preparation methods were more apparent for the PD measurements conducted to find the electric field where electrical tree growth was initiated. The average electric field for electrical tree initiation was approximately 14 kV/mm, 17 kV/mm and 21 kV/mm ranging from roughest to smoothest surface.

- Lastly, breakdown tests were conducted to measure the breakdown strength of the insulation cups. There was a significant difference between the polished and hot AC anodised electrode and the electrode sandblasted with aluminium oxide, with breakdown strengths of 26 kV/mm and 38 kV/mm respectively. Additionally, the electrode sandblasted with glass orbs had a breakdown strength in between them at 33 kV/mm. These results show that the breakdown strength is heavily impacted by surface roughness.

- All the findings in the thesis are corroborating that the surface roughness will affect the insulation performance. Increasing the surface roughness will increase the field enhancement in the insulation layer, which will contribute to reducing the electric field at electrical tree initiation and when discharge magnitudes reach 1 nC, as well as decreasing the breakdown strength. Therefore, it can be concluded that an increase in surface roughness will cause a decrease in the insulation performance.

6 Further work

The thesis has shown how some kinds of surface preparation methods can impact insulation performance. However, there are still a lot of interesting factors that can be examined further within the subject of surface roughness.

- The first part is to improve the casting process to reduce the number of insulation cups with defects. The process can be improved by for example adding heating elements around the syringe and along the tubes leading into the mould. Adding additional heating could minimise the risk of void formation due to insufficient temperature in the epoxy resin mixture.

- Another examination could be to create more test objects with polished and hot AC anodised electrode surfaces. There were only four successfully cast in this thesis, so additional test objects would give a better foundation for the insulation performance of the polished surfaces. Then, it could be examined why there were relatively large deviations between the different test objects with a polished and hot AC anodised electrode surface.

- The electrical tree initiation was only examined by PD measurements for the insulation cups. It could be interesting to make test objects and cut them open before reaching breakdown to investigate how the electrical trees are growing in the insulation. A good point to cut them open would be right after Phase 2 when some discharge magnitudes have reached over 1 nC.

- Electric tree initiation can also be examined without destroying the insulation cups by replacing the epoxy with transparent epoxy and connecting cameras in the measurement setup. By utilising this method the electrical trees can be seen in the epoxy as they are growing while a voltage is stressed over the test object.

- There are several other preparation methods that can be used on the aluminium discs. Sandblasting with different kinds of particles and particle sizes will give surface roughness parameters that have not been examined in this thesis. The results can be used to corroborate the results from this thesis. Measurements for electrode surfaces with the same S_a-values achieved with different methods could be interesting to research. This can be done by for example sandblasting with particle sizes of aluminium oxide and glass orbs that give the same S_a-value, although the glass orbs give a valley formation at the surface compared to more evenly spread with aluminium oxide. It can then be examined how the surface topography affects the results, even if the surface roughness parameters are similar.

- Other parameters such as temperature, humidity, defects and contaminants can also be examined related to the interface between the electrode and insulation material. To summarise, there are many interesting factors to examine related to this thesis.

Bibliography

[1]   Egil Bergstøl Birkeland. "Specialisation project - High Voltage Subsea Connectors for Offshore Wind – Study of Interfaces". In: (Dec. 22, 2022).

[2]   *Onshore wind energy.* URL: https://energy.ec.europa.eu/topics/renewable-energy/onshore-wind-energy_en (visited on 12/01/2022).

[3]   The SET Plan Implementation Working Group for Offshore Wind. "2nd SET Plan Implementation Plan for offshore wind March 2022". In: *The European Commission* (2022).

[4]   *High Voltage Subsea Connector for Offshore Wind - Prosjektbanken.* Prosjektbanken - Forskningsrådet. URL: https://prosjektbanken.forskningsradet.no/project/FORISS/327921 (visited on 06/01/2023).

[5]   Erling Ildstad. *TET4160 Insulating Materials for High Voltage Applications.* 2021.

[6]   *Surface Roughness - an overview | ScienceDirect Topics.* URL: https://www.sciencedirect.com/topics/chemistry/surface-roughness (visited on 09/15/2022).

[7]   Odd Christian Feet, Frank Mauseth, and Kaveh Niayesh. *Influence of Surface Roughness on Breakdown in Air Gaps at Atmospheric Pressure under Lightning Impulse.* Accepted: 2019-02-28T07:31:21Z. Institute of Electrical and Electronics Engineers (IEEE), 2018. ISBN: 978-1-5386-5086-8. DOI: 10.1109/ICHVE.2018.8642269. URL: https://ntnuopen.ntnu.no/ntnu-xmlui/handle/11250/2587895 (visited on 10/14/2022).

[8]   Scott. *Average Roughness basics.* Michigan Metrology. Jan. 23, 2021. URL: https://michmet.com/average-roughness-basics/ (visited on 11/28/2022).

[9]   Guanghui Song, Yaojin Wang, and Daniel Q. Tan. "A review of surface roughness impact on dielectric film properties". In: *IET Nanodielectrics* 5.1 (2022), pp. 1–23. ISSN: 2514-3255. DOI: 10.1049/nde2.12026. URL: https://onlinelibrary.wiley.com/doi/abs/10.1049/nde2.12026 (visited on 12/05/2022).

[10]   Erling Ildstad, Roger Dale, and Emre Kantar. "Longitudinal Breakdown Strength of Wet-mate Solid-Solid Interfaces at VLF and 50 Hz AC voltages". In: 27.1 (2022). DOI: https://doi.org/10.5324/nordis.v27i1.4897.

[11]   Daniel Qi Tan. "Differentiation of roughness and surface defect impact on dielectric strength of polymeric thin films". In: *IET Nanodielectrics* 3.1 (2020), pp. 28–31. DOI: https://doi.org/10.1049/iet-nde.2019.0031. URL: https://ietresearch.onlinelibrary.wiley.com/doi/abs/10.1049/iet-nde.2019.0031.

[12]   *Average Surface Roughness - an overview | ScienceDirect Topics.* URL: https://www.sciencedirect.com/topics/engineering/average-surface-roughness (visited on 12/07/2022).

[13]   *Surface Roughness Chart: Understanding Surface Finishes.* rapiddirect. Nov. 10, 2021. URL: https://www.rapiddirect.com/blog/surface-roughness-chart/ (visited on 12/07/2022).

[14]   You Ho Kim et al. "Dielectric Characteristics of Solid Insulation Materials With Respect to Surface Roughness". In: *IEEE Transactions on Applied Superconductivity* 25.3 (2015), pp. 1–4. DOI: 10.1109/TASC.2014.2373640.

[15]   Wei Wei, Junwen Chen, and Defa Wang. "Study on The Effect of Dielectric Film on Gap Breakdown Voltage under DC Voltage in Air, SF6 and SF6/N2 Mixture". In: *2021 International Conference on Advanced Electrical Equipment and Reliable Operation (AEERO).* 2021, pp. 1–4. DOI: 10.1109/AEERO52475.2021.9708336.

[16]   A.M. Mahdy, H.I. Anis, and S.A. Ward. "Electrode roughness effects on the break-down of air-insulated apparatus". In: *IEEE Transactions on Dielectrics and Electrical Insulation* 5.4 (1998), pp. 612–617. DOI: 10.1109/94.708280.

[17]   Emre Kantar et al. "Longitudinal AC breakdown voltage of XLPE-XLPE interfaces considering surface roughness and pressure". In: *IEEE Transactions on Dielectrics and Electrical Insulation* 24.5 (2017), pp. 3047–3054. DOI: 10.1109/TDEI.2017.006540.

[18]   Emre Kantar et al. "Tangential AC breakdown voltage of Solid-Solid Interfaces Considering Surface Roughness". In: *IEEE Transactions on Dielectrics and Electrical Insulation* 24.5 (2017), pp. 3047–3054. DOI: 10.1109/TDEI.2017.006540.

[19]   Rajendra M Patrikar, Chong Yi Dong, and Wenjun Zhuang. "Modelling interconnects with surface roughness". In: *Microelectronics Journal* 33.11 (2002), pp. 929–934. ISSN: 0026-2692. DOI: https://doi.org/10.1016/S0026-2692(02)00105-2. URL: https://www.sciencedirect.com/science/article/pii/S0026269202001052.

[20]   Y. Inagawa et al. "Effect of electrode surface roughness on breakdown conditioning process under non-uniform electric field in vacuum". In: *XXIst International Symposium on Discharges and Electrical Insulation in Vacuum, 2004. Proceedings. ISDEIV.* Vol. 1. 2004, pp. 72–75. DOI: 10.1109/DEIV.2004.1418604.

[21]   M. Taleb, G. Teyssèdre, and S. Le Roy. "Role of the interface on charge build-up in a low-density polyethylene: Surface roughness and nature of the electrode". In: *2009 IEEE Conference on Electrical Insulation and Dielectric Phenomena*. 2009, pp. 112–115. DOI: 10.1109/CEIDP.2009.5377888.

[22]   Siyu Zhang et al. "The relationship between metal electrode's surface roughness and charge injection characteristics at high temperatures". In: *2018 12th International Conference on the Properties and Applications of Dielectric Materials (ICPADM)*. 2018, pp. 253–256. DOI: 10.1109/ICPADM.2018.8401258.

[23]   Yonggang Meng. "Electrostatic Field Effects on Adhesion". In: *Encyclopedia of Tribology*. Ed. by Q. Jane Wang and Yip-Wah Chung. Boston, MA: Springer US, 2013, pp. 951–956. ISBN: 978-0-387-92897-5. DOI: 10.1007/978-0-387-92897-5_461. URL: https://doi.org/10.1007/978-0-387-92897-5_461.

[24]   Sulin Zhang, Rahul Panat, and K. Jimmy Hsia. "Influence of surface morphology on the adhesion strength of epoxy–aluminum interfaces". In: *Journal of Adhesion Science and Technology* 17.12 (2003), pp. 1685–1711. DOI: 10.1163/156856103322396749. URL: https://doi.org/10.1163/156856103322396749.

[25]   Mostafa Refaey, Tarek Negm, and A. Hossam-Eldin. "Modeling and Simulation of Internal Partial Discharge in Solid Dielectrics under Variable Applied Frequencies". In: Dec. 2016. DOI: 10.1109/MEPCON.2016.7836959.

[26]   Gian Carlo Montanari and Paolo Seri. "About the Definition of PDIV and RPDIV in Designing Insulation Systems for Rotating Machines Controlled by Inverters". In: *2018 IEEE Electrical Insulation Conference (EIC)*. 2018, pp. 554–557. DOI: 10.1109/EIC.2018.8481069.

[27]   Sebastian Aumann et al. "Measurement and diagnosis of partial discharges in low voltage applications ≤ 100 volts". In: ZVEI - German Electrical and Electronic Manufacturers Association, 2017, pp. 554–557.

[28]   Hadi Nabipour Afrouzi et al. "In-depth exploration of partial discharge modelling methods within insulations". In: *Cleaner Engineering and Technology* 6 (2022), p. 100390. ISSN: 2666-7908. DOI: https://doi.org/10.1016/j.clet.2021.

100390. URL: `https : / / www . sciencedirect . com / science / article / pii / S2666790821003505`.

[29] Antonino Imburgia et al. "Time Evolution of Partial Discharges in a Dielectric Subjected to the DC Periodic Voltage". In: *Energies* 15.6 (2022). ISSN: 1996-1073. DOI: `10.3390/en15062052`. URL: `https://www.mdpi.com/1996-1073/15/6/2052`.

[30] Zepeng Lv et al. "Evolution of partial discharges during early tree propagation in epoxy resin". In: *IEEE Transactions on Dielectrics and Electrical Insulation* 24.5 (2017), pp. 2995–3003. DOI: `10.1109/TDEI.2017.006731`.

[31] N. Shimizu and C. Laurent. "Electrical tree initiation". English. In: *IEEE Transactions on Dielectrics and Electrical Insulation* 5.5 (1998). Cited By :207, pp. 651–659. URL: `www.scopus.com`.

[32] Xiangrong Chen et al. "Electrical treeing behavior at high temperature in XLPE cable insulation samples". In: *IEEE Transactions on Dielectrics and Electrical Insulation* 22.5 (Oct. 2015), pp. 2841–2851. ISSN: 1070-9878. DOI: `10.1109/TDEI.2015.004784`. URL: `https://ieeexplore.ieee.org/document/7311063` (visited on 12/17/2022).

[33] R. Vogelsang et al. "Detection of electrical tree propagation by partial discharge measurements". In: *European Transactions on Electrical Power* 15.3 (2005), pp. 271–284. DOI: `https://doi.org/10.1002/etep.60`. URL: `https://onlinelibrary.wiley.com/doi/abs/10.1002/etep.60`.

[34] *Anodizing - an overview | ScienceDirect Topics*. URL: `https : / / www . sciencedirect.com/topics/chemistry/anodizing` (visited on 01/25/2023).

[35] Astrid Bjørgum. "Hvordan unngå korrosjon på pulverlakkert aluminium i bygg?" In: ().

[36] Ole Øystein Knudsen et al. "Anodising as pre-treatment before organic coating of extruded and cast aluminium alloys". In: *Corrosion Science* 46.8 (2004), pp. 2081–2095. ISSN: 0010-938X. DOI: `https : / / doi . org / 10 . 1016 / j . corsci . 2003 . 10 . 021`. URL: `https : / / www . sciencedirect . com / science / article / pii / S0010938X03002920`.

[37] Bernt B. Johnsen, Fabrice Lapique, and Astrid Bjørgum. "The durability of bonded aluminium joints: a comparison of AC and DC anodising pretreatments". In: *International Journal of Adhesion and Adhesives* 24.2 (2004), pp. 153–161. ISSN: 0143-7496. DOI: `https://doi.org/10.1016/j.ijadhadh.2003.09.003`. URL: `https://www.sciencedirect.com/science/article/pii/S0143749603001222`.

[38] Joe Flanagan et al. "Use of a blast coating process to promote adhesion between aluminium surfaces for the automotive industry". In: *The Journal of Adhesion* 96 (June 2018), pp. 1–22. DOI: `10.1080/00218464.2018.1486713`.

[39] W.James Stemp and Michael Stemp. "UBM Laser Profilometry and Lithic Use-Wear Analysis: A Variable Length Scale Investigation of Surface Topography". In: *Journal of Archaeological Science* 28.1 (2001), pp. 81–88. ISSN: 0305-4403. DOI: `https://doi.org/10.1006/jasc.2000.0547`. URL: `https://www.sciencedirect.com/science/article/pii/S0305440300905478`.

[40] Von Roll Switzerland Ltd. *Anti corona CoronaShield® P 8003*. 2015.

[41] Omicron Electronics GmbH. *Omicron MPD 600 User manual*. 2021.

[42] *Non-Destructive Testing - an overview | ScienceDirect Topics*. URL: `https://www.sciencedirect.com/topics/materials-science/non-destructive-testing` (visited on 12/11/2022).

[43] *Destructive Testing - an overview | ScienceDirect Topics*. URL: https://www.sciencedirect.com/topics/engineering/destructive-testing (visited on 12/11/2022).

[44] Endrerud, Pål Erik. *Private E-mail correspondance*. 2022.

[45] Seyed Rasoul Mousavi et al. "A review of electrical and thermal conductivities of epoxy resin systems reinforced with carbon nanotubes and graphene-based nanoparticles". In: *Polymer Testing* 112 (2022), p. 107645. ISSN: 0142-9418. DOI: https://doi.org/10.1016/j.polymertesting.2022.107645. URL: https://www.sciencedirect.com/science/article/pii/S0142941822001696.

[46] Akihiro Shimamura et al. "Improving the thermal conductivity of epoxy composites using a combustion-synthesized aggregated $\beta - Si3N4$ filler with randomly oriented grains". In: *Scientific Reports* 10.1 (Sept. 10, 2020). Number: 1 Publisher: Nature Publishing Group, p. 14926. ISSN: 2045-2322. DOI: 10.1038/s41598-020-71745-w. URL: https://www.nature.com/articles/s41598-020-71745-w (visited on 03/10/2023).

[47] Shania Zehra Naqvi, Janakarajan Ramkumar, and Kamal K. Kar. "12 - Fly ash/glass fiber/carbon fiber-reinforced thermoset composites". In: *Handbook of Fly Ash*. Ed. by Kamal K. Kar. Butterworth-Heinemann, 2022, pp. 373–400. ISBN: 978-0-12-817686-3. DOI: https://doi.org/10.1016/B978-0-12-817686-3.00023-2. URL: https://www.sciencedirect.com/science/article/pii/B9780128176863000232.

[48] *Relative Permittivity - the Dielectric Constant*. URL: https://www.engineeringtoolbox.com/relative-permittivity-d_1660.html (visited on 03/10/2023).

A PD screening measurements

This section will present the remaining plots from the PDIV measurements used to determine the results in Section 4.3. Only one PRPD plot for each test object is presented, even though three tests were conducted for every insulation cup. Every plot is not appended to avoid an appendix consisting of well over 100 pictures. The presented plots are chosen to represent the measurements for each test object as well as possible.

A.1 Polished and hot AC anodised electrode surface
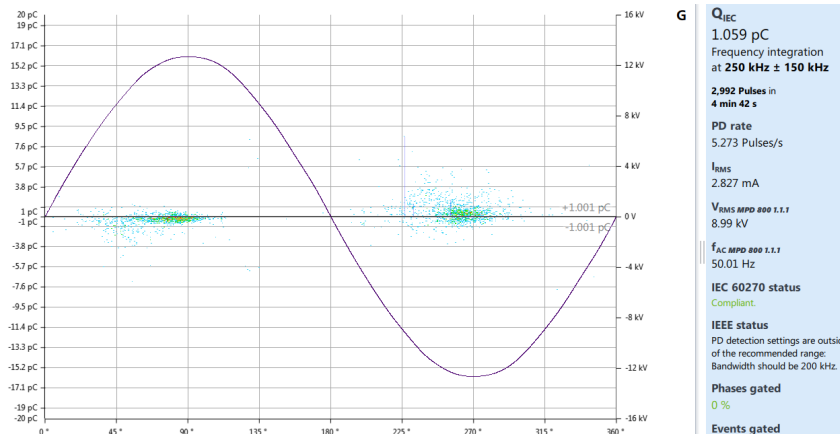
Figure A.1: *PRPD plot for the PDIV measurements conducted at test object 3 for the polished and hot AC anodised electrode surface.*
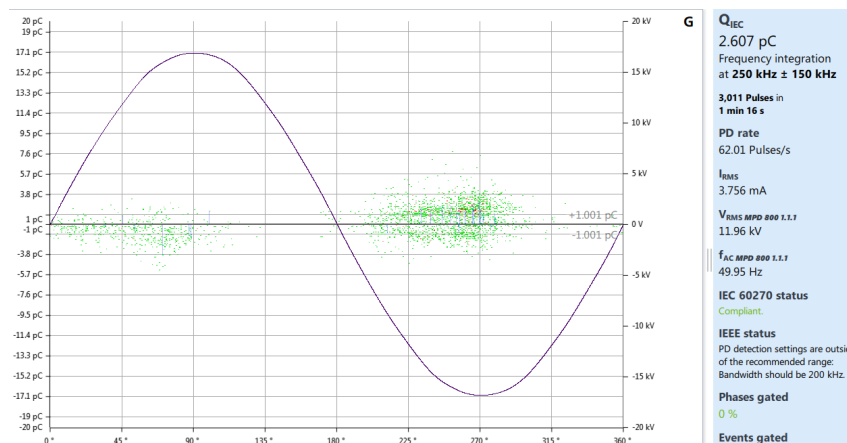
Figure A.2: *PRPD plot for the PDIV measurements conducted at test object 4 for the polished and hot AC anodised electrode surface.*
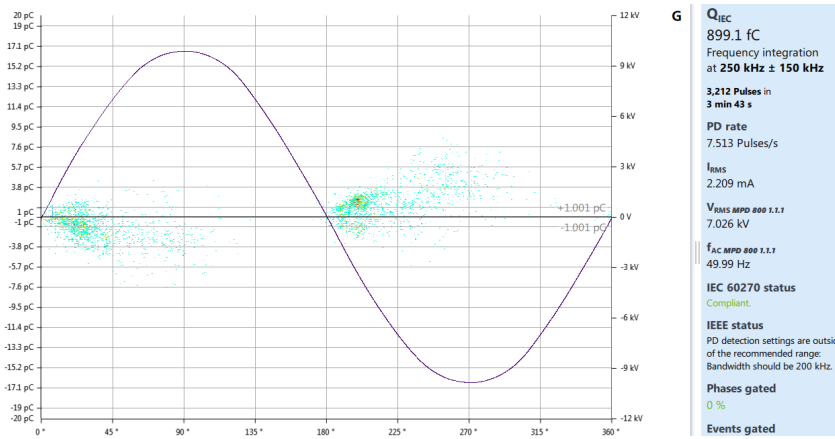
Figure A.3: *PRPD plot for the PDIV measurements conducted at test object 6 for the polished and hot AC anodised electrode surface.*
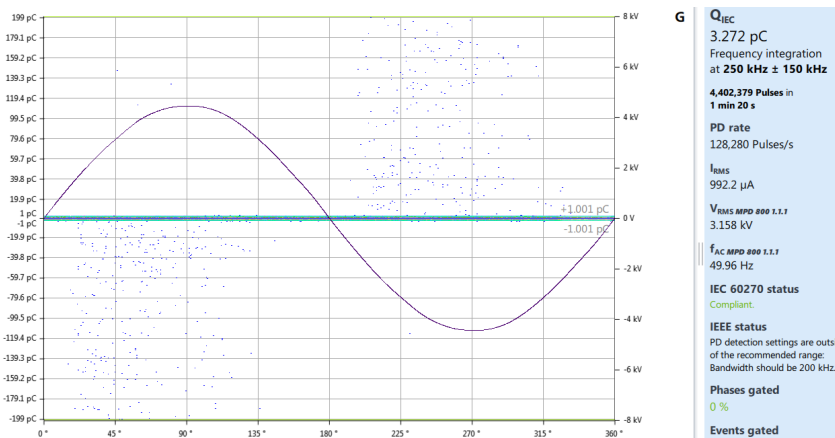
Figure A.4: *PRPD plot for the PDIV measurements conducted at test object 8 for the polished and hot AC anodised electrode surface.*
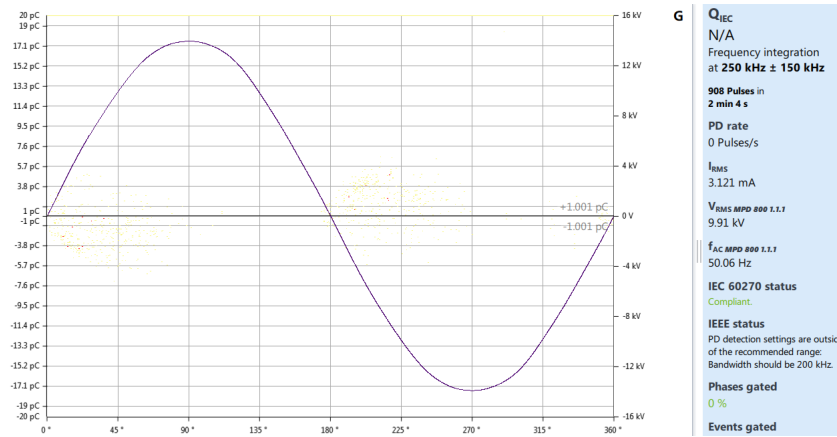
Figure A.5: *PRPD plot for the PDIV measurements conducted at test object 9 for the polished and hot AC anodised electrode surface.*
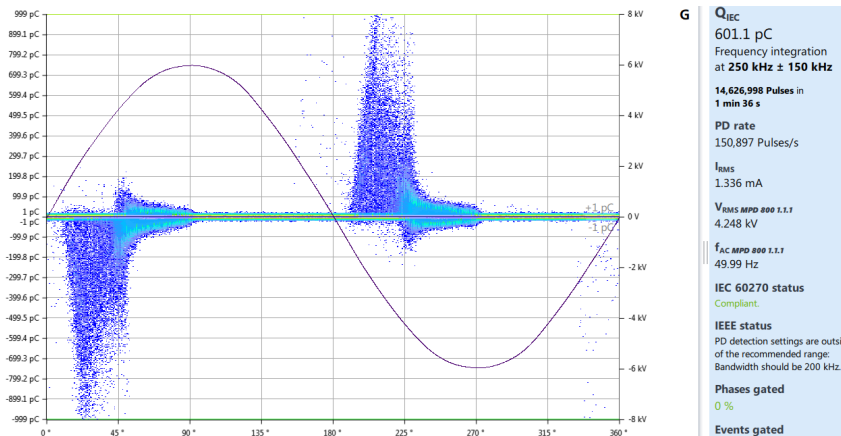
Figure A.6: *PRPD plot for the PDIV measurements conducted at test object 10 for the polished and hot AC anodised electrode surface.*

III

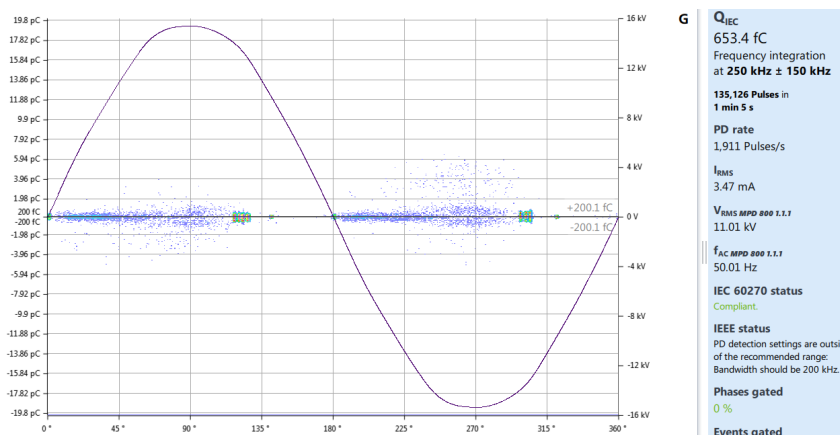## A.2 Electrode surface sandblasted with aluminium oxide(0.5-1.0 mm)
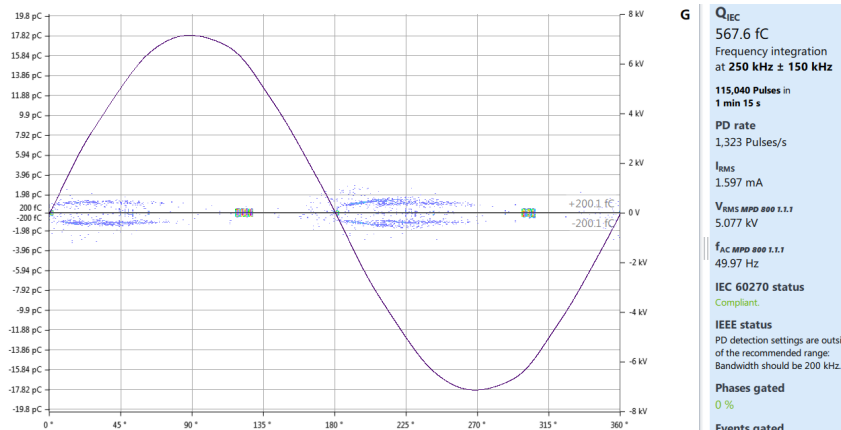
Figure A.7: *PRPD plot for the PDIV measurements conducted at test object 1 for the electrode surface sandblasted with aluminium oxide(0.5-1.0 mm).*
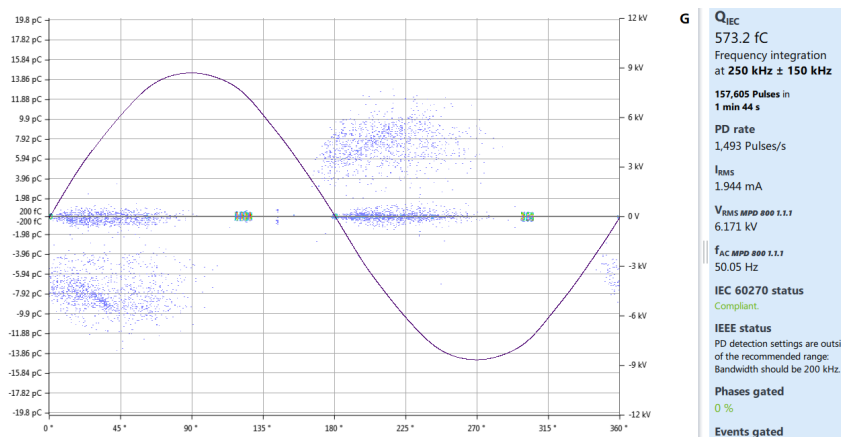
Figure A.8: *PRPD plot for the PDIV measurements conducted at test object 4 for the electrode surface sandblasted with aluminium oxide(0.5-1.0 mm).*
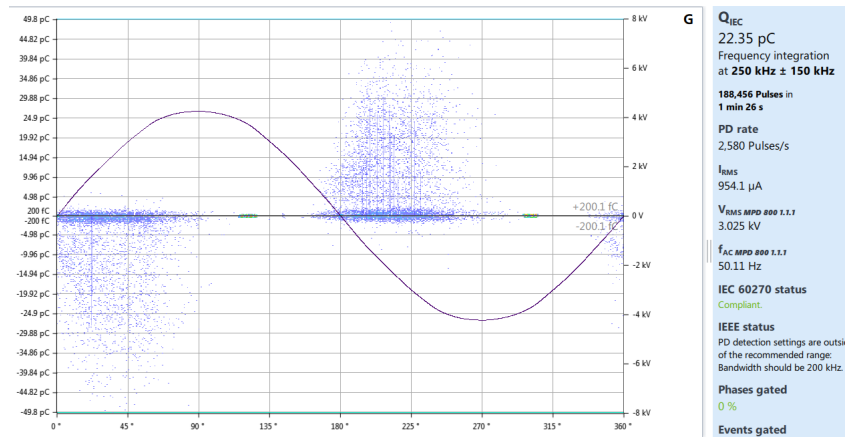
Figure A.9: *PRPD plot for the PDIV measurements conducted at test object 6 for the electrode surface sandblasted with aluminium oxide(0.5-1.0 mm).*
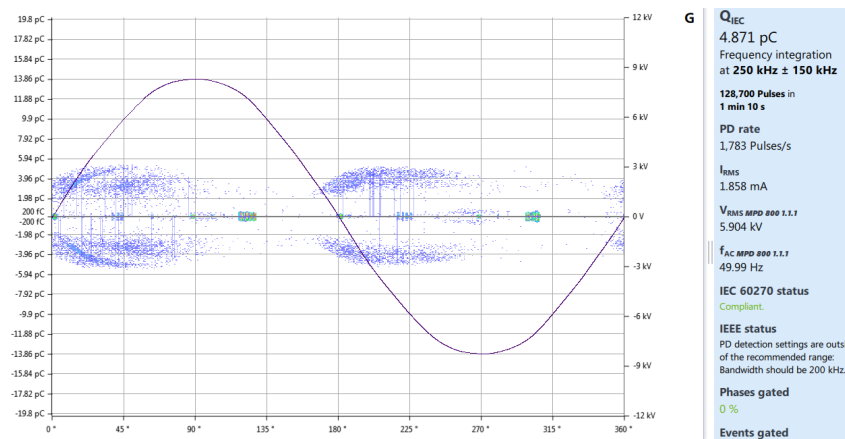
Figure A.10: *PRPD plot for the PDIV measurements conducted at test object 8 for the electrode surface sandblasted with aluminium oxide(0.5-1.0 mm).*
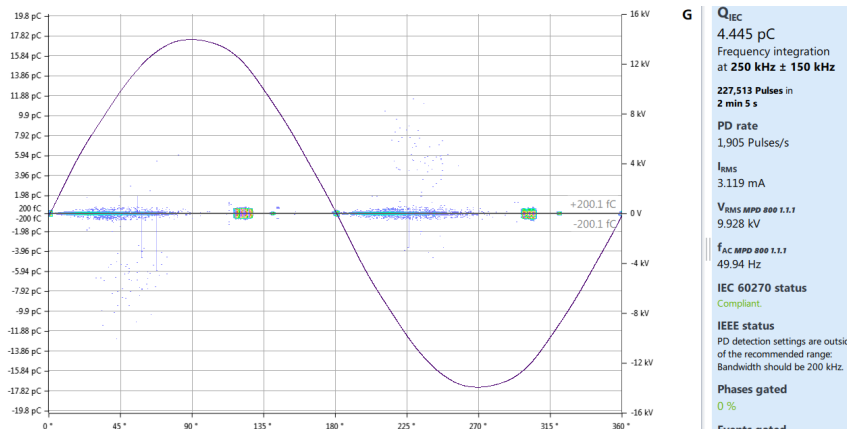
Figure A.11: *PRPD plot for the PDIV measurements conducted at test object 9 for the electrode surface sandblasted with aluminium oxide(0.5-1.0 mm).*
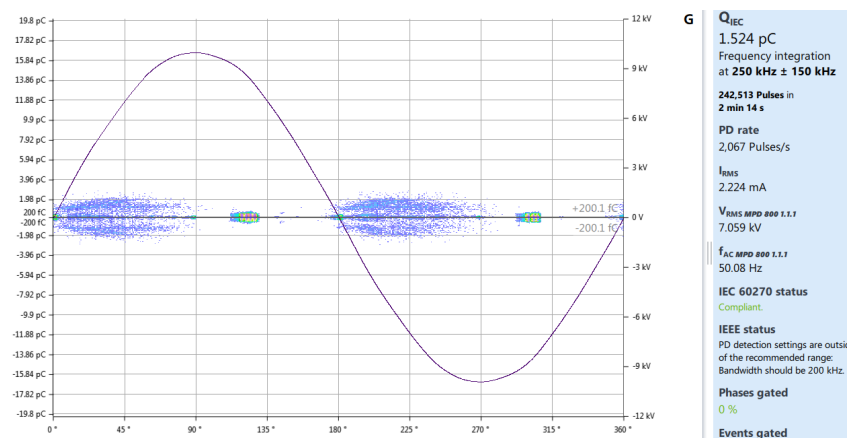
Figure A.12: *PRPD plot for the PDIV measurements conducted at test object 10 for the electrode surface sandblasted with aluminium oxide(0.5-1.0 mm).*

A.3 Electrode surface sandblasted with glass orbs(0.25-0.42 mm)
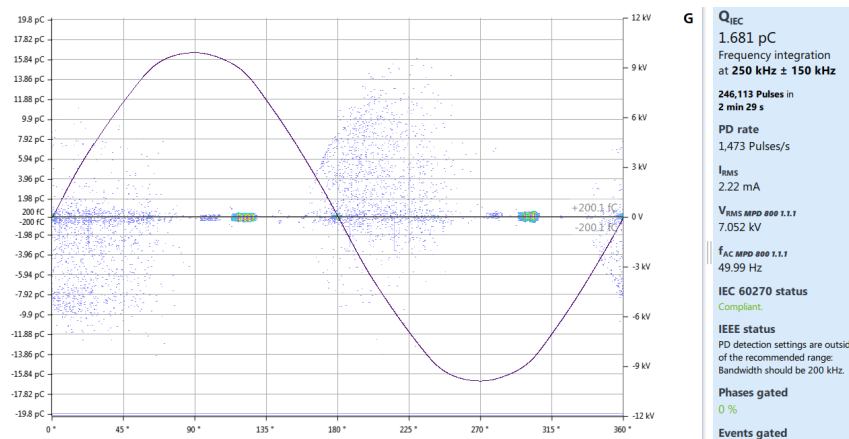
Figure A.13: *PRPD plot for the PDIV measurements conducted at test object 1 for the electrode surface sandblasted with glass orbs(0.25-0.42 mm).*
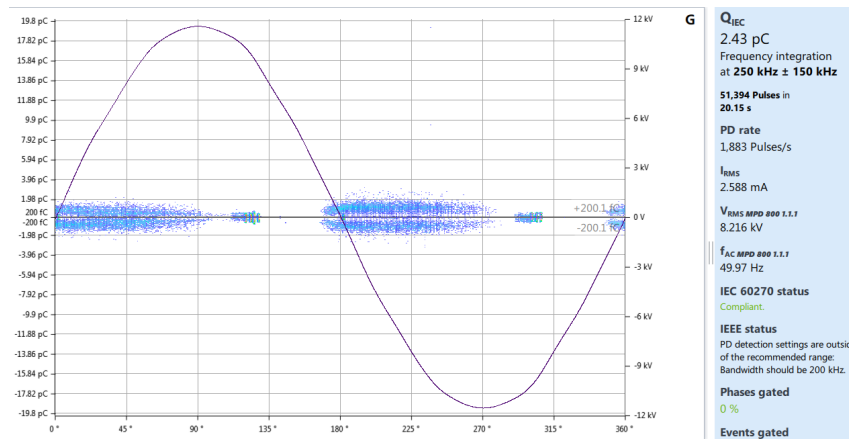
Figure A.14: *PRPD plot for the PDIV measurements conducted at test object 3 for the electrode surface sandblasted with glass orbs(0.25-0.42 mm).*
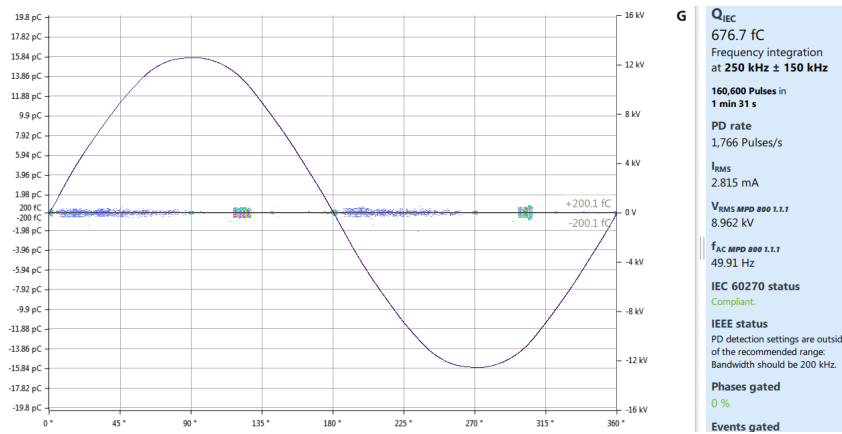
Figure A.15: *PRPD plot for the PDIV measurements conducted at test object 4 for the electrode surface sandblasted with glass orbs(0.25-0.42 mm).*
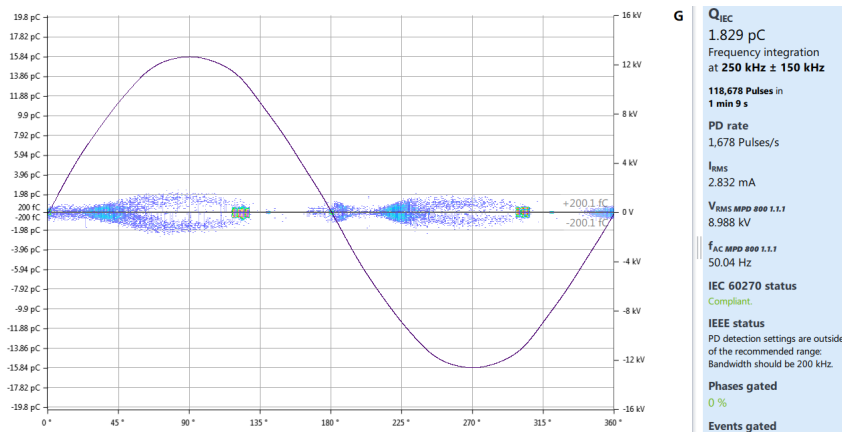
Figure A.16: *PRPD plot for the PDIV measurements conducted at test object 5 for the electrode surface sandblasted with glass orbs(0.25-0.42 mm).*
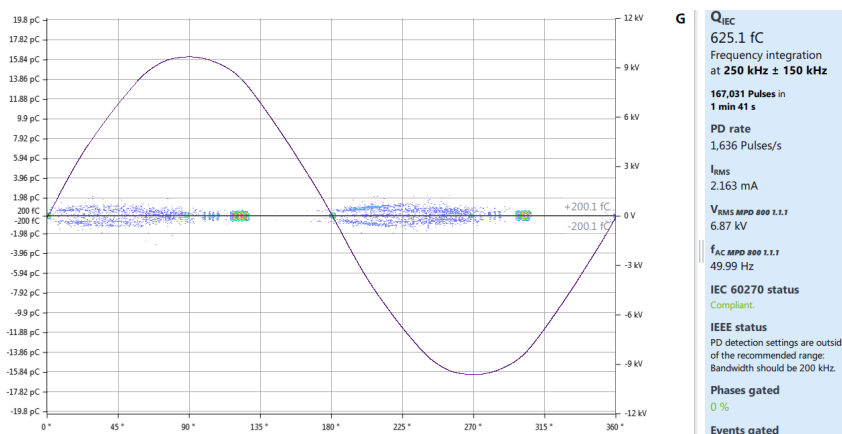
Figure A.17: *PRPD plot for the PDIV measurements conducted at test object 6 for the electrode surface sandblasted with glass orbs(0.25-0.42 mm).*
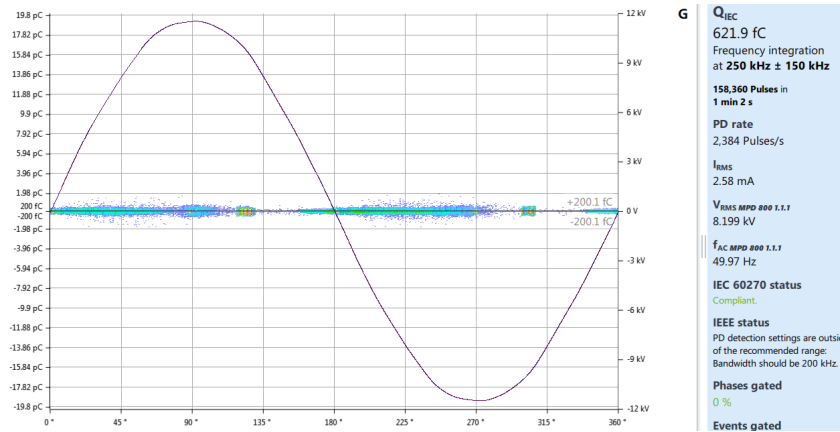
Figure A.18: *PRPD plot for the PDIV measurements conducted at test object 8 for the electrode surface sandblasted with glass orbs(0.25-0.42 mm).*
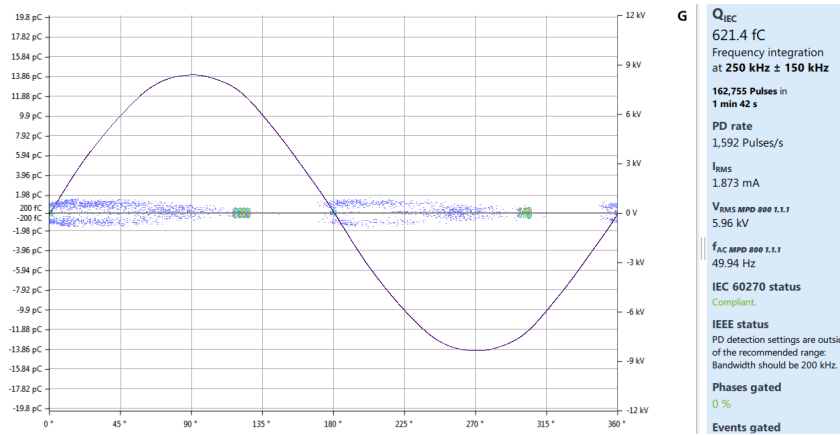
Figure A.19: *PRPD plot for the PDIV measurements conducted at test object 9 for the electrode surface sandblasted with glass orbs(0.25-0.42 mm).*

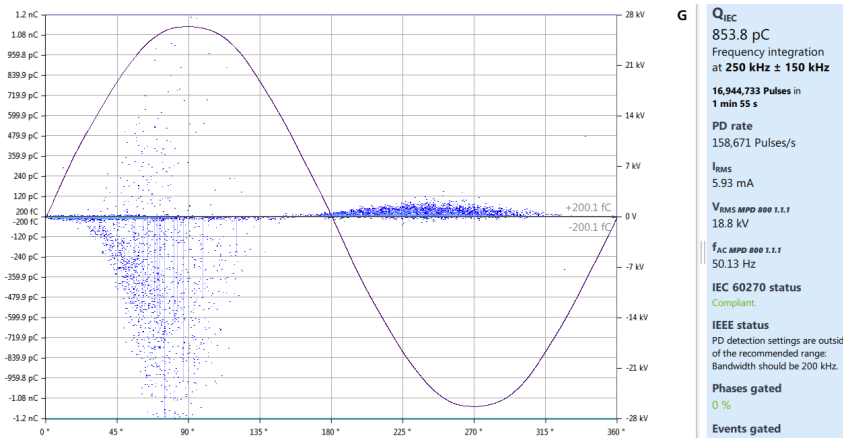**Figure A.20:** *PRPD plot for the PDIV measurements conducted at test object 10 for the electrode surface sandblasted with glass orbs(0.25-0.42 mm).*

B PRPD plots for Phase 2

This section will present the PRPD plots taken in Phase 2 when discharge magnitudes reached 1 nC.

B.1 Polished and hot AC anodised electrode surface
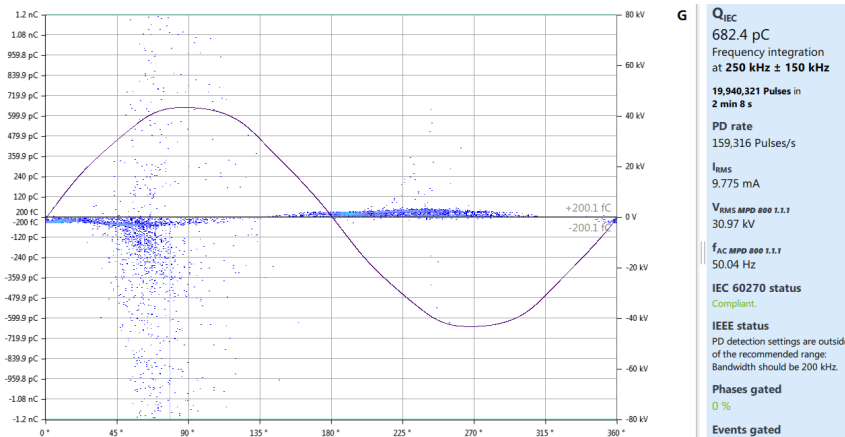
Figure B.1: *PRPD plot for the PD measurements conducted for Phase 2 at test object 3 for the polished and hot AC anodised electrode surface.*
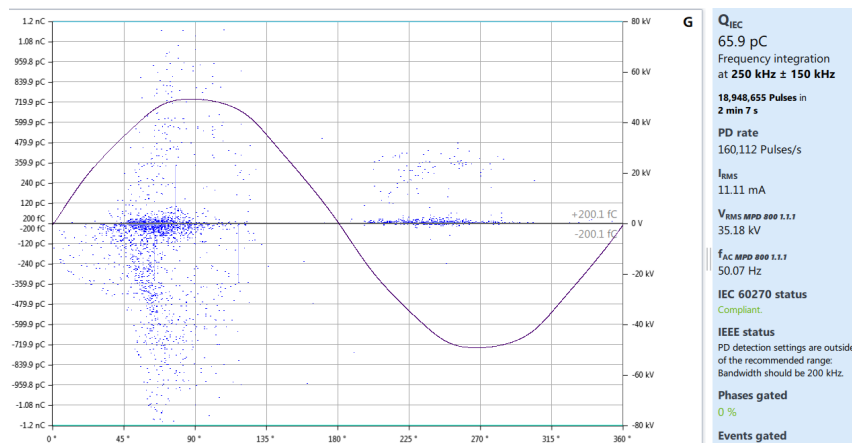
Figure B.2: *PRPD plot for the PD measurements conducted for Phase 2 at test object 4 for the polished and hot AC anodised electrode surface.*
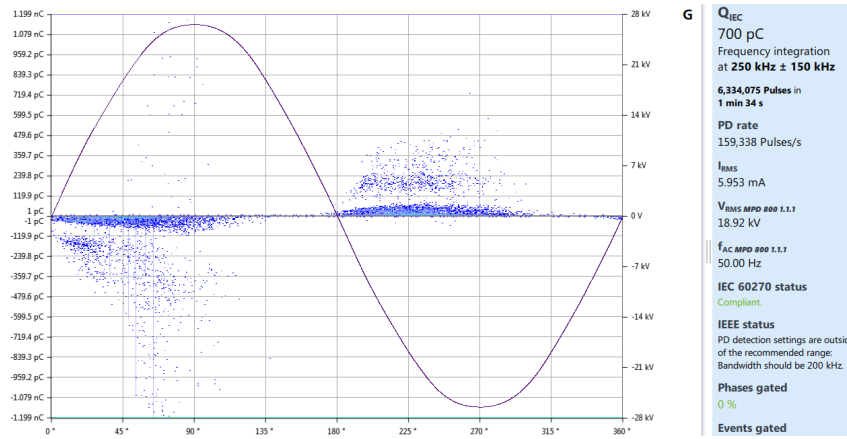
Figure B.3: *PRPD plot for the PD measurements conducted for Phase 2 at test object 6 for the polished and hot AC anodised electrode surface.*
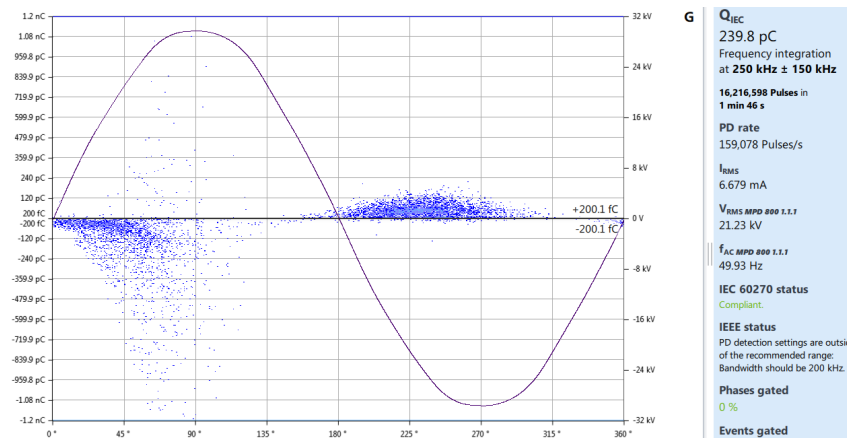
Figure B.4: *PRPD plot for the PD measurements conducted for Phase 2 at test object 11 for the polished and hot AC anodised electrode surface.*
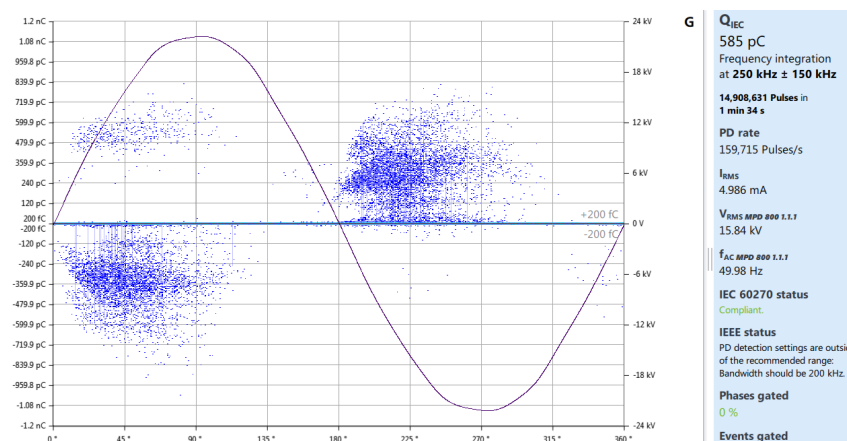
Figure B.5: *PRPD plot for the PD measurements conducted for Phase 2 at test object 12 for the polished and hot AC anodised electrode surface.*

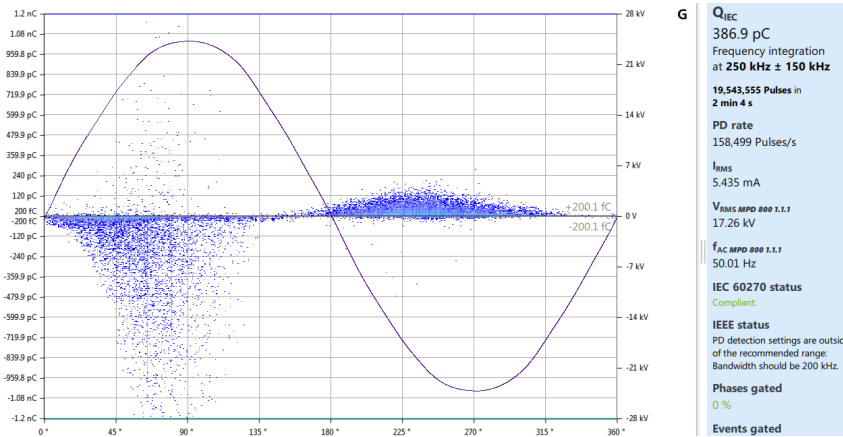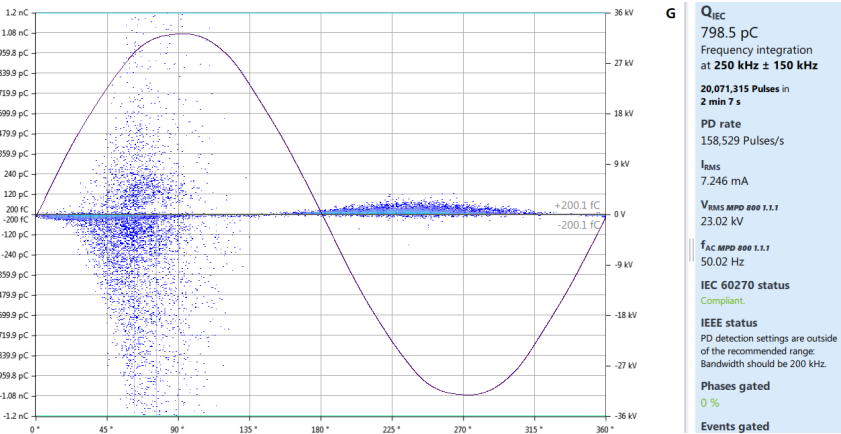## B.2 Electrode surface sandblasted with aluminium oxide(0.5-1.0 mm)
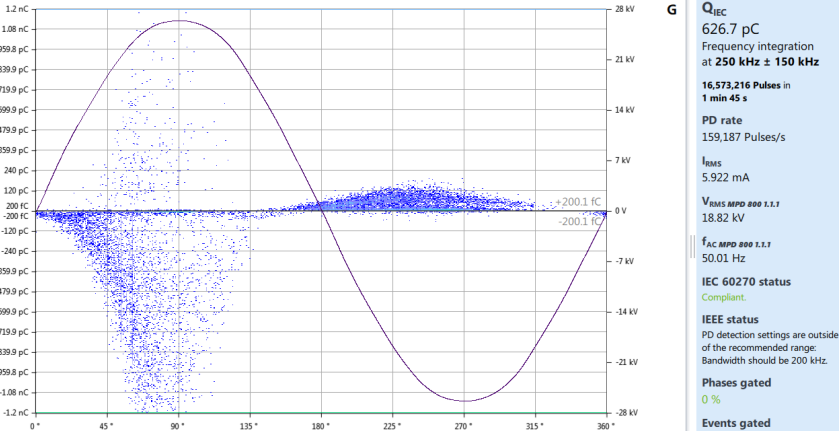
Figure B.6: *PRPD plot for the PD measurements conducted for Phase 2 at test object 1 for the electrode surface sandblasted with aluminium oxide(0.5-1.0 mm).*
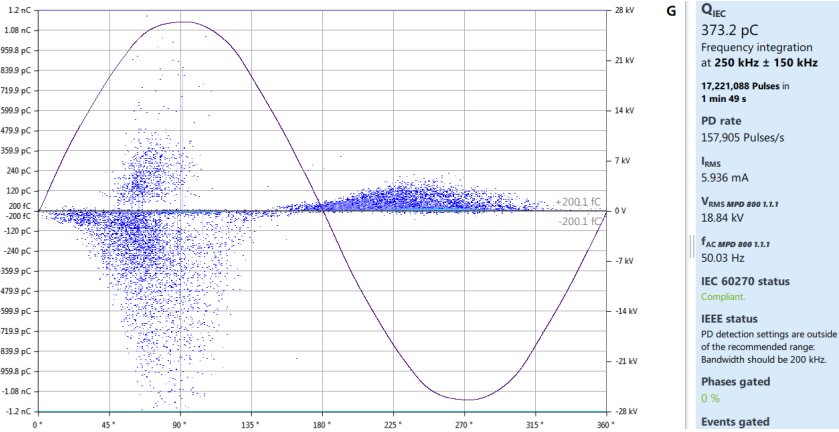
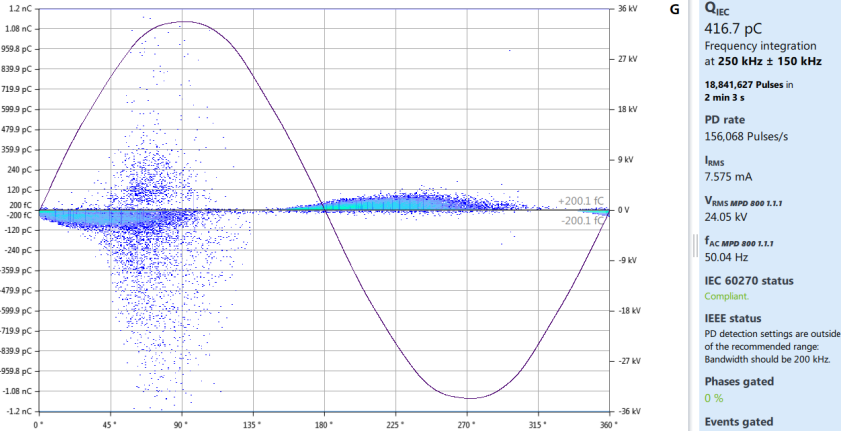**Figure B.7:** *PRPD plot for the PD measurements conducted for Phase 2 at test object 4 for the electrode surface sandblasted with aluminium oxide(0.5-1.0 mm).*
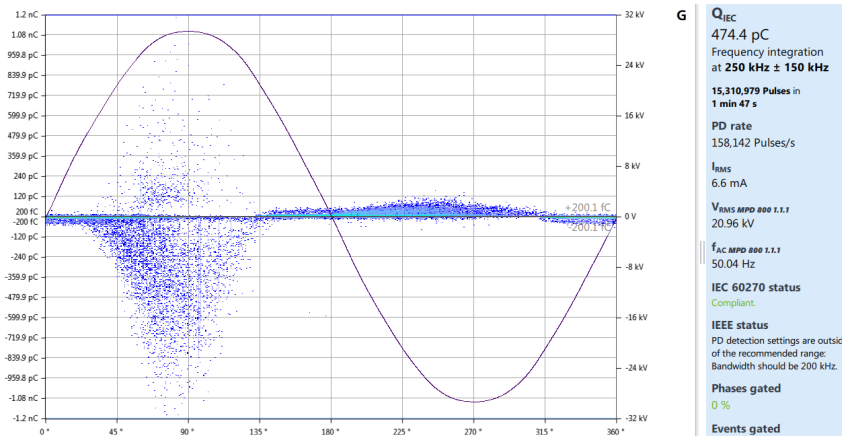
Figure B.8: *PRPD plot for the PD measurements conducted for Phase 2 at test object 6 for the electrode surface sandblasted with aluminium oxide(0.5-1.0 mm).*
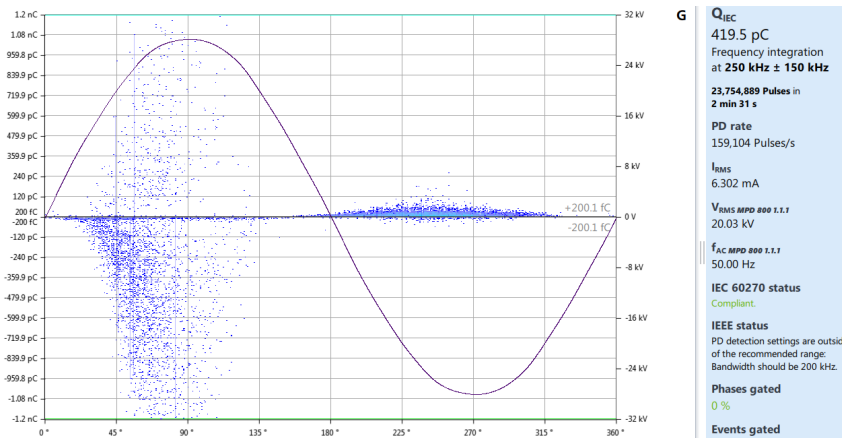
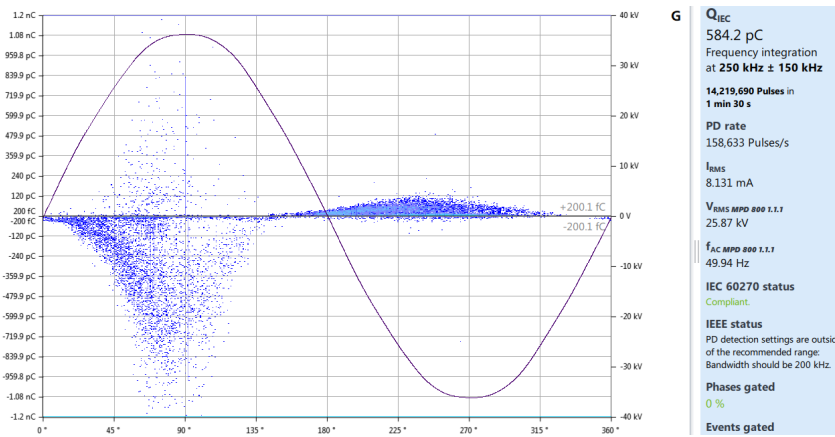**Figure B.9:** *PRPD plot for the PD measurements conducted for Phase 2 at test object 8 for the electrode surface sandblasted with aluminium oxide(0.5-1.0 mm).*

Figure B.10: *PRPD plot for the PD measurements conducted for Phase 2 at test object 9 for the electrode surface sandblasted with aluminium oxide(0.5-1.0 mm).*

Figure B.11: *PRPD plot for the PD measurements conducted for Phase 2 at test object 10 for the electrode surface sandblasted with aluminium oxide(0.5-1.0 mm).*

B.3 Electrode surface sandblasted with glass orbs(0.25-0.42 mm)

Figure B.12: *PRPD plot for the PD measurements conducted for Phase 2 at test object 1 for the electrode surface sandblasted with glass orbs(0.25-0.42 mm).*
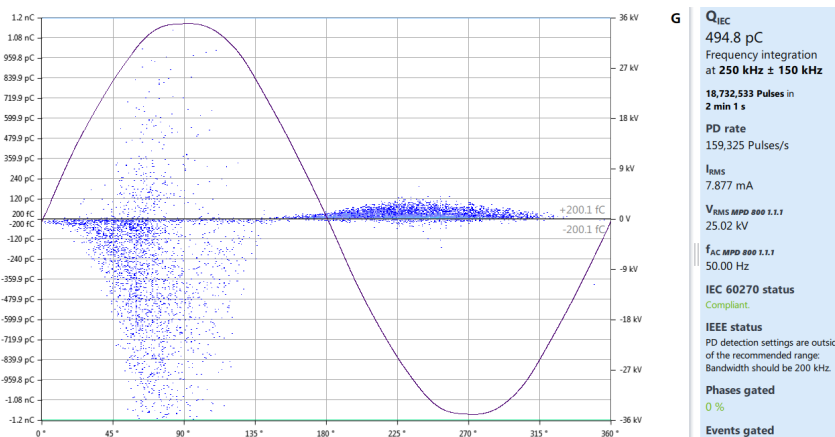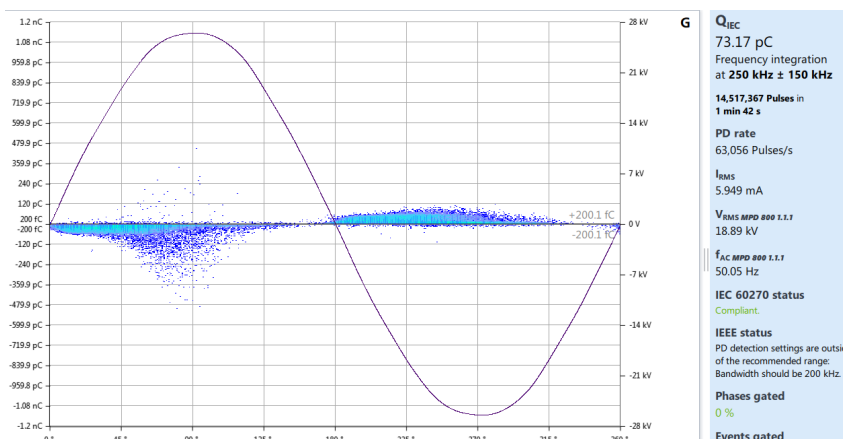

Figure B.13: *PRPD plot for the PD measurements conducted for Phase 2 at test object 3 for the electrode surface sandblasted with glass orbs(0.25-0.42 mm).*
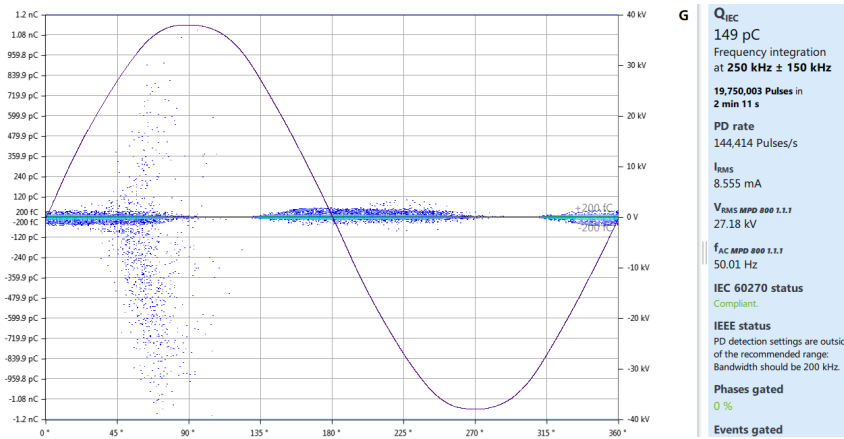
Figure B.14: *PRPD plot for the PD measurements conducted for Phase 2 at test object 4 for the electrode surface sandblasted with glass orbs(0.25-0.42 mm).*

Figure B.15: *PRPD plot for the PD measurements conducted for Phase 2 at test object 5 for the electrode surface sandblasted with glass orbs(0.25-0.42 mm).*
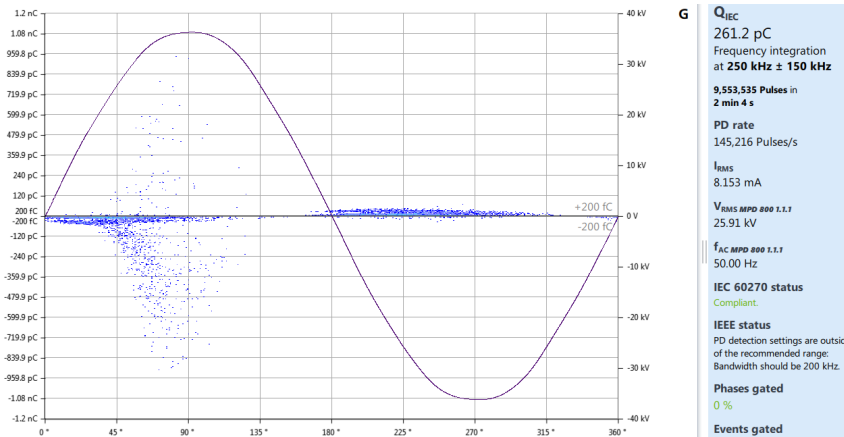

Figure B.16: *PRPD plot for the PD measurements conducted for Phase 2 at test object 6 for the electrode surface sandblasted with glass orbs(0.25-0.42 mm).*

Figure B.17: *PRPD plot for the PD measurements conducted for Phase 2 at test object 8 for the electrode surface sandblasted with glass orbs(0.25-0.42 mm).*

Figure B.18: *PRPD plot for the PD measurements conducted for Phase 2 at test object 9 for the electrode surface sandblasted with glass orbs(0.25-0.42 mm).*
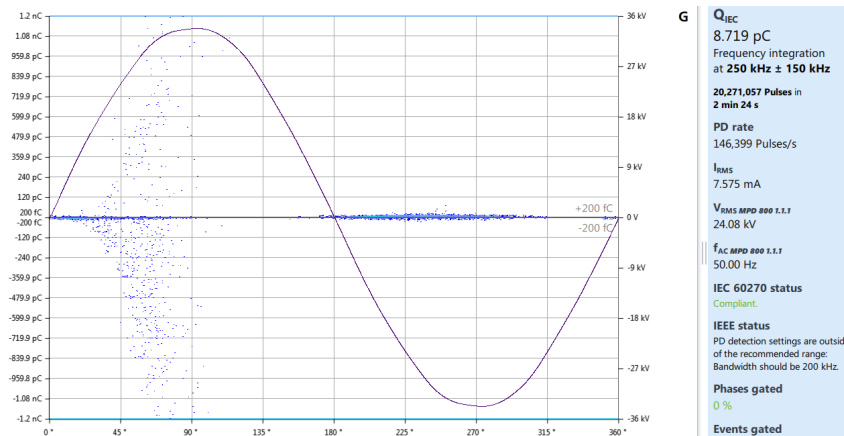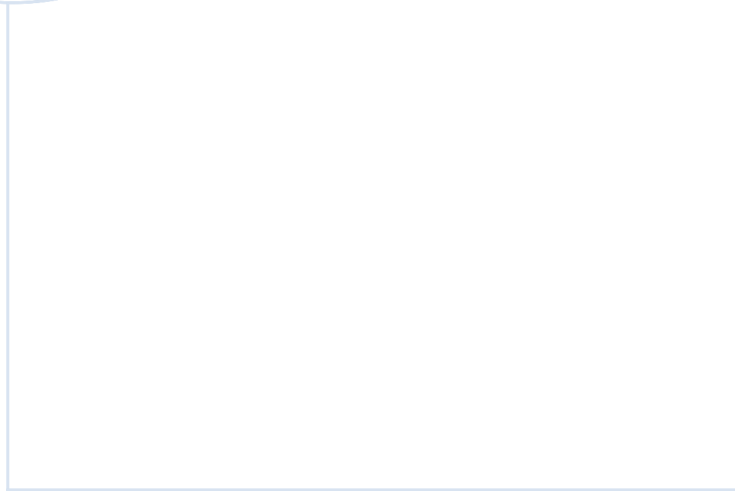

Figure B.19: *PRPD plot for the PD measurements conducted for Phase 2 at test object 10 for the electrode surface sandblasted with glass orbs(0.25-0.42 mm).*